Protein Target Identification and Characterization for Antibiotic Discovery

BY
PAULINE KABRE
B.S. University of Illinois at Chicago, 2010

THESIS
Submitted as partial fulfillment of the requirements for the degree of
Doctor of Philosophy in Chemistry in the Graduate College of the
University of Illinois at Chicago, 2018

Chicago, Illinois

Doctoral Dissertation Defense Committee:

Dr. Leslie W.-M. Fung, Chair and Advisor, Department of Chemistry, UIC
Dr. Leslie Aldrich, Department of Chemistry, UIC
Dr. Shahila Mehboob Christie, Neugenica LLC
Dr. Stephanie Cologna, Department of Chemistry, UIC
Dr. Scott Shippy, Department of Chemistry, UIC

ACKNOWLEDGMENTS

First I would like to sincerely thank my advisor Dr. Leslie W.-M. Fung for taking me in her lab and guiding me throughout the years. Her guidance, support and dedication are empowering greatly appreciated.

I would like to thank the Chemistry Department at UIC for providing me financial support as a Teaching Assistant during my time in the graduate program.

I would like to thanks my committee members Dr. Leslie Aldrich, Dr. Shahila Mehboob Christie, Dr. Stephanie Cologna, and Dr. Scott Shippy, for their time, expertise and insight into improving the quality of my thesis.

Many thanks goes to my undergraduate research adviser, Dr. Richard Kasner for exposing me to undergraduate research and encouraging me to join the program.

My special thanks and gratitude to Dr. M.E. Johnson and members of his entire lab for their continued support, excellent suggestion and allowing me in their lab for countless number of experiments. Their generous gifts of cells, plasmids are mostly helpful and greatly appreciate.

I particularly want to thank Dr.Tina Mistry for the construct of *Sa*FabI WT in pHT370 and preparing the sample for the initial round of whole genome sequencing.

I want to thank Dr. Shahila Mehboob Christie for providing me with a protocol to generate mutants, without which part of my work would not have been possible.

To Dr. Hyunwoo Lee and his lab, thank you so much for making yourself available, both for my experiments and my endless questions. Your scientific expertise was greatly appreciated.

My sincere gratitude goes to Dr. Mankin and members of his lab. Thank you for showing

me how to set-up an MIC plate, setting the initial mutant selection, and generously providing your scientific expertise. Without all of this input, my project on Target Identification of 1, 3, 4 Oxadiazole Compounds in *Staphylococcus aureus* would not have been possible.

I want to thanks Dr. James Cook for the initial screening of the oxadiazole compounds.

To Dr. T. Bae for readily providing the *S. aureus* USA300 strain which was instrumental in getting the knockout of TetR-PK in the *S. aureus* Newman strain.

I want to thank past members of the Fung lab for the helpful discussion, their insight and suggestions at the beginning of my project. My special thanks to Drs. Marta Witek, Nina Wolf, Mike Tuntland, and Anna Kim Jones for providing a great environment around the lab and providing their great insights into project related discussion.

To Robel Demissie, thank you for everything. Thank you for synthesizing the CAIR, and being a great collaborator on many project.

To my family and friends, I asked too much, and you delivered. I am so grateful for your patience and understanding.

To my parents, Vincent De Paul Kabre and Genevieve Nikiema Kabre, thank you for setting up a great example of work ethic. Your love, support and prayers carried me every day.

Finally, I thank God for my health and strength which were both instrumental to getting through the PhD program.

TABLE OF CONTENT

TABLE OF CONTENT (continued)

TABLE OF CONTENT (continued)

LIST OF TABLES

LIST OF FIGURES

LIST OF FIGURES (continued)

LIST OF ABBREVIATIONS

1XMP	PDB code for *Ba*PurE
3KUU	PDB code for *Yp*PurE
3OOW	PDB code for *Ft*PurE
A260	Absorbance at 260 nm
A280	Absorbance at 280 nm
ACP	Acyl-carrier-protein
Amp^R	Ampicillin resistant gene
*Ba*PurE	*Bacillus anthracis* PurE
BHI	Brain heart infusion
BWA	Bio-informatics program for NGS
$CaCl_2$	Calcium chloride
CAIR	4-Carboxy-5-aminoimidazole ribonucleotide
CD	Circular dichroism
CFU	Colony forming units
CRI	Core for research informatics
DMSO	Dimethylsulfoxide
DNA	Deoxyribonucleic acid
DNTP	Deoxyribonucleotide triphosphate

DPNI	Restriction enzymes
E. coli	Escherichia coli
epPCR	Error prone PCR
Erm	Erythromycin
erm^R	Erythromycin resistant gene
FabI	Enoyl-acyl carrier protein reductase
FPLC	Fast performance liquid chromatography
*Ft*PurE	PurE from *Francisella tularensis*
GATK	Bio-informatics program for NGS
gDNA	Genomic DNA
GSH	Glutathione, reduced
GST	Glutathione S-transferase
IDT	Integrated DNA technology
IMP	Inosine monophosphate
IPTG	Isopropyl β-D-1-thiogalactopyranoside
I-TASSER	Program for protein structure prediction
K_{AV}	Partition coefficient
K_{cat}	Turn over number
K_m	Michaelis Menten constant
LB	Luria broth (medium)

LIST OF ABBREVIATIONS (continued)

LC2	2, 5-Dichlrobenzene 2-carboxamido-1, 3, 4-oxadiazole 2-phenyllepidine
LC5	2, 5-Dimethylbenzene 2-carboxamido-1, 3, 4-oxadiazole 2, 5-chlorothiophene
MEM	Bio-informatics analysis tool
MIC	Minimum inhibitory concentration
MRSA	Methicillin resistant *staphylococcus aureus*
MSSA	Methicillin sensitive *Staphylococcus aureus*
N^5-CAIR	N^5-Carboxyaminoimidazole ribonucleotide
NaCl	Sodium chloride
$NADP^+$	Nicotinamide adenine dinucleotide phosphate
NGS	Next generation sequencing
OD_{600}	Optical density at 600 nm
ORF	Open reading frame
PBS	5 mM Phosphate buffer saline at pH 7.4 with 150 mM NaCl
PCR	Polymerase chain reaction
PDB	Protein data bank
pHT370	Shuttle vector
pHT370-*Sa*FabI-A33V	Shuttle vector containing FabI gene from *Staphylococcus aureus* with an A33V mutation
pHT370-*Sa*FabI-WT	Shuttle vector containing FabI WT gene from *Staphylococcus aureus*

LIST OF ABBREVIATIONS (continued)

pI	Isoelectric Point
PIP	Phage Infusion Protein
PMSF	Phenylmethylsulfonyl fluoride
PurE	N^5-Carboxyaminoimidazole ribonucleotide mutase
RRC	Research resources center
Sa	*Staphylococcus aureus*
SAICAR	4-(N-Succino)-5-aminoimidazole-4-carboxamide ribonucleotide
*Sa*FabI	FabI from *Staphylococcus aureus*
SE	Size exclusion
SNP	Single Nucleotide Polymorphism
SnpEff	Bio-informatics program for NGS
SPANDx	Bio-informatics program for NGS
T/N	Triclosan/$NADP^+$
TetA	Tetracycline induced efflux pump
TetR	Repressor protein of tetracycline resistance element
TetR-PK	TetR from ORF 2165 in *Staphylococcus aureus* identified in this study
Tm	Boltzmann transition temperature in thermal denaturation
$TolC^-$	Cured from efflux pump TolC gene.
Tris	Tris (hydroxymethyl) aminomethane
TSA	Tryptic soy agar

UIC	University of Illinois at Chicago
USA300	Community-associated methicillin resistant *Staphylococcus aureus*
VCF	Bio-informatics program for WGS
WGS	Whole Genome Sequencing
YhgE	Un-characterized membrane-spanning protein
*Yp*PurE	PurE from *Yersinia Pestis*
ΔANR	*Bacilus antracis* Ames strain
Φ85	Phage 85 from *Staphylococcus aureus*

SUMMARY

Antibiotic discovery requires a multilevel approach to finding candidates. My projects involved three approaches toward the antibiotic discovery: (1) the identification of additional targets of bio-active oxadiazole compounds, (2) understanding a drug resistant mechanism for the next generation drug modification, and (3) the characterization of a drug target of multiple pathogens for both narrow and broad spectrum drug development.

In the identification of additional targets of oxadiazole compounds, *Staphylococcus aureus* resistant strains were developed against two compounds. The genomic DNA analysis of the resistant strains revealed different mutations in the same gene, a gene in the tetracyline repressor (TetR) family (we named it TetR-PK). To identify the gene that TetR regulates, a transposon insertion was used to knock-out the TetR-PK gene, and further selected resistant strains. The genomic DNA analysis of the resistant TetR-PK knock-out colonies showed a single nucleotide insertion in an intergenic region in - between YhgE and TetR-PK genes. Further studies are needed to determine the function of this intergenic region.

In the second approach, we used error prone PCR to generate 326 mutations in an essential enzyme enoyl-acyl carrier protein reductase (FabI). Forty two genes with single mutations were introduced individually into an expression vector. The expressed proteins were then tested for triclosan binding. MIC measurement of a mutant A33V show 450 fold increase in triclosan concentration required to inhibit bacterial growth, clearly demonstrating its resistance toward Triclosan. This mutational studies allow us to understand the mechanism(s) leading to triclosan resistance and to provide possible modifications on triclosan rendering bio-activities again.

The third approach focused on the biochemical and biophysical characterization of an enzyme being targeted for drug development, the PurE enzyme in the purine biosynthesis pathway of *Bacillus anthracis*, *Francissella tularensis* and *Yersinia pestis*. The solution properties of the three homologous enzymes were mostly the same except the surface hydrophobicity. The results defined a frame work for narrow and broad spectrum antibiotic development.

Antibiotic resistance is one of our most serious health threats, so we need to develop antibiotics faster than the rate at which bacteria develop mutations that render them resistant. My studies on target identification, target mutation and target characterization are all essential components in antibiotic discovery.

1 Introduction

1.1 Emergence of Antibiotic Resistant Pathogens

Natural evolution has the ability to create bacterial cells with many mutations in many genes and/or with foreign plasmids from other bacterial cells. With the application of antibiotics, many bacterial cells are killed by antibiotics and they are antibiotic sensitive bacterial cells. Those with certain mutations or plasmids such that they are able to continue to grow in the presence of antibiotics are left to grow and multiply, and they are antibiotic resistant bacterial cells. The more antibiotics are used, the more resistant bacterial cells dominate, as stated in the Center for Disease Control and Prevention (CDC) publication (https://www.cdc.gov/drugresistance/threat-report-2013/pdf/ar-threats-2013-508). As we apply different antibiotics, we eradicate all susceptible and sensitive bacteria present. The resistant bacteria eventually take over and some of the resistant pathogens transfer their resistant genes or plasmids to other pathogens that were still susceptible to the given antibiotic. This transfer will create new resistant strains and the resistance continues spreading (Figure 1.1).

The persisting threat of antibiotic resistant pathogens infection is a serious peril for medicine. The need for new antibiotics to clear infection has created some unforeseen problems that are threatening the efficacy of modern medicine. As we are increasingly relying on existing antibiotics, the need to develop new antibiotics is more urgent than ever, given the rapid emergence of antibiotic resistant pathogens. As stated above, antibiotic resistant pathogens emerge from antibiotic sensitive bacteria with only a hand full of the bacteria being resistant to our antibiotic.

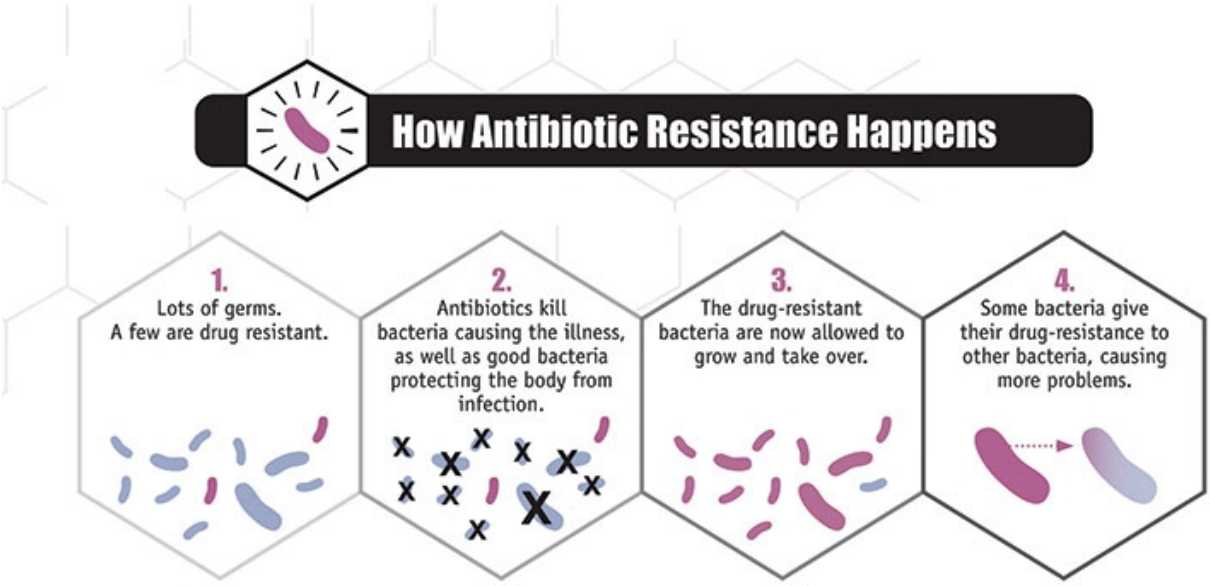

Figure 1.1: Process of antibiotic resistant pathogen emergence. Blue depict pathogens that are susceptible to the antibiotics, red refer to pathogens that are resistant to the antibiotics either by having a resistant mutation in the genome or by having a resistant gene. X on blue describe the susceptible bacteria that have been killed by the antibiotic. Purple depict a susceptible bacteria in the process of acquiring a resistant gene (https://www.cdc.gov/drugresistance/about.html).

1.2 Common Antibiotics, Targets and Resistance Mechanisms

Up to the present days, we still rely heavily on antibiotics discovered during the "golden era" of (1950 - 1970). Since the discovery of penicillin in 1928, more than 100 antibacterial compounds have been discovered to treat infections mostly in that era. Since then, the pace at which new class of antibiotic entered the clinics slowed down to the point where no new class of antibiotic has been approved since the approval of damptomycin in1987 (Davies *et al.*, 2010; Lewis *et al*; 2013). This time span coincides with the accelerated emergence of antibiotic resistant pathogens (Rogers *et al.*, 2012). For example β-lactam, cycloserine, fosfomycin, glycolipids, lantibiotic, lipoglycopeptides plectasin, and polypeptides target the cell wall synthesis; amphenicols, lincosamides, macrolides and ketolides, oxazolidinones, pleuromutillin, streptogramins, and thiopeptides, target the 50s in protein synthesis; aminocyclitols, aminoglycosides, edeine pactamycin, and tetracyclines target the 30s in protein synthesis; actinomycins, ansamycins, rifamycins, tiacumicins target RNA polymerase; aminocoumarins and fluoroquinolones target DNA gyrase; diaminopyrimidines and sulfonamides target folate synthesis mechanism; lipopeptides and polymyxins, target the cell membrane structure (Figure 1.2). Some of the prominent molecular antibiotic targets discovered so far also included DNA topoisomerase II and IV, RNA polymerase, penicillin-binding proteins, peptidoglycan units, the cell membrane, the 30s ribosome and 50s ribosome subunit, folic acid synthesis as reviewed in (Kohanski et al., 2010; and Chellat *et al.*, 2016; Figure 1.2). Resistant pathogens strains to these classes of antibiotics (sulfonamides, β-lactams, aminoglycosides, tetracyclines, macrolides, glycopeptides, streptogamins, lincosamides, linezolid, phenicols, rifammyins, fluroquinolones,

and lipopeptides (Kohanski *et al.*, 2010)) have emerged since the introduction of most of them in the clinic. The observed methods of resistance included over-expression of efflux pump to expel the antibiotics from the intracellular environment, destruction of the antibiotics, target mutation or cellular membrane alteration to prevent the crossing of the antibiotic from outside of the cell to inside of the cell (Chellat *et al.*, 2016; Figure 1.2).

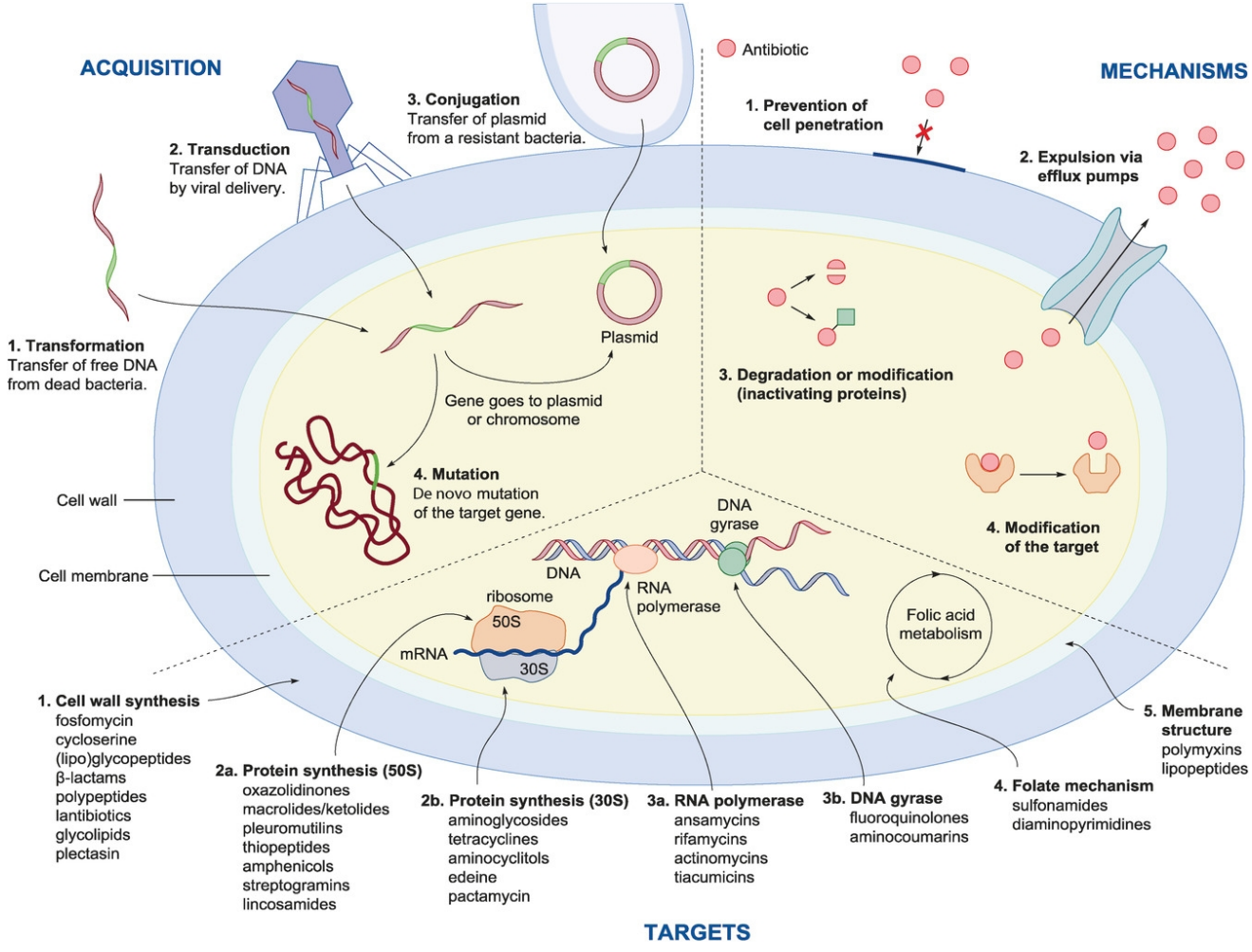

Figure 1.2: Mechanism of intrinsic resistance development, resistance acquisition and common antibiotic targets (Chellat *et al.*, 2016). The "Targets" refer to the molecules inside the cells known to be acted on by antibiotics. "Mechanism" is the intrinsic methods developed by the bacteria to resist the antibiotics. "Acquisition" is getting foreign elements from the environment that render the bacteria resistant to the antibiotics (Reprinted with permission from Wiley and Sons).

1.3 Impact of the Emerging Antibiotic Resistant Pathogens

Given the estimations by the Center for Disease Control and Prevention (CDC), 2,000,000 illnesses and 23,000 deaths in human cost each year are directly attributed to the resistant pathogens. In addition to the human cost, these resistant pathogens are responsible for $20 billion dollar in excess direct health care costs each year, and if we take into account the lost in productivity regarding everyone involved, the cost can be as high as $35 billion dollar each year. Pathogens of high priority includes *Bacillus anthracis*, *Francissella tularensis* and *Yersinia pestis*, all classified as Category A Biothreat Agents by the CDC in part due to the fact, that they can be easily disseminated, and their spread can result in a high mortality rate. (https://emergency.cdc.gov/agent/agentlist-category.asp). *Bacillus anthracis* can be treated with common antibiotics, however, resistance to ciprofloxacin (the first choice for anthrax treatment) has been reported (Lance *et al.*, 2003). *Francissella tularensis* and *Yersinia pestis* are often treated with streptomycin, however resistant *Yersinia pestis* to multiple antibiotic have been detected (Marc *et al.*, 2006). *Francissella tularensis* show resistance to beta lactam and azithromycin (Ikaheimo *et al.*, 2000). The possibility of using *B. anthracis*, *F. tularensis* and *Y. pestis* as a biological weapon raises the stakes for finding antibiotics for these pathogens. The high priority in methicillin resistant *Staphylococcus aureus* (MRSA) come from the fact that these pathogen is labeled as a "superbug" due to it resistance to many antibiotics.

1.4 Current Approaches to Antibiotic Discovery

Currently explored methods of antibiotic discovery to counter the rapid emergence of resistant pathogens includes finding new classes of antibiotics and finding novel molecular drug targets. In the process of antibiotic discovery, finding new chemicals is essential in developing the next generation of antibiotics. Meanwhile, with the identification of new targets, we can identify molecules with different mechanism of action than currently exist. For these new compounds to become antibiotics, they need to be **on target**, in order to have minimal side effects in human.

Multiple approaches have been used along with the information from the mechanism of resistance to design new class of antibiotics as well as create analogs of the existing antibiotics to combat the resistant bacterial strains. It is a combination of learning from the mechanism of resistance, designing new or alternate scaffold in order to conquer the emerging resistant pathogens (Chellat *et al.*, 2016; Figure 1.3).

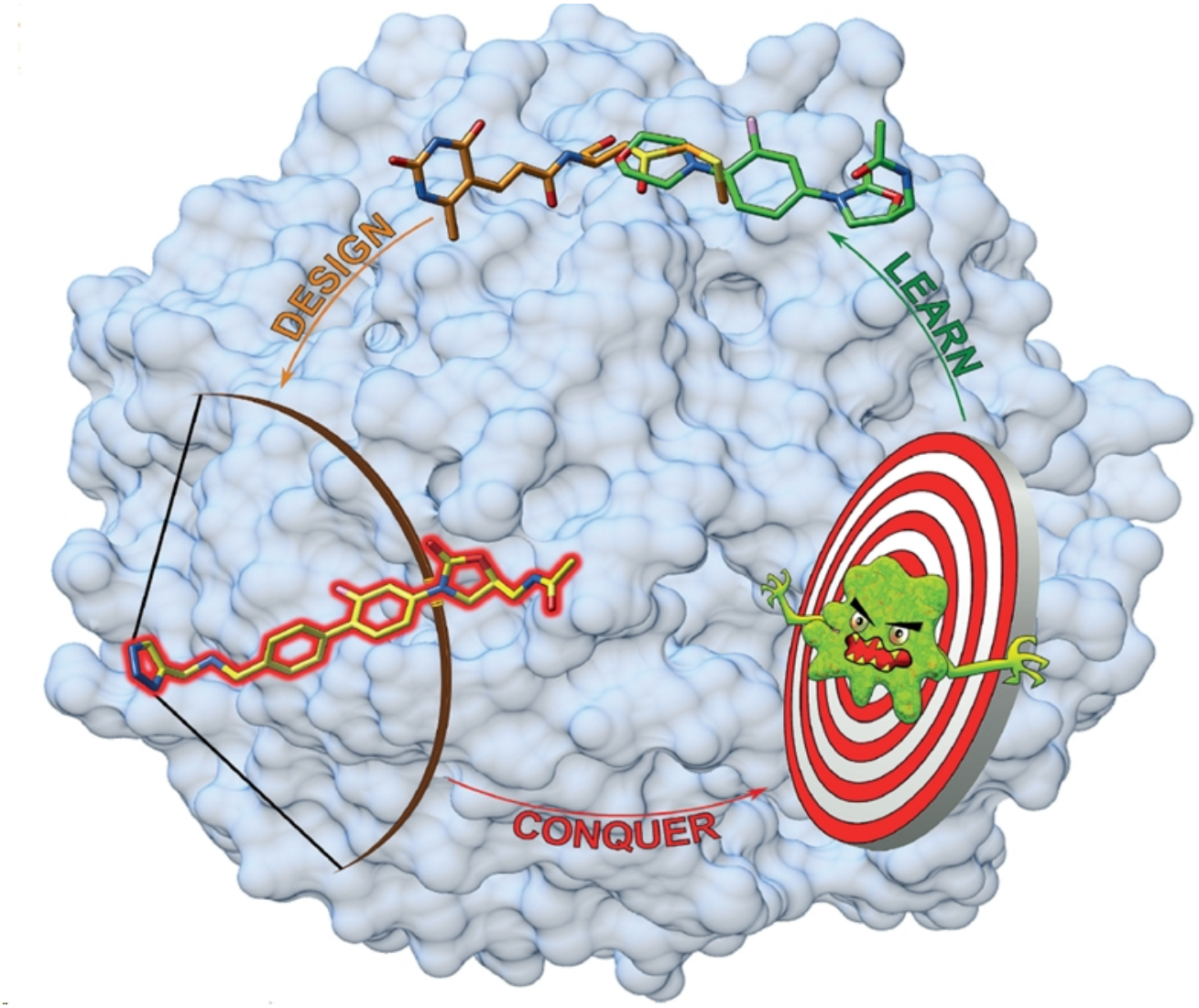

Figure 1.3: The process of antibiotic discovery and re-development. A new bio-active molecule is discovered, the bacteria develop resistance to that molecule, scientists learn about the mechanism of resistance, develop an analogue that can overcome the resistance, apply the new molecule to the sensitive and resistant bacteria, and if the bacteria develop resistance to the new molecules, the cycle continues (Chellat *et al.*, 2016). (Reprinted with permission from Wiley and Sons).

Since whole genome sequencing (WGS) became accessible (Quainoo *et al.*, 2017), almost all the genes have been identified in different bacteria and in human which facilitate the targets identification and target validation. Due to the advances and ease in gene manipulation and recombinant protein production, many structures have been solved (Kroemer *et al.*, 2007), facilitating structure-based drug discovery. Structure-based drug discovery is becoming a method of choice for high throughput screening of natural products and synthetic molecules. It is also increasingly being used to uncover mechanism of action of antibiotic lead molecules. Whole genome sequencing is also being used in the sequencing of the genome of clinical isolates or laboratory evolved strains for resistant mutants identification.

1.5 Second Generation of Drug Development

A derivative or an analogue of existing antibiotics may become effective in fighting resistant strains. Medicinal chemistry methods are used to improve an existing antibiotic molecule to become useful in resistant strains.

1.5.1 Rational Identification of Target and Structure-Based Drug Discovery

Methods used to identify targets include understanding metabolic pathways of both human and pathogens, particularly the enzymes involved in each step of metabolism. With a target identified, structure-based drug discovery platform is often used to screen for inhibitors. The method yields a molecular level information on target engagement as well as the mode of action of a particular compound. A major difficulty encountered in this approach is that the identified compounds may also interact with other targets. Coupling structure-based drug design

approaches and other methods can lead to a unique target identification and therefore a positive outcome in drug discovery.

1.5.2 Mutant Selection and Whole Genome Sequencing

Antibiotic resistant bacterial strains are selected and the genes in the entire genome are sequenced to identify those genes that are mutated. Whole genome sequencing uses both the process of sequencing to gather the sequence of the fragments and the bio-informatics to assemble the genome as well as align it to a reference wild type genome. Crucial mutations are identified in the sequencing, and the mutations can be confirmed to be responsible for the resistance by measuring the concentrations of antibiotics required to kill the native bacterial cells compared to a strains with plasmids consisting of the mutations introduced into these strains.

1.5.3 Gene Knockout by Transposon Insertion

Transposons are named since they are mobile and able to be dislocated around a given genome. Transposable elements are DNA fragments often used to study the function of a given gene. They can be inserted through integration during replication (Opijnen *et al.*, 2013), or pasted into the genome by an enzyme. A pathogen gene with a transposon inserted in its sequence will lose its function leading to a distinct phenotype in the pathogen. Thus, transposon insertion can be used in a high throughput fashion to randomly knockout different genes and screen for the phenotypic effect, or the transposon can be used to knockout a specific gene, and study the function(s) of that gene (Mesarich *et al.*, 2017). Transposable element can be genes that are resistant to antibiotic (Craig *et al.*, 1997) or it can code for a particular phenotype. Though transposon insertion can be used to identify gene function, other gene characteristics are necessary for viable drug target identification/verification.

1.5.4 PurE as a Viable Target for Drug Discovery

N^5-Carboxyaminoimidazole ribonucleotide mutase (PurE) is an essential enzyme in the *de novo* purine biosynthesis pathway that catalysis the conversion of N^5-CAIR to CAIR (Zhang *et al.*, 2008) and is an octameric enzyme (Mathews *et al*., 1999). This N^5-CAIR to CAIR conversion step is important in drug discovery, since the substrate in bacteria differs significantly from that in human (Figure 1.4). PurE knockout of *Bacillus anthracis* (*B. anthracis*) cells exhibited reduce pathogenicity in blood (Samant *et al.*, 2008), attesting to the essentiality of the enzyme in the *de novo* purine biosynthesis pathway. Also, a transposon site hybridization in *Mycobacterium tuberculosis* showed that PurE is essential for optimum growth (Sassetti *et al.*, 2003).

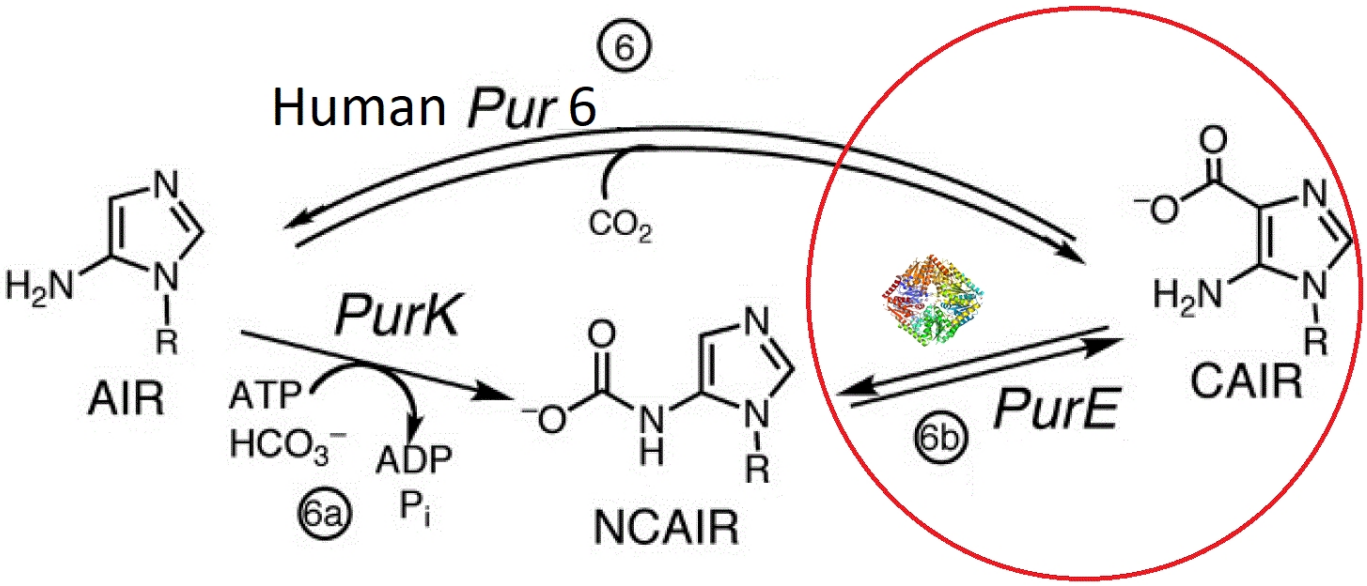

Figure 1.4: Conversion of AIR to CAIR catalyzed by different enzymes. In higher eukaryote including human the conversion is a one step process, catalyzed by Pur6 with CO_2 as a cofactor. In prokaryote, AIR is irreversibly first converted to N^5-CAIR followed by the interconversion between N^5-CAIR and CAIR catalyzed by PurE found in bacteria. Adapted from Zhang *et al.*, 2008.

1.6. Summary

Using *B. anthracis* PurE as a target, high throughput screening has identified several 1, 3, 4 oxadiazole compounds to be inhibitors and some were shown to be potent against a wide range of both gram positive and gram negative bacteria (Kim *et al.*, 2015) (TABLE I). Though different approaches have been proven successful for developing antibiotics in different settings, this study focused on target identification, target mutation and characterization of targets. They are discussed in the next three chapters. In the second chapter, I focused on the identification of the molecular target of 1, 3, 4 oxadiazole compounds in *Staphylococcus aureus* (*S. aureus*). In the third chapter, I identified the effect of mutations in target enoyl-acyl carrier protein reductase (FabI) in *S. aureus* cells. In the fourth chapter, I characterized the target (enzyme PurE) in *Bacillus anthracis, Francisella tularensis,* and *Yersinia pestis* pathogens. Antimicrobial resistance is one of our most serious health treats. New antibiotics need to be developed faster than the rate bacteria develop mutations that render resistance. Multiple antibiotic development platforms are available for us to obtain new antibiotics.

TABLE I: PERCENT INHIBITION OF 1, 3, 4 OXADIAZOLE COMPOUNDS ON *BA*PURE, AND MIC OF OXADIAZOLE COMPOUNDS ON DIFFERENT BACTERIAL STRAINS. ADAPTED FROM KIM *ET AL.,* 2015.

Compound	% Inhibition[a]	MIC (μg/mL)					
	*Ba*PurE	*Ba*[b]	*Ft*[b]	*Yp*[b]	MSSA[b]	MRSA[b]	EcTolC[-b]
LC1	27	0.15	6.25	>12.5	0.29	0.39	0.29
LC2	19	0.10	3.1	>12.5	>12.5	6.25	0.39
LC3	13	0.10	>12.5	>12.5	>12.5	>12.5	>12.5
LC4	19	0.10	6.3	>12.5	0.2	>12.5	0.02
LC5	20	0.05	1.6	3.1	0.78	1.95	0.07
LC6	15	0.78	1.2	3.1	1.56	3.13	0.39
Cipro	ND[c]	0.11	0.03	0.04	0.35	0.34	0.01
Linezolid	ND	2	32	ND	2	ND	ND

[a]Inhibition: reported values were obtained from a range of 2 to 4 trials with an average of 7% error.

[b]*Ba* = *B. anthracis* (ΔANR strain) cells; *Ft* = *F. tularensis* cells; *Yp* = *Y. pestis* cells; MSSA = *S. aureus* (methicillin susceptible strain 29213) cells; MRSA = *S. aureus* (methicillin-resistant strain 43300) cells; *Ec*TolC$^-$ = *E. coli* (BW25113 TolC$^-$) cells.

[c]ND = not determined

Chapter Two

Target Identification of 1, 3, 4 Oxadiazole Compounds in *Staphylococcus aureus*

2.1. Introduction

Finding the target for a bioactive small molecule and unraveling it mechanism of action inside a bacterial cell are still major road blocks in drug discovery (Neggers *et al.,* 2018). Cell-based antibiotic discovery is a method of choice as it ensures successfully jumping the major hurdle of cell membrane permeability in the antibiotic discovery process (Ioerger *et al.*, 2013). Genetic and cell-based approaches are also shown to be powerful methods to find as well as to characterize bioactive molecule targets (Zheng *et al.*, 2004). PurE is an essential enzyme in the building block formation of the purine bases. It catalyzes the interconversion of N^5-CAIR to CAIR in prokaryote and is a domain of Pur6 in human. Pur6 catalyzes the conversion of AIR to CAIR in the presence of CO_2 in human. This key difference in substrate intake made PurE an essential target for antibiotic development. A high throughput screening of target PurE from *Bacillus anthracis* (*Ba*PurE) yielded potent compounds against *Bacillus anthracis*, *Staphylococcus aureus* - both methicillin sensitive (MSSA) and methicillin resistant (MRSA), *Escherichia coli* TolC$^-$, *Francisella tularensis* and *Yersinia pestis* (Kim *et al.*, 2015). These potent compounds are members of the azole family with (1, 3, 4 oxadiazole) as a common component.

An observed discrepancy between minimum inhibitory concentration (MIC) and the compound concentration required for *Ba*PurE inhibition (IC_{50}) led to the suggestion that other target(s) are also responsible for the high potency of the compounds (Kim *et al.*, 2015). The goal of my study was to identify the additional target(s) in *S. aureus*. Among the identified potent

compounds, LC2 (2, 5-dichlrobenzene 2-carboxamido-1, 3, 4-oxadiazole 2-phenyllepidine) and LC5 (2, 5-dimethylbenzene 2-carboxamido-1, 3, 4-oxadiazole 2, 5-chlorothiophene) were selected at random for this study. There are 3065 genes in *S. aureus* (2.9×10^6 nucleotides). How to find just one or two gene products that interact with LC2 and LC5 was the challenge.

Using drug resistant pathogenic strains to locate mutant proteins is a mean to identify drug target(s) (Cloete *et al.*, 2016). We have used this method to identify the other target(s) of LC2 and LC5 in this class of potent compounds that retard the growth of several pathogens.

2.2. Materials and Methods

Materials were from Thermo Fisher (Waltham, Massachusetts) otherwise specified.

2.2.1. Bacterial Cell Growth

Cells of *Staphylococcus aureus* Newman strain (a laboratory strain; Nair *et al.*, 2011) (*S. aureus* cells) were obtained from Dr. M. Johnson lab of UIC. Cells of *Bacillus anthracis* Ames strain (ΔANR, a non-pathogenic strain) (*B. anthracis* cells) were from Dr. J. Cook lab of Loyola University of Chicago. Cells of *Escherichia coli* with the *TolC* efflux pump knocked out (*E. coli* $TolC^-$ cells) were obtained from Dr. A. Mankin lab of UIC. Cell growth was started with either a single colony or a frozen stock (4 μL) in 4 mL medium solution. The medium for *S. aureus* cells is brain heart infusion (BHI) medium, and *B.anthracis* and *E. coli* $TolC^-$ cells is Luria broth (LB) medium. The cell culture was incubated at 37 ºC while shaking with 240 rotation per minute (rpm) overnight (16 to 18 h). This overnight culture was diluted 100-fold and incubated at 37 ºC with 240 rpm shaking until a desire optical density at 600 nm (OD_{600}) was reached. Since most of the compounds used in this study were dissolved in DMSO, cells were grown in 0-2% DMSO to

an OD_{600} of 1. For cell growth on agar plates, agar (3 gm) in BHI or LB medium (200 mL) with the appropriate concentration of the compound was used.

2.2.2. Miles and Misra Cell Count (Colonies Forming Unit)

The Miles and Misra cell counting method (Miles *et al.*, 1938) was used to determine the colony forming unit (cfu) in a given inoculum. A cfu is the number of viable bacterial cells in a sample and was determined using serial volume dilutions, starting from cells at an OD_{600} of 1, with 100-fold dilution, followed by 100- or 10-fold dilution until a 10^9-fold dilution was achieved. With each dilution, the cell solution (100 L) was plated and incubated at 37 °C for 18 h. The plates with 10 or fewer colonies were counted, and the dilution factors of the plates were noted. For example, for 5 cells counted on the 10^9 dilution plate represented 5 x 10^9 cfu for the original sample.

2.2.3. MIC of *S. Aureus* Cells in Liquid Medium

Cell culture of a single colony was used for overnight culture, and the overnight culture (20 µL) was diluted 100-fold in fresh BHI and incubated at 37 °C with shaking at 240 rpm for 2.5 to 3 h to give an OD_{600} of 0.2 to 0.6 (mid log phase).

During the cell incubation time, a 96-well flat bottom plate was prepared for MIC determination using the micro-dilution method (Hevener *et al.*, 2012), with slight modifications. BHI medium (146 µL) was added to the 12^{th} well of a specific row, and BHI (75 µL) was added to each of the remaining wells of the same row. 4 µL of a specific compound, LC2 or LC5 (Kim *et al.*, 2015; section 2.1) at a specific concentration was added to the 12^{th} well to give a final volume of 150 µL. 75 µL solution of this well was pipetted and introduced to the 11^{th} well to

give a total volume of 150 μL in this well and thus half of the concentration of the compound in this well. This step was repeated for the 10th to the 2nd wells. The 75 μL from the 2nd well was discarded leaving the first well without compound as a negative control. Different rows were used for different compounds and/or different cell types if needed.

At the end of the cell incubation, the cell culture was diluted to an OD_{600} of 0.004. The diluted cells (75 μL) were added to each of the 12 wells on the plate prepared above to give a calculated final OD_{600} of 0.002. The plate was sealed and incubated with no shaking at 37 ºC for overnight (18 to 20 h growth). The next morning, the wells were visually inspected for turbidity as a sign for cell growth. The well with the lowest compound concentration to give no visible turbidity (cell growth) was noted, and this compound concentration was reported as the MIC value of the compound for the cells used.

Using the method above, we also tested the MIC of antibiotics with known mode of action on *S. aureus* Newman and *B. anthracis* ΔANR cells, in order to narrow down the pathway on which, our compound might be acting on. The idea was that if our compounds have a target similar to the antibiotic, they will have similar MIC increase and/or decrease on wild type (WT) strain, mutant strains and knockout strains. This antibiotic were ciprofloxacin (targeting DNA gyrase), tetracycline (targeting the ribosome), chloramphenicol and erythromycin (targeting 50s ribosome), triclosan (targeting fatty acid metabolism and specifically FabI enzyme) and ampicillin (targeting the cell wall synthesis). Also, the MIC values of several compounds sharing the same core structure as LC2 and LC5 were determined on *S. aureus* Newman, *B. anthracis* ΔANR and *E. coli* TolC^{-} cells in order more compounds that are potent against our bacterial strains.

2.2.4. Compound Resistant Cells (Mutants) Selection

Agar plates containing LC2 or LC5 at a concentration of 0.5x, 1x, 2x, 5x, 10x, 20x or 40x, with x as the MIC value of the WT cells, were prepared. *S. aureus* Newman or *B. anthracis* ΔANR cell culture with 10^9 cfu was centrifuged, re-suspended in medium (100 µL or less) and spread to each plate. Only colonies that appeared after 24 h incubation at 37°C were picked and re-streaked on new agar plates with the same compound concentration. The colonies that grew on the new plates were kept and processed for DNA sequencing. The plates with no growth were discarded.

2.2.5. MIC on Resistant Mutants

The MIC values of compounds LC2 and LC5 on the selected resistant cells were tested and compared to that of the wild-type strain to confirm their resistance by the increase of their MIC compared to the MIC of the wild-type strain. To check whether efflux pumps on the membrane was over expressed in the mutant colonies, the MIC of kanamycin, a known antibiotic, was also used to compare its MIC on the wild-type and on the mutant colonies. If the pump was over expressed in the resistant cells, kanamycin MIC value would be higher in the resistant cells than in the wild-type cells. BHI medium was used for *S. aureus* Newman cells, and LB was used for *B. anthracis* ΔANR and *E. coli* ($TolC^-$) cells.

2.2.6. Genomic DNA Extraction

Overnight culture (4 mL) was pelleted, re-suspended in water (600 µL), and pelleted again. The genomic DNA (gDNA) from *B. anthracis* cells were obtained by lysing the cells at 90 °C for 10 m to release the cell content including the gDNA. The gDNA from *S. aureus* Newman cells was extracted by adding 10 units/mL of lysostaphin to help break down the cell

wall, and using MoBIO genomic DNA extraction kit (MoBio, Germantown, Maryland). Small amounts of gDNA were extracted by this method suitable for PCR fragment amplification. When a large amount of gDNA was needed for whole genome sequencing, GenElute bacterial genomic DNA Kit (Sigma Aldrich, St. Louis, Missouri) was used to extract the gDNA from *S. aureus* colonies with slight variation. Overnight culture (4 mL) was pelleted, washed with water and pelleted once more. The cell suspension was supplemented with 10 unit/mL of lysostaphin and 10^5 unit/mL lysozyme before eluting the DNA using water.

2.2.7. Genomic DNA Sequencing and Sequence Analysis

The extracted gDNA from *S. aureus* was sent to the UIC Research Resource Center (RRC) for Illumina whole genome sequencing. Samples were prepared according to RRC protocols. Briefly, DNA samples were extracted at a concentration of 100 ng/μL with an A_{260} to A_{280} ratio of greater than 2. The bioinformatics analyses of the generated sequence were carried out by the Center for Research Informatics (CRI) at UIC, including raw data quality control, alignment of the sequence to the reference genome (wild type *S. aureus*, NC_009641.1) the identification of mutants with SPANDx and annotation of the mutants. SPANDx relied on BWA MEM to align the individual reads to the reference genome, then utilized GATK to identify the mutants and finally employed SnpEff for mutant annotation. The CRI team then generated a summary table of detailed mutants from VCF files that identified and compared mutations between colonies sequenced with special attention to the difference between wild type and mutant sequence. The annotated mutants were used to identify the genes involved. Each of the gene carrying the appropriate mutants was translated into amino-acid sequence and was aligned to the wild type amino-acid sequence to identify mutated residues. With the mutated gene of two

colonies identified, the other colonies were subjected to PCR amplification of the same gene. The PCR products of these colonies were sequenced and analyzed for amino-acid residue mutation. This was a cheaper and more efficient method than a gDNA sequencing of each resistant colony.

2.2.8. Mutated Gene Product Identification and Knockout

With the gene annotation, we searched the gene product (corresponding protein) in the National Center for Biotechnology Information web site. The gene, here referred to as "Gene A", was subjected to knockout by transposon insertion. Gene A was searched and identified in the Nebraska transposon library of *S. aureus* USA300. The transposon, a 3000 base pair DNA fragment including an erythromycin resistant gene, was inserted within the first third portion of Gene A. This *S. aureus* USA300 "Gene A knockout" strain (from Dr. T. Bae at the Indiana University School of Medicine- Northwest) was used to prepare the *S. aureus* Newman Gene A knockout strain (Figure 2.1), following published method (McNamara *et al.*, 2008).

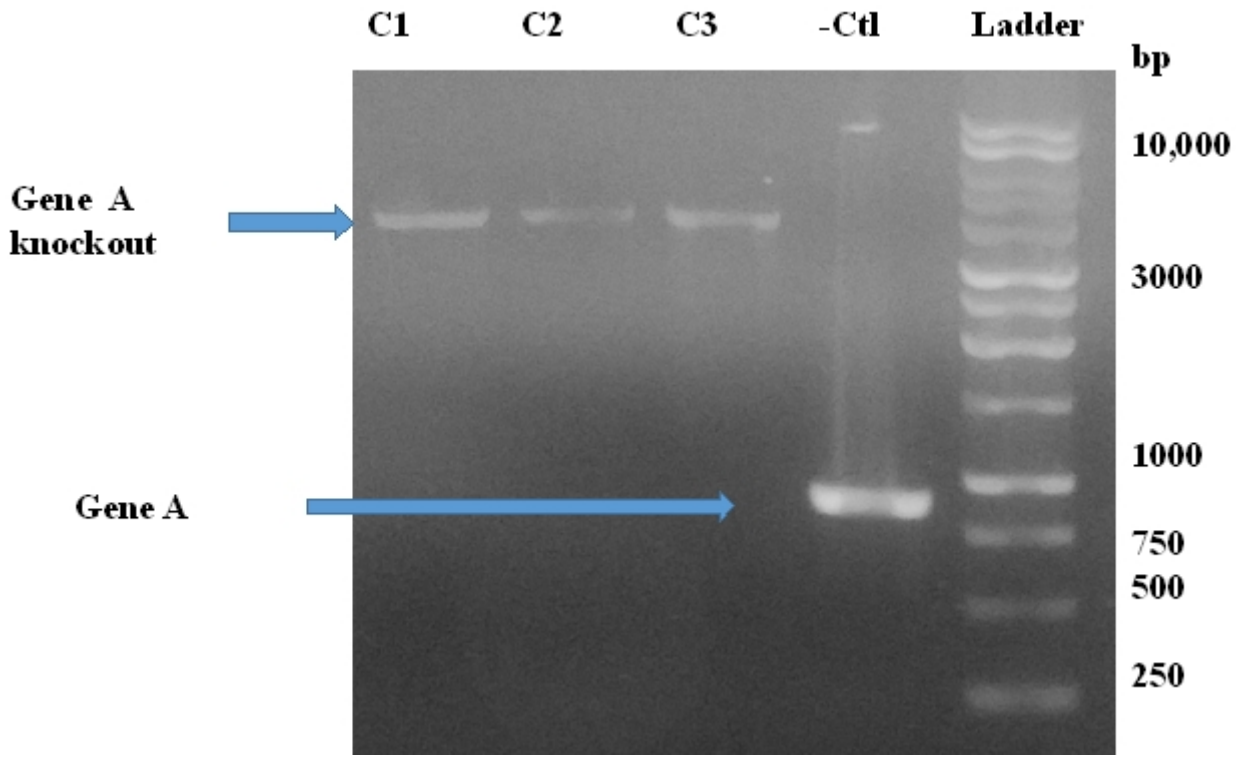

Figure 2.1: USA300 (Transposon donor) DNA gel screening for contaminants screening. Genomic DNA was extracted from the *S. aureus* USA300 strain, and the primers for Gene A amplification was used to amplify the transposon inserted gene. The size of the amplified fragment was used to identify the clones containing the transposon in Gene A. A size of 800 base pairs was expected for Gene A and that of 4,000 base pairs was expected for transposon inserted Gene A. C1, C2 and C3 are the single colonies, - Ctl is the negative control, and it represents the size of Gene A in *S. aureus* Newman before the transposon insertion. The Ladder is a 1 Kb ladder and has DNA fragment sizes going from the molecular size of 250 to 10,000 base pairs.

2.2.8.1. Phage 85 Stock Preparation

Phage 85 (Φ85, from Dr. Hyunwoo Lee lab, UIC) was used to transfer the Gene A knockout from *S. aureus* USA300 to *S. aureus* Newman. Since the sample of Φ85 was frozen for more than one year, it was revived by preparing an overnight culture (2 mL) of *S. aureus* Newman in BHI. This overnight culture (50 µL) was diluted 100-fold with fresh BHI containing 5 mM $CaCl_2$ and incubated with shaking at 37 ºC for 2.5 h. The culture was then split in two. To one, the phage stock solution (1 volume) was added to 1,000 cell culture volume. Both tubes were incubated overnight. The phage in the medium was extracted by centrifugation and filtering the supernatant through a 0.45 µm filter.

2.2.8.2. Transducing Phage Preparation

A transducing phage preparation was started by making an overnight culture of *S. aureus* USA300 cells with 10 µg/mL erythromycin. The *S. aureus* USA300 overnight culture was diluted 1:100 with fresh BHI (5 mL) containing 10 µg/mL erythromycin and 5 mM $CaCl_2$ to activate the phage and incubated at 37 ºC with shaking for 2.5 h to an OD_{600} of 0.6. Freshly prepared phage solution at various volumes (0, 5, 10, 25, 50 and 100 uL) were added into *S. aureus* USA300 culture aliquots (1 mL) and incubated overnight at 37 ºC. The sample(s) with sufficient Φ85 to give ~ 30 colonies was/were used to extract the transducing phage.

2.2.8.3 Phage Transduction

Overnight culture of *S. aureus* Newman (1 mL) in BHI containing 5 mM $CaCl_2$, and 5 µg/mL nalidixic acid (a quinolone antibiotic for Newman selection) was prepared. Agar plates were made with sodium citrate (to de-activate the phage) to select colonies. The colonies selected were then plated on a plate without both $CaCl_2$ and sodium citrate to obtain clean colonies.

Following this step, fresh BHI (20 mL) was used to dilute the overnight culture of *S. aureus* Newman (1 mL) and incubated for 1 h at 37 ºC with shaking. An aliquot (1 mL) of *S. aureus* Newman cells were pipetted into a fresh sterile Eppendorf micro-centrifuge tube and 0, 10, 50 and 100 µL of transducing phage solution was added. The diluted culture was incubated for 30 m at 37 ºC with shaking, and the cells were spun down with a table top centrifuge at room temperature for 30 s at the top speed. The supernatant was decanted, and the cell pellets were washed with 1 mL of ice-cold 40 mM sodium citrate solution, and spun down for 30 s. The washed cells were suspended in 100 µL of 40 mM sodium citrate solution and plated on tryptic-soy-agar plates with sodium citrate (40 mM) and erythromycin (10 mM). These plates were incubated at 37 ºC for 2 days, and 2-4 colonies were streaked on plates with erythromycin (10 mM) but without sodium citrate.

2.2.8.4. Verification of *S. aureus* Newman Gene A Knockout

The gDNA of Gene A knockout *S. aureus* Newman cells was extracted as previously described in "Genomic DNA Extraction". Primers specific to the inserted transposon and a pair of primers specific to Gene A were used to amplify the DNA fragment of Gene A containing the transposon by PCR. The amount of PCR product generated and the size of the amplified fragment were used to identify colonies with and without the transposon in Gene A (Figure 2.2).

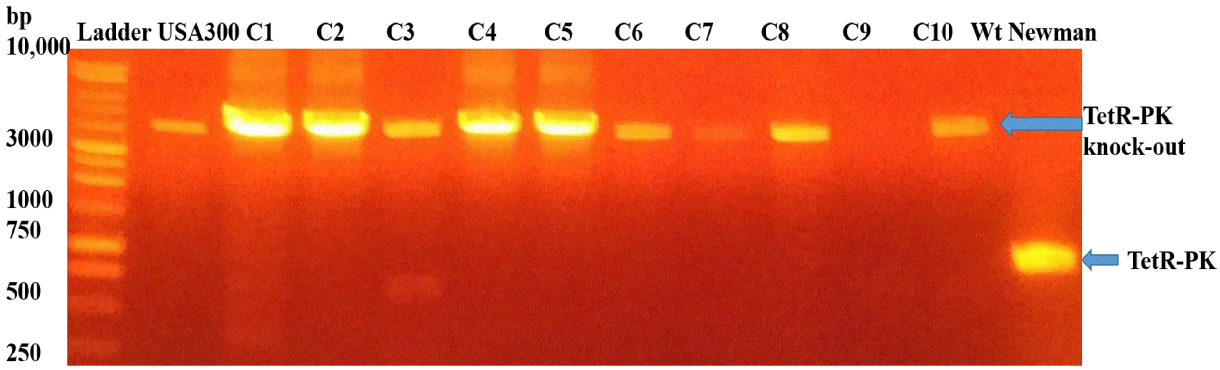

Figure 2.2: Colonies screening for *S. aureus* Newman positive clones. *S. aureus* Newman WT is erythromycin sensitive and the transposon carries an erythromycin resistant gene. Erythromycin was used to select for clones containing the transposon and PCR was used to ensure that the selected clones had the transposon in Gene A. C1 to C10 denote the colony number that the fragment was amplified from. The expected band size for the wild type Gene A is 800 bps and that of the transposon (Gene A knockout) inserted is 4,000 bps. Colonies without fragment around 4,000 bps were considered to be contaminants.

2.2.9. Protein Structural Speculation

The amino-acid sequence of unknown gene was submitted to the I-TASSER program (https://zhanglab.ccmb.med.umich.edu/I-TASSER), which identifies the top 10 templates in the Protein Data Bank (PDB), and predicts the most likely structure, possible location for ligand binding, enzyme commission number and the molecular function.

2.3. Results

2.3.1. Cell Growth

The cell growth was found to be not affected by DMSO, up to 2%, in the growth medium. About 3 h were needed for *S. aureus* Newman cells and 3.5 h for *B. anthracis* ΔANR cells to reach an OD_{600} of 1. For 1 mL of *S. aureus* Newman cells with OD600 of 1 correspond to 1.5 x 10^9 cfu and for *B. anthracis* ΔANR cell culture, 3.6 x 10^7 cells.

2.3.2. MIC of LC2 and LC5 on Wild Type *S. aureus* Strains

For the wild types of *S. aureus* Newman cells, the MIC of LC2 ranged from 0.0.20-0.80 μg/mL (n = 5), and that of LC5 was 0.31 (n = 6) μg/mL.

The MIC values was 0.25 g/mL for ciprofloxacin, 0.03 g/mL for tetracycline, 4.00 g/mL for chloramphenicol, 0.25 g/mL for erythromycin, 0.03 g/mL for triclosan, and 0.13 g/mL for ampicillin on *S. aureus* Newman wild type strain.

2.3.3 MIC of Other Compounds on Wild Type *B. anthracis*, *E. coli* TolC$^-$ and *S. aureus*

Other 1, 3, 4 oxadiazole compounds with substituents different than that found in LC2 and LC5, and were not tested for PurE inhibition were found to have MIC values ranging from 0.07 μg/mL to 1.1 μg/mL against the 3 bacterial strains tested (TABLE II). Under the same

conditions tested, some of these MIC values were comparable or lower than the MIC of ciprofloxacin and linezolid.

TABLE II: MIC OF 1, 3, 4 OXADIAZOLE BIO-ACTIVE SMALL MOLECULES ON *S. AUREUS* NEWMAN, *B. ANTHRACIS* (ΔANR) AND *E. COLI* (TOLC$^-$). THIS COMPOUNDS WERE OBTAINED FROM THE LIFE CHEMICAL LIBRARY AND ARE ANALOGOUS TO LC2 AND LC5, HAVE SIMILAR CORE, BUT DIFFERENT SUBSTITUENTS. THE MIC ARE DETERMINED AS DESCRIBED IN METHOD AND WAS RECORDED IN MM, THEN CONVERTED TO MG/ML.

Compound ID	MIC on *S. aureus* Newman (μg/mL)	MIC on *B. anthracis* ΔANR (μg/mL)	MIC on *E. coli* TolC$^-$ (μg/mL)
F2518-0474	0.07	0.07	0.26
F2518-0504	0.14	1.10	2.30
F2518-0085	0.26	1.10	1.10
F2518-0481	0.28	0.28	0.28
F2518-0445	0.49	0.25	0.49
F2518-0447	0.29	1.10	1.10
F2518-0477	0.07	0.07	0.14
F2518-0039	0.14	0.07	0.28
F2518-0183	0.12	0.12	0.12
Ciprofloxacin	0.25	0.3	0.3
Linezolid	1.00	0.8	4.0

2.3.4. Resistant Mutant Colonies Selection

Application of 10^9 cfu of *B. anthracis* ΔANR to plates containing LC2 or LC5 compound with concentrations at 0.5 MIC-WT and 2 MIC-WT yielded a lawn of colonies, and with concentration at 3 MIC-WT yield no colony after 18 h incubation. Repeated attempt to select resistant colonies from ΔANR was unsuccessful.

For wild type *S. aureus* Newman cells, 1 colony was found on the plate with 40 MIC-WT (20 μg/mL) LC2 (Colony-LC2-1), 1 colony with 25 MIC-WT (12.5 μg/mL) LC2 (Colony-LC2-2), and 13 colonies with 20 MIC-WT (10 μg/mL) (Colony-LC2-3 to Colony-LC2-15).

For LC5 compound, 2 colonies (Colony-LC5-1) and (Colony-LC5-2) were obtained on plate with 10 MIC-WT (3 μg/mL) and 1 colony (Colony-LC5-3) with 5 MIC-WT (1.5 μg/mL) (TABLE III).

TABLE III: NUMBER OF RESISTANT COLONIES SELECTED AS A FUNCTION OF COMPOUNDS CONCENTRATION. 40 MIC-WT MEANS 40 TIME THE MIC OF THE WILD TYPE *S. AUREUS* NEWMAN. THE MIC OF LC2 ON *S. AUREUS* NEWMAN WT RANGED FROM 0.20-0.80 (N = 5) MG/ML FOR LC2 AND 0.31 (N = 6) FOR LC5. ALL RESISTANT COLONIES WERE SELECTED ON AGAR PLATE.

		Compound Concentration	Colonies
S. aureus Newman WT	LC2	40 MIC-WT (20 μg/mL)	1
		25 MIC-WT (12.5 μg/mL)	1
		20 MIC-WT (10 μg/mL	13
	LC5	10 MIC-WT (3 μg/mL	2
		5 MIC-WT (1.5 μg/mL	1
TetR-PK knockout	LC2	10 MIC-WT (5 μg/mL)	2
		5 MIC-WT (2.5 μg/mL)	1
	LC5	2 MIC-WT (1 μg/mL)	1
		1 MIC-WT (0.5 μg/mL)	3

2.3.5. Whole Genome Sequencing of Resistant Cells

Whole genome sequencing result of the resistant Colony-**LC2**-1 showed a DNA mutation of ***a*** to ***g*** at position 2,501,537 of the *S. aureus* Newman (NC_009641.1) genome. This nucleotide belong to a protein-coding gene (position 2,501,066 to 2,501,689), which translates to a 207- residue hypothetical protein in the tetracycline transcription repressor (TetR) protein family, with a locus tag NWMN_2277 or a protein ID: WP_000656771.1 (GenBank accession number BAB43467). The nucleotide mutation ***a*472*g*** was translated to a ***T158A*** mutation in the protein (we will refer to this protein as TetR-PK). The PCR amplification in the TetR-PK region for Colony-LC2-2 and for Colony-LC2-3 of the TetR-PK gene yielded a ***g347t*** nucleotide mutation (***R116L*** mutation in the protein) (Figure 2.3).

Interestingly, the whole genome sequencing result of the resistant Colony-**LC5**-1 showed a single nucleotide substitution (***a*** to ***t***) at position 2,501,247, of the same gene (TetR-PK). The ***a182t*** mutation in that gene translated to ***E61V*** mutation in the protein. The PCR amplification for TetR-PK in colony-LC5-2 yielded a ***g361a*** nucleotide mutation (***E121K***) (TABLE IV).

```
TetR-PK-WT  MKEDRRIRKTKSSIKQAFTKLLQEKDLEKITIRDITTRADINRGTFYLHYEDKYMLLADM 60
E61V        MKEDRRIRKTKSSIKQAFTKLLQEKDLEKITIRDITTRADINRGTFYLHYEDKYMLLADM 60
R116L       MKEDRRIRKTKSSIKQAFTKLLQEKDLEKITIRDITTRADINRGTFYLHYEDKYMLLADM 60
E121K       MKEDRRIRKTKSSIKQAFTKLLQEKDLEKITIRDITTRADINRGTFYLHYEDKYMLLADM 60
T158A       MKEDRRIRKTKSSIKQAFTKLLQEKDLEKITIRDITTRADINRGTFYLHYEDKYMLLADM 60
            ************************************************************

TetRWt      EDEYISELTTYTQFDLLRGSSIEDIANTFVNNILKNIFQHIHDNLEFYHTILQLERTSQL 120
E61V        VDEYISELTTYTQFDLLRGSSIEDIANTFVNNILKNIFQHIHDNLEFYHTILQLERTSQL 120
R116L       EDEYISELTTYTQFDLLRGSSIEDIANTFVNNILKNIFQHIHDNLEFYHTILQLELTSQL 120
E121K       EDEYISELTTYTQFDLLRGSSIEDIANTFVNNILKNIFQHIHDNLEFYHTILQLERTSQL 120
T158A       EDEYISELTTYTQFDLLRGSSIEDIANTFVNNILKNIFQHIHDNLEFYHTILQLERTSQL 120
             ********************************************************* ****

TetR-PK-WT  ELKINEHIKNNMQRYISINHSIGGVPEMYFYSYVSGATISIIKYWVMDKQPISVDELAKH 180
E61V        ELKINEHIKNNMQRYISINHSIGGVPEMYFYSYVSGATISIIKYWVMDKQPISVDELAKH 180
R116L       ELKINEHIKNNMQRYISINHSIGGVPEMYFYSYVSGATISIIKYWVMDKQPISVDELAKH 180
E121K       KLKINEHIKNNMQRYISINHSIGGVPEMYFYSYVSGATISIIKYWVMDKQPISVDELAKH 180
T158A       ELKINEHIKNNMQRYISINHSIGGVPEMYFYSYVSGAAISIIKYWVMDKQPISVDELAKH 180
            :**********************************:**********************

TetR-PK-WT  VHNIIFNGPLRIMAENRLHKSNLDSLT 207
E61V        VHNIIFNGPLRIMAENRLHKSNLDSLT 207
R116L       VHNIIFNGPLRIMAENRLHKSNLDSLT 207
E121K       VHNIIFNGPLRIMAENRLHKSNLDSLT 207
T158A       VHNIIFNGPLRIMAENRLHKSNLDSLT 207
            ***************************
```

Figure 2.3: Multiple sequence alignment of wild type TetR-PK using CLUSTAL Omega. The TetR-PK of each resistant strain was amplified by PCR, Sanger sequenced, and each revealed a point mutation in the same gene. Highlighted area denote a position where a residue substitution was observed. TetR-PK-WT is describing the *S. aureus* Newman containing the wild type gene of TetR-WT. E61V, R116L, E121K and T158A are in reference to TetR-PK with the respective mutations in the gene.

TABLE IV: MIC OF COMPOUNDS AND ANTIBIOTICS ON VARIOUS S. AUREUS NEWMAN STRAINS. LC2 AND LC5 ARE THE COMPOUNDS TESTED IN THIS STUDY. WILD TYPE IS REFERRING TO THE *S. AUREUS* NEWMAN STRAIN. ΔTETR-PK DESCRIBES THE *S. AUREUS* NEWMAN WITH RESISTANT MUTATIONS IN THE TETR-PK GENE. TETR-PK KNOCKOUT IS THE *S. AUREUS* NEWMAN WITH A TRANSPOSON INSERTED IN THE TETR-PK GENE AND "Δ INTERGENIC REGION" IS THE *S. AUREUS* NEWMAN STRAIN WITH THE TRANSPOSON IN THE TETR-PK GENE AND A NUCLEOTIDE INSERTION IN THE DNA FRAGMENT BETWEEN THE TWO GENES TETR-PK AND YHGE.

		MIC (μg/mL)							
Compounds / Strains		LC2	LC5	Amp[g]	Chlo[g]	Cipro[g]	Erm[g]	Tcl[g]	Tetra[g]
Wild Type - Literature		0.78[a]	0.29[a]	0.5 - 2.0[b]		0.12 - 0.5[b]			
Wild Type - This Work		0.2-0.8 (n=5)	0.31 (n=6)	0.13 (n=2)	4.00 (n=3)	0.25 (n=2)	0.25 (n=2)	0.03 (n=2)	0.03 (n=6)
ΔTetR-PK	E61V[c]	25 (n=6)	1.25[f] (n=4)	0.50[f] (n=2)	8.00[f] (n=3)	0.50[f] (n=2)	0.25[f] (n=2)	0.03[f] (n=2)	0.03-0.13 (n=6)
	R116L[d]	37.5 (n=4)							
	E121K[c]	25 (n=4)							
	T158A[d]	100 (n=2)							
TetR-PK knockout		0.20 (n=3)	0.31 (n=2)	8.00 (n=2)	8.00 (n=3)	64.00 (n=2)	64.00 (n=2)	0.03 (n=2)	0.03-0.13 (n=6)
Intergenic Region		50.00 (n=3)	1.25 (n=2)	8.00 (n=2)	8.00 (n=3)	64.00 (n=2)	64.00 (n=2)	0.03 (n=2)	0.03-0.13 (n=6)

[a]Kim, A., Wolf, N.M., Zhu, T., Johnson, E.M., Deng, J., Cook, L.J., Fung, W.-M. L. (2015) Bioorganic and Medicinal Chemistry 23, 1492.

[b]The range was due to values obtained from different strains of *S. aureus*

[c]Mutation generated with LC5 compound

[d]Mutation generated with LC2

[e]The n values for the average and standard deviation values presented were 2 - 6.

[f]The MIC for all four ΔTetR-PK mutants were the same.

[g]Antibiotic abbreviations used are Amp = Ampicillin, Chlo = Chloramphenicol, Cipro = Ciprofloxation, Erm = Erythromycin, Tcl = Triclosan and Tetra = Tetracycline see text for the different *S. aureus* Newman strains.

2.3.6. MIC Determination on Knockout and Knockout Resistant Strains

The knockout cell growth on agar plates yielded yellow and white colonies. The white colonies were contaminants and the yellow colonies had the transposon insertion (Figure 2.4). The MIC of the LC2 on the knockout colonies was 0.20 μg/mL and that for LC5 was 0.31 μg/mL. These values were similar to those obtained for wild-type (Figure 2.5; TABLE IV) suggesting that the knockout of TetR family protein had no effect on the MIC values, or there was little effect of LC2 and LC5 on *S. aureus* knockout cells. The MIC of ciprofloxacin on the knock out colonies was increased to 64 μg/mL, and ampicillin rose to 8 μg/mL. Since the knockout colonies contained erythromycin resistant gene in the transposon region, the MIC for erythromycin was increased to 64 μg/mL.

The whole genome sequence of the knockout resistant colony showed a single adenine ***"a"*** insertion at position 2,500,968, or 98 nucleotides upstream of the TetR-PK gene. The intergenic region is located at positions 2,500,806-2,500,967 (162 base pairs) between NWMN_2276 a hypothetical protein (YhgE) and NWMN_2277 (TetR-PK) genes. The gene product of YhgE, a counterclockwise gene, is an unknown protein (Figure 2.6). A mutation in the intergenic region between TetR-PK and YhgE may impact both genes. However, at this time, the function of this region is not clear.

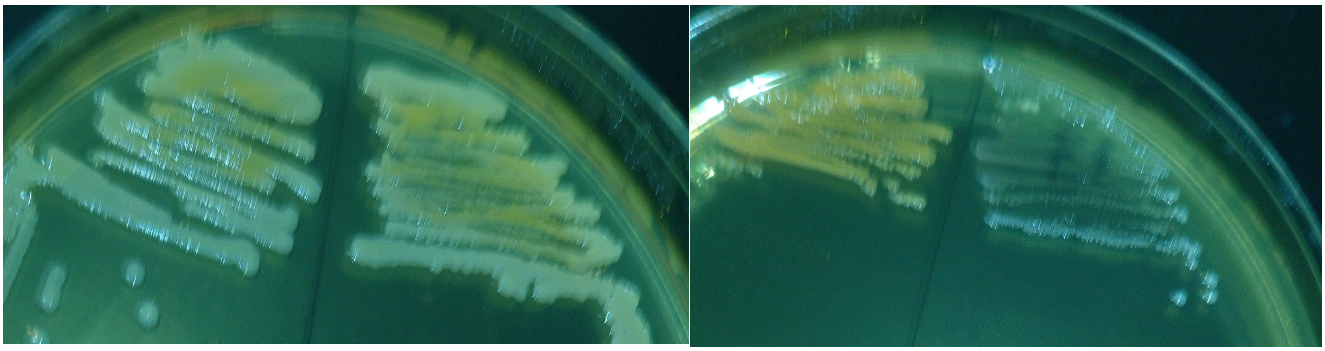

A B

Figure 2.4: Visual image of white and yellow colonies derived from TetR-PK knockout. A): White colonies were separated from the yellow colonies by both re-streaking and confirming by PCR amplification of the transposon-inserted fragment by using transposon specific primer along with TetR-PK primer. B): Some colonies were only made of contaminants.

		µg/mL											
LC2	*Sa* Newman WT	0	0.1	0.2	0.4	0.8	1.6	3.1	6.3	12.5	25	50	100
	T158A	0	0.1	0.2	0.4	0.8	1.6	3.1	6.3	12.5	25	50	100
	E61V	0	0.1	0.2	0.4	0.8	1.6	3.1	6.3	12.5	25	50	100
	E121K	0	0.1	0.2	0.4	0.8	1.6	3.1	6.3	12.5	25	50	100
	R116L	0	0.1	0.2	0.4	0.8	1.6	3.1	6.3	12.5	25	50	100
	TetR-PK knock out	0	0.1	0.2	0.4	0.8	1.6	3.1	6.3	12.5	25	50	100
	Δ Intergenic Region	0	0.1	0.2	0.4	0.8	1.6	3.1	6.3	12.5	25	50	100
LC5	*Sa* Newman WT	0	0.01	0.02	0.04	0.1	0.2	0.3	0.6	1.25	2.5	5	10
	T158A	0	0.01	0.02	0.04	0.1	0.2	0.3	0.6	1.25	2.5	5	10
	E61V	0	0.01	0.02	0.04	0.1	0.2	0.3	0.6	1.25	2.5	5	10
	E121K	0	0.01	0.02	0.04	0.1	0.2	0.3	0.6	1.25	2.5	5	10
	R116L	0	0.01	0.02	0.04	0.1	0.2	0.3	0.6	1.25	2.5	5	10
	TetR-PK knock out	0	0.01	0.02	0.04	0.1	0.2	0.3	0.6	1.25	2.5	5	10
	Δ Intergenic Region	0	0.01	0.02	0.04	0.1	0.2	0.3	0.6	1.25	2.5	5	10
				Growth	No growth								

Figure 2.5: MIC display of LC2 and LC5 on the different strains of *S. aureus* Newman generated. The values shown in the table are that of the compounds concentration in µg/mL dispensed in the 96 well plate. T158A, E61V, E121K and R116L are mutations generated in the TetR-PK gene. "TetR-PK knockout" denote a *S. aureus* Newman with 3 kilo bases inserted in the wild type TetR-PK gene. "Δ Intergenic Region" describes a new resistant strain with a base pair inserted in the intergenic region between the divergent adjacent (YhgE) gene and TetR-PK which is the precedent strain described.

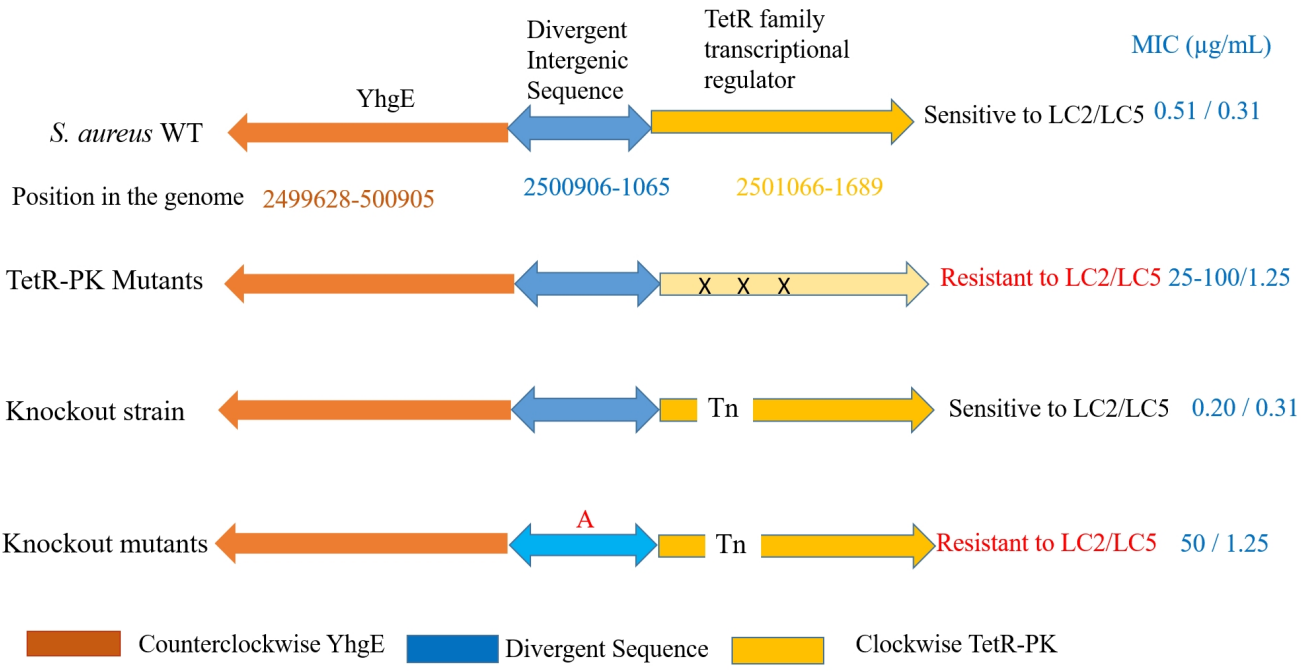

Figure 2.6: Display of gene orientation in the altered region following exposure of sensitive stains to higher than MIC concentration of compounds. The TetR family transcriptional regulator gene displayed a single point mutation in all the strains that was resistant to the compounds. The TetR-PK knockout strains were sensitive to the compounds while the resistant knockout strains have and adenine nucleotide insertion in the intergenic region of the adjacent and divergent genes (YhgE/TetR-PK).

The MIC for resistant mutant colonies of the knockout *S. aureus* cells was found to be 50 μg/mL for LC2 and 1.25 μg/mL for LC5 (Figure 2.5; TABLE IV). The MIC for ciprofloxacin was increased to 64 μg/mL (256-fold over the wild-type), for ampicillin was 8 μg/mL (60-fold increase), for tetracycline was 0.25 μg/mL (8-fold increase), for chloramphenicol was 8.0 μg/mL (2-fold increase) and for triclosan was 0.03 μg/mL (no change) (TABLE IV).

2.3.7. Summary of Results

In summary, the native *S. aureus* Newman was found to be sensitive to LC2 and LC5 with a MIC of 0.20-0.80 μg/mL (n=5) for LC2 and that of 0.31 μg/mL for LC5 (n=6). The knockout strains became slightly more sensitive to LC2 and the MIC did not change for LC5. Resistant colonies generated from the knockout strains had a MIC increase to 50 μg/mL for LC2 and 1.25 μg/mL for LC5 (TABLE V).

2.3.8. Structural Prediction of TetR-PK and YhgE

The knockout resistant colonies showed a single nucleotide insertion in the divergent intergenic region between TetR-PK and YhgE. Since neither of their function is clear, we used structural prediction to get some insights into the structural and functional insight. The unknown protein (YhgE) was predicted to be an all helical bundle possibly spanning the cellular membrane. The probability of prediction that are almost certain have a value of one. The probability of the location of the different residues as all close to one in this case. Roughly one half of the residues in the protein reside outside of the membrane while the other half is in between the two layers of the membrane with only a few residues in the inner membrane (Figure 2.7 A, B, C). The single chain representation of TetR-PK is also shown to be an all helical protein (Figure 2.7 D). YhgE

was labeled as a membrane phage infusion protein (PIP) of unknown function which is in line with the prediction.

TABLE V: SUMMARY OF RESULTS. A): MIC OF LC2, LC5, AMP, CIPRO AND ERM ON WILD TYPE AND TETR-PK KNOCKOUT *S. AUREUS*. THE MIC DID NOT INCREASE IN THE TETR-PK KNOCKOUT WHICH WAS NOT EXPECTED. WORKING HYPOTHESIS: WHEN THE TETR-PK GENE IS KNOCKOUT, ANOTHER REGULATOR BECOMES ACTIVE. B): SECOND ROUND OF SELECTING RESISTANT COLONIES IN THE KNOCKOUT CELLS. C): WHOLE GENOME SEQUENCING FOR MUTATION(S). GENOMIC ANALYSIS: "A" INSERTION AT GENOMIC LOCATION 2,500,968.

A

	MIC (μg/mL)				
Strains /Compounds	LC2	LC5	Amp	Cipro	Erm
S. aureus wild type	0.20-0.80 (n=5)	0.31 (n=6)	0.13 (n=2)	0.25 (n= 2)	0.25 (n= 2)
TetR-PK knockout	0.20 (n=3)	1.25 (n= 2)	8.00 (n=2)	64.00 (n= 2)	64.00 (n=2)

B

Strains	Compounds	Compounds concentration	Colonies
Resistant *S. aureus* with TetR-PK Knocked out	LC2	10 MIC-WT (5 μg/mL)	2
		5 MIC-WT (2.5 μg/mL)	1
	LC5	2 MIC-WT (1 μg/mL)	1
		1 MIC-WT (0.5 μg/mL)	3

C

		MIC (μg/mL)			
Strains /Compounds	LC2	LC5	Amp[a]	Cipro[b]	Erm[c]
Resistant Knockout	50.00 (n=3)	1.25 (n=2)	8.00 (n=20	64.00 (n=2)	64.00 (n=2)

[a]Amp: Ampicillin

[b]Cipro: Ciprofloxacin

[c]Erm: Erythromycin

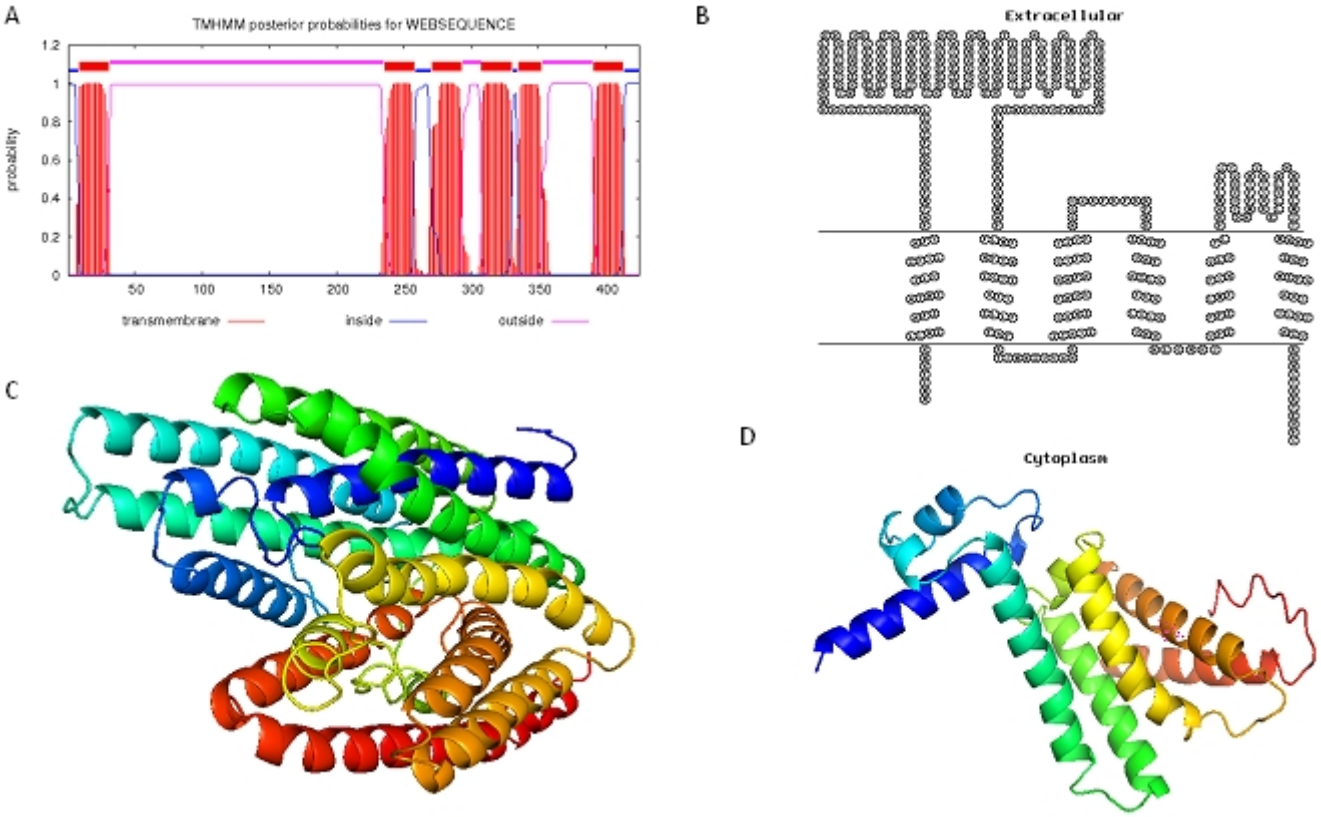

Figure 2.7: Predicted membrane topology of YhgE and structural prediction of unknown proteins. A): Trans-membrane prediction of the probability of YhgE being a membrane protein. B): Step by step display of extracellular residues, residues between the membranes and residues inside the membrane. C): Structural prediction using I-TASSER from https://zhanglab.ccmb.med.umich.edu/I-TASSER. YhgE shows an all alpha helical bundle with high similarity to membrane protein. D): The structural prediction of TetR-PK using QUARK and I-TASSER.

2.4. Discussion

As shown in the previous publication by members of the Fung group (Kim *et al.*, 2015), the MIC values of LC2 and LC5 and known antibiotics (ciprofloxacin and linezolid) on *S. aureus* Newman, *B. anthracis* ΔANR and *E. coli* TolC^{-} show that these compounds (LC2 and LC5) exhibit comparable or even better MIC than the known antibiotics. The MIC for LC2 was as low as 0.51 μg/mL and for LC5, 0.31 μg/mL on the same strains. In this study, with the generation of *S. aureus* cells resistant to LC2 and LC5, we found four mutations rendering *S. aureus* resistant to both LC2 and LC5 compounds. All mutations were shown to be on the same gene, expressed as a hypothetical protein, TetR-PK. Some of the mutations in the resistant colonies were identified by PCR method. These colonies might have other mutations in their genome, however, the results show that all the resistant colonies have a mutation in the TetR-PK gene. The MIC values for LC2 were much higher in cells with mutations generated from both LC2 and LC5 (25 -100 μg/mL). A four-fold increase in MIC values was seen for LC5 in cells with mutations in the TetR-PK gene (all 1.25 μg/mL). It was interesting to find lower MIC values for the TetR-PK knockout for LC2. The cells became sensitive again to LC2 (MIC of 0.20 μg/mL) and to LC5 (MIC of 0.31 μg/mL), values very similar to those in the wild-type. The MIC values were increased to 50 μg/mL when the intergenic region was mutated. We propose the following working hypothesis. The LC2 and LC5 do not inhibit TetR-PK directly, but inhibited a gene (Gene X) product (Protein X) regulated by TetR-PK. When either TetR-PK or the intergenic region are mutated, Protein X concentration is increased and requires more LC2 or LC5 to inhibit Protein X. However, when TetR-PK was knockout, another regulation system

kicks in to regulate Protein X and thus returning the MIC values to those of the wild-type. This working hypothesis needs to be proven in the future.

It is also interesting to find that the MIC values for ciprofloxacin for colonies with TetR-PK knockout and with intergenic region mutant increased to 64 μg/mL. Ciprofloxacin is a DNA gyrase inhibitor. The increase in MIC values for erythromycin in TetR-PK knockout and intergenic region mutant were expected since we introduced erythromycin resistant gene in the transposon used to knockout TetR-PK.

The TetR-PK protein was identical to a 207-residues protein reported earlier as TetR21, and it binds to the promoter of Tet38 to repress its expression (Truong-Bolduc *et al.*, 2015). Since the open reading frame of the gene is ORF SA2165, it is named TetR21. It is obvious that we will also pursue Tet38 in the future.

2.5. Conclusion

At this stage of the project, we found that the gene region shown in Figure 2.6 (YhgE, intergenic region and TetR-PK) was important for the action of compounds LC2 and LC5. Further work is needed to identify the mode of action for this two compounds.

Chapter Three

A Library of FabI Mutants from Triclosan-Resistant *Staphylococcus aureus* Strain

3.1. Introduction

Infections related to antibiotic resistant pathogens are increasingly becoming a public health matter (Priyadarshi *et al.,* 2009; Freire-Moran *et al.*, 2011). Triclosan is a common and effective antimicrobial agent used to eradicate pathogens such as *Staphylococcus aureus* (*S. aureus*) in general and particularly methicillin-resistant *Staphylococcus aureus* (MRSA). Since triclosan is shown to target the enzyme enoyl acyl carrier protein reductase (FabI), some mutations in the FabI gene, identified through clinical isolates or through laboratory directed evolution, render the pathogens resistant to triclosan. About ten resistant mutants have been observed in clinical isolates or evolved in the laboratory. They are (R40Q, K41N, A95V, I193S and F204S (Xu *et al.*, 2008), D101T, A198G and F204C (Ciusa *et al.*, 2012) and Y147H, L208F (Brenwald *et al.,* 2003). All mutations but two (D101T and L208F) are found in the active site and/or at the dimer interface of FabI, as defined in a publication (Schiebel *et al.*, 2012). FabI is homodimer. The impact of mutations outside of these regions is largely unexplored. Identification of the resistant mutations in *Sa*FabI is imperative in the effort to better understand resistant strains. We used an error prone polymerase chain reaction (epPCR) method to randomly generate numerous FabI mutants to establish a mutant library. The cellular thermal shift assay and the minimum inhibitory concentration (MIC) screening were used to identify the mutations in the FabI protein that rendered triclosan resistance. We found that mutations included single/multiple insertion, deletion, and substitutions. A total of 134 colonies was generated consisting of FabI mutants and 42 of these colonies consisted of single amino-acid

mutation in FabI. Of these single substitution FabI mutants, 19 did not bind Triclosan/$NADP^+$. One of the colony consisting of FabI mutation of A33V exhibited an MIC value against Triclosan/$NADP^+$ 30-fold higher than that of the wild type FabI.

In addition to understanding the mechanism(s) leading to Triclosan resistance, this triclosan-resistant library generated in this project will serve as a checklist for clinicians to identify resistant strains in deciding a course of action. My work in this project focuses on using error prone PCR to generate mutants, and on determining the MIC of a resistant-mutant which will be described in detail below. The assays for triclosan binding to these mutants were done by a collaborating group member (Robel Demissie). The discovery of these mutations highlights the value of obtaining insights into the types of mutation that render *S. aureus* resistant to triclosan and other inhibitors binding to the FabI active site region.

3.2. Materials and Methods

3.2.1. Error Prone PCR

3.2.1.1. Primer Design

Two pairs of primers were designed with comparable length and melting temperature (Tm). One pair was used for obtaining mutated *Sa*FabI gene in the epPCR reaction, and the other pair was used for the vector linearization. Primers were designed for In-Fusion ligation (Clontech; Mountain View, California). In order to randomly introduce mutation in the *Sa*FabI gene but keep the integrity of the remaining DNA sequence in the vector, epPCR was used on the gene, and high-fidelity PCR on the vector pET-15b. The two pairs of primers were designed to have overlapping 5' ends for the subsequent ligation of the insert (*Sa*FabI gene) into the

expression vector (pET-15b; Novagen; Madison, Wisconsin). Primers were ordered from Integrated DNA Technologies (IDT; Coralville, Iowa).

3.2.1.2. Mutated *Sa*FabI Genes by Error Prone PCR

For the error prone PCR to mutate the *Sa*FabI gene, the PCR reaction was carried out using a commercially available kit (GeneMorph II, Agilent Technology, Santa Clara, California), with a few modification. The forward primer was 5'- CGG CAG CCA TAT GCT CGA GAT GTT AAA TCT TGA -3' and the reverse primer 5'- GTT AGC AGC CGG ATC CTT ATT TAA TTG CGT GG -3'. The template (*Sa*FabI gene; 100 ng or 1 µL), the forward primer and the reverse primer (125 ng or 0.5 µL each), dNTP (1 µL of 40 µM) and Mut II Polymerase (1µL; Agilent Technology) in Mut II reaction buffer were mixed with H_2O (46 µL) to give a reaction volume of 50 µL. With this mixture, error prone PCR was carried out with a thermal cycler (Eppendorf AG 22331, Hamburg, Germany) with an initial denaturation at 95 °C for 2 m, then x cycles (x to be determined below) of 95 °C for 30 s, 50 °C for 30 s, and 72 °C for 1 m followed by a final extension at 72 °C for 10 m.

To estimate the amount of error prone PCR product generated, gel electrophoresis was performed with 0.6 µL of the PCR product and increasing amounts of known concentration of *Sa*FabI-WT DNA. The PCR amount (yield) was used to determine the number of doubling and the expected mutation rate. It was found that 25 cycles were sufficient to provide the mutants needed. This PCR product is called “mega-primer” per company specification. Thus our mega-primer was the mutated *Sa*FabI gene, to be used as a primer for insertion into the vector (pET-15b).

3.2.1.3. Vector Linearization

High-fidelity amplification of the expression vector pET-15b was carried out using a forward primer 5'-CCA CGC AAT TAA ATA AGG ATC CGG CTG CTA AC -3' and a reverse primer 5'- TCA AGA TTT AAC ATC TCG AGC ATA TGG CTG CCG -3'. pET-15b (50 ng) was combined with 26 µL of pfuUltra hot start PCR master mix (Agilent Technologies), the forward primer (0.5 µL at 100 mM to give a final concentration of 1 mM); the reverse primer (0.5 µL at 100 mM), and H_2O to make a 50 µL reaction volume. pET-15b containing *Sa*FabI-WT gene was used as the starting template for the vector amplification. The primers were designed to NOT include the WT gene in the amplification and thus resulting a linear vector. The mixture was subjected to an initial denaturation at 95 °C for 5 m, followed by 40 cycles of 95 °C for 30 s, 59 °C for 30 s, and 72 °C for 6.5 m, ending with a final elongation at 72 °C for 15 m.

3.2.2. Mutated Expression Vector

The PCR product of the mutated *Sa*FabI gene generated with the epPCR method was used as the mega primer to amplify the linearized empty vector. Briefly, 3 µL of mega primer, 30 ng of linearized pET-15b along with 25 µL 2x ez-clone enzyme mix and 3 µL of ez-clone solution were assembled into a 50 µL reaction mixture. The mixture was subjected to 95°C for 2 m followed by 40 cycles of 95 °C for 50 s, 70 °C for 50 s and 68 °C for 15 m, ending with a final extension at 72 °C for 15 m. Product yield was minimal (~1 µg). Optimization might improve the yield. At the end of the reaction, 1 µL DPNI was added to the entire sample and incubated at 37 °C for 2 h to digest the methylated parent template plasmid. The expression vector consisted of ampicillin resistant gene, a lac repressor for isopropyl β-D-1-

thiogalatopyranoside (IPTG) binding and a hexa-histidine on the N-terminal end for affinity purification.

3.2.3. Expression Vector Transformation and *E. coli* Colonies Generation

DH5α Z-Competent *E. coli* cells (Zymo; Irvine, California) was used for transformation. Briefly, DPNI treated expression vector of mutated *Sa*FabI (5 µL) was added to DH5α Z-competent cells (50 µL) (Zymo) and the mixture was incubated on ice for 5 m before being plated on agar plates containing ampicillin (100 µg/mL).

3.2.4. DNA Extraction, Sequencing and Analysis

DNA was extracted using PureYield plasmid miniprep kit (Promega; Madison, Wisconsin) with a slight modification. Overnight cell culture (4 mL) was pelleted by centrifugation. The pellet was washed with H_2O to remove residual culture medium and re-suspended in H_2O for DNA extraction, according to company protocol. The DNA was then eluted with H_2O rather than the buffer provided by the company. With this modification, the DNA sample was more suitable for DNA sequencing. The DNA sample with a concentration 100 ng/µL was sent to the Research Resources Center (RRC) at the University of Illinois at Chicago (UIC) for Sanger sequencing. Sequencing results were obtained as a zip file containing the sequencing chromatogram and the nucleotide bases associated with the chromatogram. Finch TV (a free software program) was used to open, extract and align the sequenced raw data to the expected sequence and identify similarities and differences in the sequences. The sequence of a mutant FabI was aligned with that of the wild type. The sequences that displayed single nucleotide polymorphism was checked against the sequencing chromatogram to confirm the validity of the mutations.

3.2.5. Mutated Residue Characterization

Using the hydrophobicity scale developed by Zhu and coworkers (Zhu *et al*., 2016), the polarity of each of the mutated residues was examined and compared to the hydrophobicity of the original residues.

3.2.6. Construction of a Shuttle Vector pHT370 Containing *Sa*FabI-A33V

To introduce a *Sa*FabI mutant gene into *S. aureus* cells rather than *E. coli* cells, a plasmid different from that used in *E. coli* cells was prepared. *E. coli-Bacillus thuringiensis* shuttle vector pHT370 containing *Sa*FabI WT gene and it promoter in *E. coli* (a kind gift from Dr. M. Johnson lab, UIC) was used to insert the A33V mutation into the *Sa*FabI gene to be introduced into *S. aureus* RN4220 cells. The vector contained erythromycin and ampicillin resistant genes as well as *Sa*FabI-WT gene and its promoter. This vector was used as a template to generate *Sa*FabI-A33V gene. Primers containing the A33V mutation were used. Template (50 ng) was mixed with forward primer (100 ng), reverse primer (100 ng), pfuUltra hotstart PCR master mix (26 µL) (Agilent Technology) and H_2O to prepare a 50 µL reaction mixture. The mixture was incubated at 95 °C for 3 m, followed by 30 cycles of 95 °C for 30 s, 50 ºC for 30 s, and 72 °C for 15 m concluding with a final elongation at 72 °C for 15 m and a cool down to 4 °C.

The schematic diagram of the procedures is shown below.

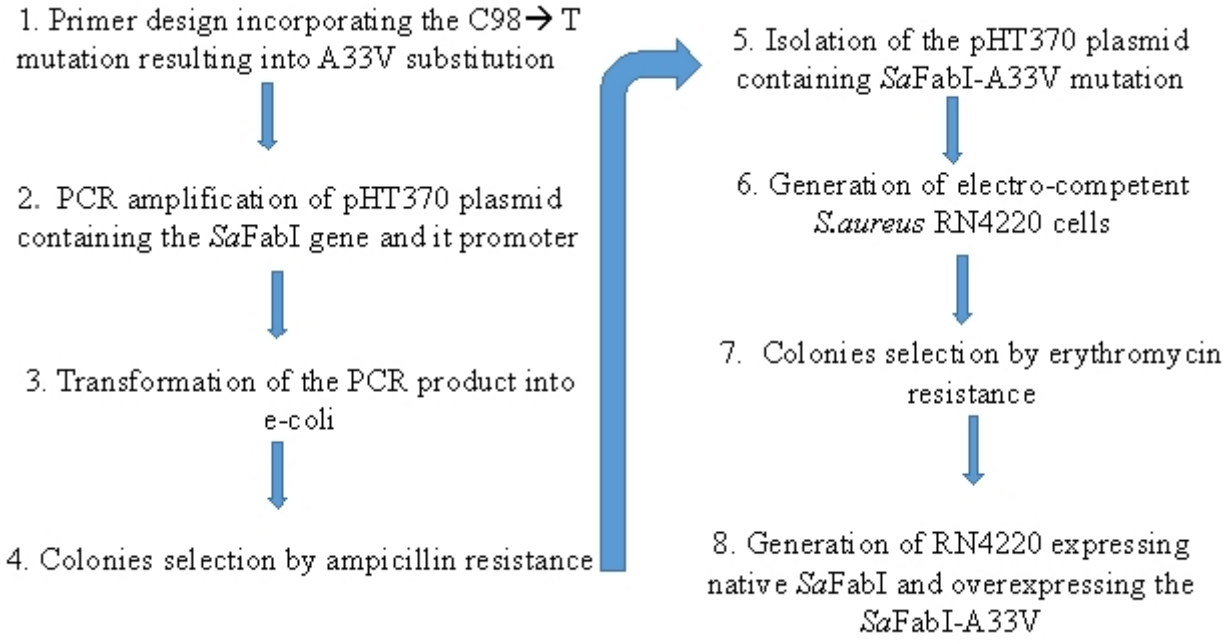

Scheme 1: Schematics of mutant generation into pHT370 plasmid, transformation into *E. coli* cells and electroporation into *S. aureus* RN4220 cells. This virtual screening protocol was used to acquire pHT370-*Sa*FabI-A33V into *S. aureus* RN4220 cells.

3.2.7. *S. aureus* RN4220 Cells with *Sa*FabI-A33V Gene

RN4220 competent cells were generated following published methods (Mistry *et al.*, 2017) with minor adjustment. Briefly, RN4220 cells were grown in BHI (5 mL) in a 250-mL flask to an OD_{600} of 2.7. The culture was diluted into pre-warmed fresh BHI medium (100 mL) to an OD_{600} of 0.3 and incubated at 37 °C for 60 m to an OD_{600} of 0.6. The culture was chilled on ice for 10 m, washed 3 times with equal volume of chilled H_2O and recovered by a centrifugation (15 m) at 3000 g. The cells were then re-suspended in 10% glycerol (10 mL) followed by another suspension in 10% glycerol (4 mL first then 1 mL), all in sterile H_2O. The cells were then suspended in sterile electroporation solution of 10% glycerol and 0.5 M sucrose in chilled sterile H_2O and centrifuged as before. The supernatant was discarded with portion of the cells to ensure complete supernatant removal. The previous step was repeated with 1 mL of the same electroporation solution, re-suspended and divided into 100 µL aliquots. The aliquots were centrifuged at 3000 g for 2 m, and then re-suspended in 50 µL of electroporation solution. DNA (5 µg or 10 µL) was then added to the *S. aureus* RN4220 competent cells for immediate electroporation. The cells should be in solution with very low salt content for the electroporation to be successful.

The *E. coli* competent cells (Stellar competent cells from Clontech, for high efficiency transformation) were thawed on ice. 5 µL of the PCR product of pHT370-*Sa*FabI-A33V was added to 50 µL of the competent cells, and incubated on ice for 5 m. The cells were then heat-shocked at 42 °C for 45 s, and on ice for 2 m before shaking at 37 °C for one hour for recovery. The resulting culture was plated on 100 µg/mL ampicillin plates, and single colonies were picked and grown in liquid LB medium for DNA extraction. DNA extraction was carried out as

previously described in section 3.2.4, sequenced, and used for the electroporation to introduce it to *S. aureus* cells.

3.2.8. Electroporation of *S. aureus* Cells

Micropulser electroporator from Bio-rad in Dr. A. Mankin lab (UIC) was used to introduce one pulse of 1.8 KV for 2.5 ms to a pre-chilled 0.2 cm cuvette containing the DNA sample mixed with the cells. 900 µL of 0.5 M sucrose in BHI was immediately added to the electroporated cells, mixed, transferred to a 15 mL Falcon tube and incubated at 37 °C for 1 h for recovery. The recovered cells were spread on a petri-dish plate containing 2 µg/mL erythromycin. Colonies that appeared before 14 h incubation were picked, and their identities were determined by testing their resistance to erythromycin, and triclosan/$NADP^+$.

3.2.9. Resistance Testing by MIC Determination

In-vivo resistance testing was determined by the MIC experiments as described in Chapter 2 section 2.2.3. MIC for erythromycin and triclosan on (1) the native *S. aureus* RN4220 with no vector, (2) RN4220 with *Sa*FabI WT vector, and (3) RN4220 with *Sa*FabI-A33V vector were determined.

3.3. Results

3.3.1. Error Prone PCR

The gel electrophoresis of the epPCR product showed a band of 800 bp, similar to that of the wild type control (Figure 3.1). Calibration curve of DNA amount vs. DNA band intensity appeared to be linear with the R^2 of the fitted data to be 0.99 (Figure 3.1). From the gel, the PCR band intensity corresponded to 53 ng. A total of 10 µg of PCR product of *Sa*FabI mutants was generated. According to the company guidelines for GeneMorph II (Agilent Technology) this

product-yield corresponded to a medium mutation frequency. With this yield, we obtained zero to six mutations per plasmid.

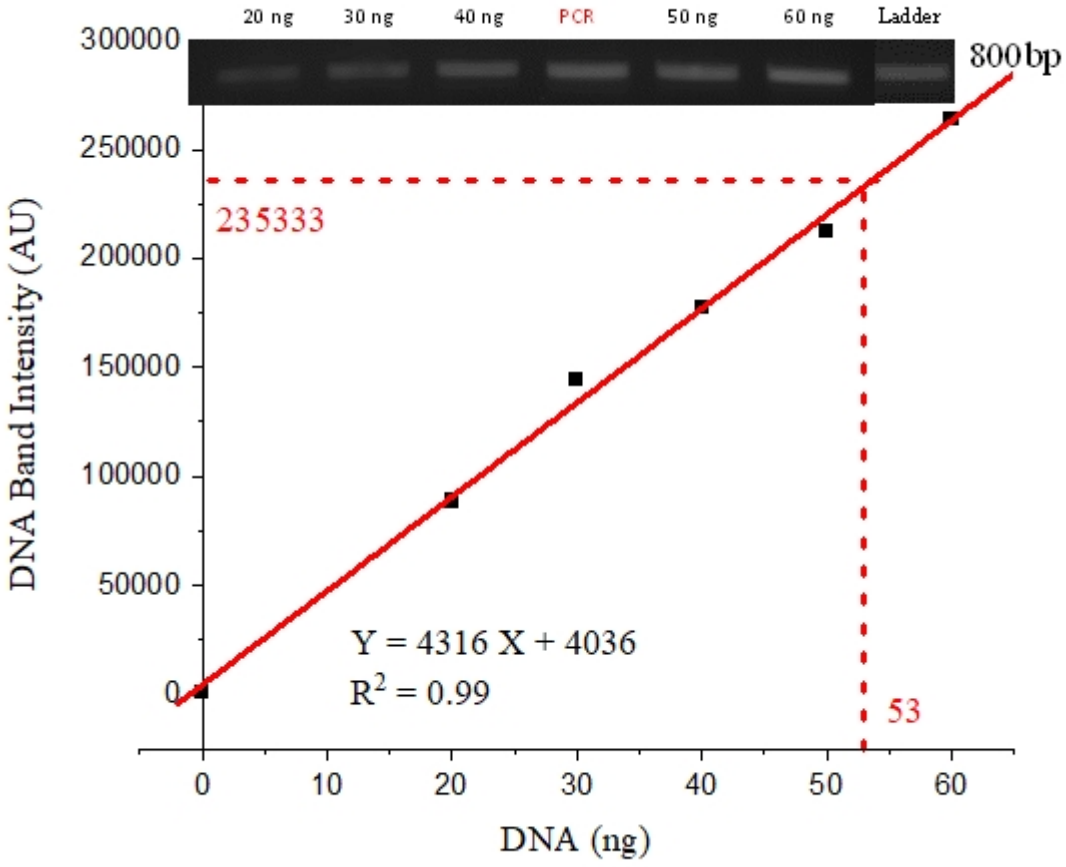

Figure 3.1: Calibration curve used to quantify the epPCR product.

The amount of a standard DNA sample was determined by its absorbance value at 260 nm (A260) to give its concentration and the sample volume. The band intensity measured the brightness of the band in arbitrary units (AU). The band intensity directly correlated with the amount of DNA with a correlation coefficient of 0.99. PCR refer to the amount of PCR product loaded into the well. The amount of PCR product was found to be 53 ng.

As indicated earlier, the PCR amplification of 25 cycles was found to be optimum for achieving a mutation frequency of one to six mutation per individual gene. The amount of initial DNA template was adjusted to 100 ng (*Sa*FabI portion), to give a product yield of 10 μg.

3.3.2. *Sa*FabI Mutant Gene Analysis

DNA sequence analysis of plasmids containing *Sa*FabI mutant samples indicated that there were 22 A to C, 91 A to T and 125 A to G changes to give a total of 238 adenine substitutions (TABLE VI). Similarly, there were 122 G, 187 T and 67 ^{o}C substitutions to give a total of 614 substitution (TABLE VI). A total of 219 colonies were analyzed. Forty two colonies consisted of single amino-acid mutation in *Sa*FabI protein (Figure 3.2), 38 colonies with double residues mutations and 27 colonies with three mutations. In addition, fourteen, eight, and five colonies with four, five and six mutations in the *Sa*FabI protein. The mutations covered 191 residue positions in FabI throughout the length of this 256-amino-acid-residue protein. Eighty four colonies consisted of silent mutations as well as frame shifts insertions and deletion and were discarded.

TABLE VI: SUMMARY OF BASE PAIR CHANGE DURING ERROR PRONE PCR (EPPCR). EACH OF THE FOUR BASES IN THE TEMPLATE GENE WAS ALTERED TO THE OTHER THREE IN THE RESULTING VARIANT GENE UPON COMPLETION OF THE EPPCR. WT DESCRIBE THE NUCLEOTIDE ORIGINALLY FOUND IN THE WILD TYPE GENE. Δ REFER TO THE NUCLEOTIDE SUBSTITUTED TO, IN THE MUTANT STRAIN. THE TOTAL IS EITHER OF BASE CHANGED OR THE TOTAL OF NEW ALTERED BASES. RED INDICATES THE INDIVIDUAL BASE SUBSTITUTION AND BLACK IS THE TOTAL CHANGES THAT OCCURRED.

WT	Δ	C	T	G	A	Total
A		22	91	125	-----	138
G		9	24	-----	89	122
T		106	-----	11	70	187
C		-----	36	9	22	67
Total		137	151	145	181	614

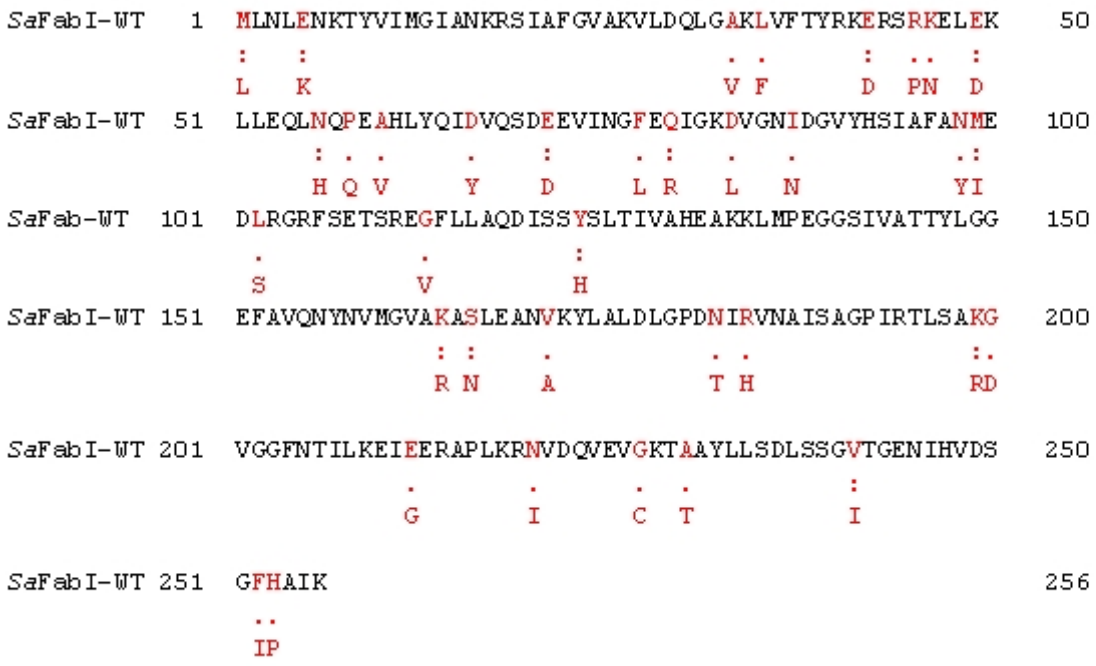

Figure 3.2: Sample representation of single mutations generated on pET-15b during the error prone PCR and mega primers ligation. Each of the point mutation was generated on a separate plasmid containing the S*a*FabI gene. "*Sa*FabI-WT" refers to the wild type sequence of the *Sa*FabI gene, and red residues denote each of the position where a single mutation was observed in a plasmid construct. The numbers indicate the nucleotide position in the wild type gene.

3.3.3. Mutants *Sa*FabI Expression Vector

A total of 326 amino-acid-residue mutations were found in one hundred and thirty four (134) pET-15b plasmids (*Sa*FabI proteins) (TABLE VII). This included 1, 2, 3, 4, 5, or 6 mutations in the FabI protein. Forty two (42) were plasmids containing single mutation in the FabI, thirty eight (38) had two mutations, twenty seven (27) had three, fourteen (14) had four mutations, eight (8) had five mutations and five (5) had six mutations. Only the 42 mutants with a single mutation in FabI were considered for triclosan binding study. These mutations were M1L, E5K, A25T, A33V, L35F, E42D, R45P, K46N, E49D, N56H, N56K, P58Q, A60V, D66V, E71D, F77L, F77S, Q79R, V84L, I87L, N98Y, M99I, L102S, T109I, E112D, G113V, Y123H, G140C, K164R, S166N, V171A, N182T, R184H, K199R, G200D, E212G, N220I, G227C, A230T, V241I, F252I and H253P.

TABLE VII: OVERVIEW OF THE AMINO-ACID SUBSTITUTED DURING THE ERROR PRONE PCR (EPPCR) REACTION. “WILD TYPE RESIDUES” REFERS TO AMINO-ACIDS FOUND IN THE WILD TYPE TEMPLATE STRAIN. “SUBSTITUTED RESIDUES” ARE THE RESIDUES FOUND IN THE *SA*FABI AFTER EPPCR. SINGLE RESIDUE MUTATIONS ARE LABEL IN GREEN. YELLOW IS THE RESIDUE WITH THE HIGHEST NUMBER OF MUTATIONS. TOTAL REFER EITHER TO THE NUMBER OF TIMES A RESIDUE WAS MUTATED OR THE NUMBER OF TIMES, IT HAS BEEN MUTATED TO, FROM THE WILD TYPE RESIDUES.

Wild Type Residues \ Substituted Residues	G	A	V	L	I	S	T	C	D	E	K	R	M	P	H	Q	N	F	Y	W	Total
G			3			6		9	13			5									36
A	4		10			4	8		1	3		1		1							32
V		6		1	6		1		6	1								1			22
L			1		8	3												8			20
I			2	1			7										4	6			20
S	5			1			2	2				4					7				21
T		4			4	2						1		1			2				14
C																					0
D	1	1	4												1		1		1		9
E	7	1	4						12		5										29
K					8		1			3		5	1			2	5				25
R	1			1		5		4						2	6						19
M				3	2		2				1										8
P				1		2										2					5
H				3										3					2		8
Q				1								4			4						9
N					9	3	3		4		3				1				1		24
F			2	2	3	7		1											3		18
Y						1			2						1		1	2			7
W																					0
Total	18	12	26	14	40	33	24	16	38	7	9	20	1	7	13	4	20	17	7	326	326

3.3.4. Mutation Characterization

Out of the 326 mutations, we found a mixture of inter-conversion between polar and non-polar substitution, polar to other polar mutations or non-polar to other non-polar alterations were observed. 36 mutations were in the active site, as defined in a publication (Schiebel *et al.*, 2012); from which 12 involved polar to non-polar or non-polar to polar change and the other 24 mutations maintained the polarity of the residues. In addition, 72 mutations involved interface residues (Schiebel *et al.*, 2012), from which 24 residues changed polarity while the other 48 maintained their polarity. The remaining mutations (152) were with the residues not in the active site or interface. Within this class of 152 mutations, 103 maintained polarity and the other 49 changed polarities. Throughout the gene, 5 of the mutations changes from charged residues to non-charge residues and vice versa.

3.3.5. MIC for *Sa*FabI-A33V

The MIC values of triclosan/$NADP^+$ toward *S. aureus* RN4220 cells with the plasmid pHT370 containing FabI-A33V gene were greater than 100 μg/mL, whereas those for the controls were 0.4 μg/mL on native RN4220 and 3.1 μg/mL on RN4220 containing pHT370-*Sa*FabI-WT (Figure 3.3).

The MIC of erythromycin was found to be 0.39 μg/mL in the native RN4220, and 64 μg/mL in both strains containing pHT370-*Sa*FabI-WT and pHT370-*Sa*FabI-A33V plasmids (Figure 3.3).

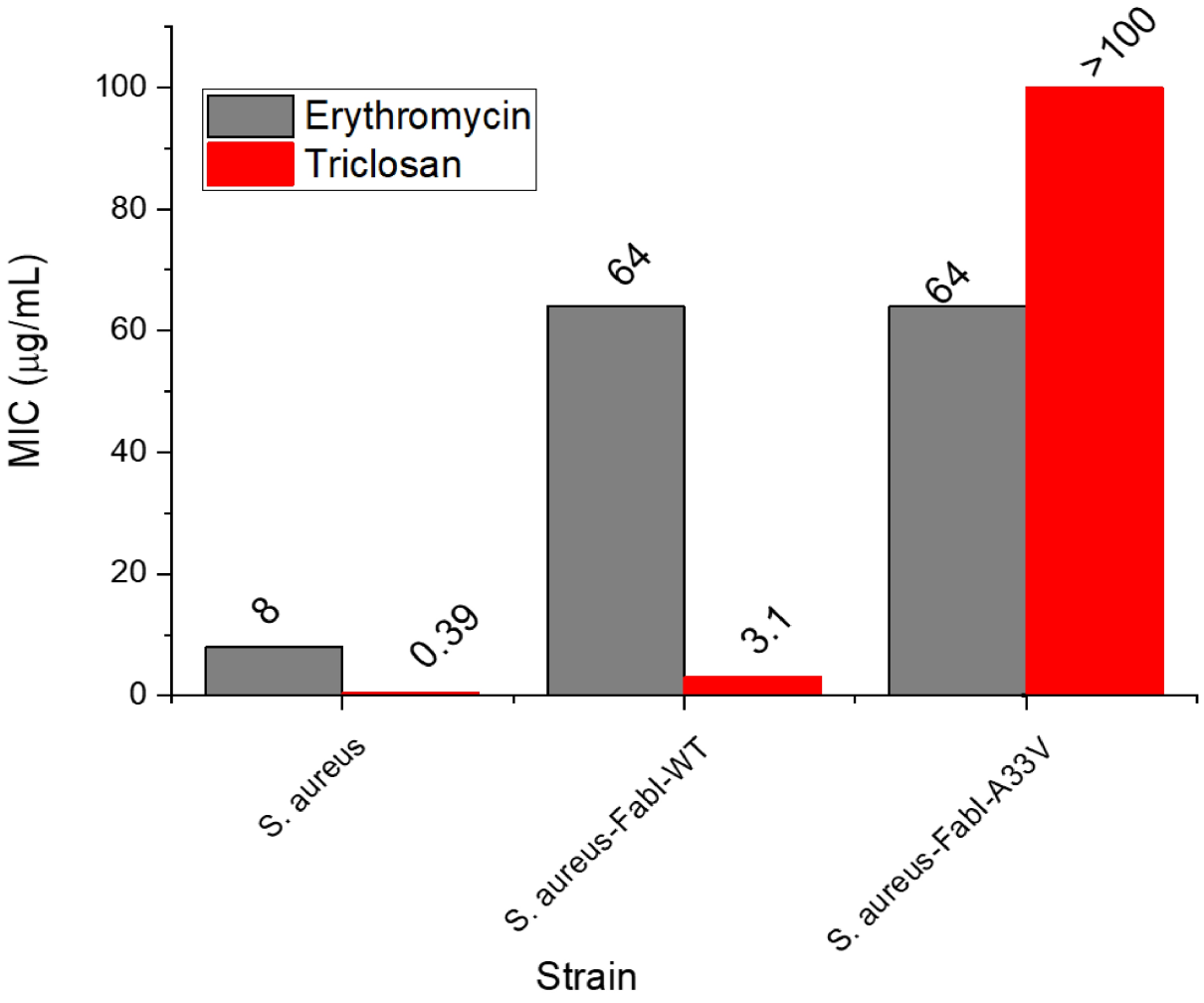

Figure 3.3: Minimum Inhibitory Concentration (MIC) of erythromycin, and triclosan on native *S. aureus* RN4220, RN4220 containing pHT370-*Sa*FabI wild type (WT), and RN4220 containing pHT370-*Sa*FabI-A33V. PHT370 contain erm resistant genes. The native RN4220 was used to verify the presence of the plasmid, and the wild type was used as a control to access the effect of the mutations on the bacterial resistance.

3.4. Discussion

Triclosan exhibits antibacterial activity against *Staphylococcus aureus* (McBride *et al.*, 1984; Chen *et al.*, 2009), and is a major class of antibacterial and antifungal agent used in many commercial products (Heath *et al.*, 1999). However, triclosan resistant strains have since appeared. Particular mutations in the enoyl-acyl carrier protein (ACP) reductase (ENR/FabI) confer high resistance to triclosan (Skovgaard *et al.*, 2013). It is crucial to identify potential resistant mutations, their mechanism of resistance and to develop method of inhibition before they are observed clinically. The error prone PCR (epPCR) enabled the substitution of nucleotides in a gene to give a small library of single, double, triple and multiple mutations in the *Sa*FabI protein. The single mutations in *Sa*FabI that were conferring resistance to triclosan included two mutations that involves active site residues, nine mutations involves interface residues and nine mutations that do not involve either active site residue or interface residues, but prevent triclosan binding. Polar residues are key players in electrostatic interaction, and therefore, their mutation may influence the enzyme conformation. The mutation analysis showed that 67% of the mutations maintained their polarity while 33% changed the polarity indicating that most of the mutations did not affect the electrostatic interaction in FabI directly.

The MIC of erythromycin in the native RN4220 being eight-fold lower than that on both *S. aureus* RN4220 *Sa*FabI-WT and *S. aureus* RN4220 *Sa*FabI-A33V was a proof that the latter two strains contained the plasmid carrying the erythromycin resistant gene. The MIC value of triclosan on *Sa*FabI-WT in RN4220 strain (3.1 µg/mL) was 8-fold higher than that in native RN4220 (0.4 µg/mL) reported previously (Mistry *et al.*, 2017). This result provided a good control for

interpreting the mutant results. The further increase of MIC of triclosan on A33V to greater than 100 μg/mL was indicative of extra resistance due to the point mutation in the FabI gene.

3.5. Conclusion

Directed evolution allows mutations in the *Sa*FabI gene that resist triclosan binding to become a serious threat to public health. Today, there is a pressing need to predict, identify and prevent or alleviate the evolution of resistance to triclosan, which remain a widely used antibacterial agent. Accelerated gene evolution is a useful tool in resistant mutations identification before they emerge as a clinical isolates. EpPCR allowed us to generate a small library of mutants that did not bind triclosan. In this project, nineteen different mutants were identified that did not bind triclosan. This list of mutations will serve as a checklist for clinicians to identify resistant strains in deciding a course of action.

3.6. Future Direction

The next logical step will be to identify the mechanism of resistance by simulating the structures of the mutants in the presence of the substrate and co-factors. Simulation is currently under way in Fung lab to access the mode of resistance for the various mutant and eventually propose a mechanism of resistance development.

Chapter Four

Comparison of the Solution Properties of N^5-Carboxyaminoimidazole Ribonucleotide Mutase (PurE) from *Bacillus anthracis*, *Francisella tularensis*, and *Yersinia Pestis*

4.1. Introduction

Structure-based drug discovery requires not only the validation of the protein target as essential for growth and or virulence, but also a detail understanding of the structural features of the protein to allow for a potent inhibitor development. Purine nucleotides are indispensable in the DNA molecule synthesis and therefore essential for the survival of the bacterial cells. Inhibiting one of the enzymes in a key step in the *de novo* purine biosynthesis pathway will create a significant shortage of the purine molecules necessary for bacterial growth. The *de novo* purine biosynthesis pathway is required for complete virulence in several pathogens including *Yersinia pestis* and *Bacillus anthracis* (Jenkin *et al.*, 2011). With N^5-carboxyaminoimidazole ribonucleotide (N^5-CAIR) mutase (PurE) in the *de novo* purine biosynthesis pathway knocked out, the murines showed little virulence of *B. anthracis* (Samant *et al.,* 2008). In addition, knocking out the PurE gene attenuates the growth of *Mycobacterium tuberculosis* (Sassetti *et al.,* 2003). Given the difference in the substrate between N^5-carboxyaminoimidazole ribonucleotide (N^5-CAIR) mutase from human (Pur6), which contains a PurE domain, and the bacterial PurE, PurE protein becomes a viable target for selective antibiotic development (Brugarolas *et al.*, 2011).

All bacterial PurE enzymes studied so far exist as an octamer in solution and are found to have the same substrate. However, the condition for obtaining octameric homogeneity with the optimum enzymatic activity is not clear. The octameric enzyme has 8 active sites, with each site

formed by three subunits each (Mathews *et al.*, 1999), but is shown to have variable level of occupancy, with four active sites occupied in *E. coli* PurE (Hoskins *et al.*, 2007). It is therefore important to characterize and identify the optimal conditions for inhibitor screening.

For PurE from Gram positive *B. anthracis*, a "sub-stable" state was selected for high throughput screening (Kim *et al*., 2015). For *F. tularensis,* causative agents of rabbit fever, and Gram negative *Y. pestis*, causative agent for black plague, it is not clear whether similar conditions can be used for inhibitor screening. Kinetics evaluation will help to obtain information on catalytic efficiencies of PurE in these species, and the full biochemical and biophysical characterization may reveal similar and/or distinct structural features that can be exploited in the development of both a narrow and a broad spectrum antibiotic development.

4.2. Materials and Methods

4.2.1. Plasmid Construction and Transformation

The PurE genes from cDNA of *Bacillus anthracis* Ames strain (ΔANR; locus tag Ba_0288), *Francisella tularensis* SHU4 (locus tag FTT_0896) and *Yersinia pestis* (locus tag YPO3076) were individually inserted in pDEST -15 expression vector (Invitrogen; Carlsbad, California), containing an ampicillin resistant gene, an N-terminal glutathione S-transferase (GST) tag, a 20 amino-acid linker followed by a thrombin cleavage site. Briefly, primers designed for In-Fusion ligation (Clontech) were used to amplify the gene and another set of vector amplification primers was used to linearize the pDEST-15 vector. The PCR product of the gene was treated with DPNI (New England Biolabs; Beverly, Massachusetts) and column purified. The gene and the linearized vector were mixed in a molar ratio of three to one in the presence of 2 μL of In-Fusion

enzyme. The mixture was incubated at 50 ºC for 30 m and proceeded with transformation with DH_5-α competent cells (Zymo). Cells were spread on ampicillin containing agar plates. The DNA sequence of the construct in the cells was confirmed by the results of Sanger sequencing done by the Research Resources Center (RRC) at UIC. The plasmids were then extracted and transformed into BL21-CodonPlus (DE3)-RIL (Agilent Technologies; Cedar Creek, Texas) competent cells, for optimal protein expression.

4.2.2. Cell Growth and Protein Expression

A starter culture was prepared by inoculating a single colony in LB medium containing 100 µg/mL ampicillin and incubated overnight at 37 ºC with shaking at 240 rpm. A glycerol stock was prepared, flash frozen in liquid nitrogen to give freeze-down samples and stored at -80 ºC for the downstream processing. For the protein expression, freeze-down (50 µL) was added to Luria-Broth (LB) (50 mL) and incubated overnight (16 - 18 h) to an optical density at 600 nm (OD_{600}) of about 1.7. The next day, the overnight culture was added to one litter of fresh LB and incubated to an OD_{600} of 0.5. Isopropyl β-D-1-thiogalactopyranoside (IPTG; Gold Biotechnology; St Louis, Missouri) was added to a final concentration of 0.5 mM to induce the protein expression. Cells were harvest after an additional 3 h growth. The collected cells were weighted and stored at -80 ºC if not used immediately.

4.2.3. Purification of Recombinant Proteins *Ba*PurE, *Ft*PurE and *Yp*PurE

About 12 grams of cells was re-suspended in 50 mL of 5 mM phosphate buffer at pH 7.4 with 150 mM NaCl (PBS7.4) and 1% triton and stirred at 4 ºC to homogeneity. Lysozyme (1 mg/mL) was added and stirred. The final mixture was sonicated in a Rosetta cell for 15 m with a

sonicator (Vibra Cell; Danbury, Connecticut) with a power output set at 30. The cell lysate was centrifuged at 30,000 g for 30 m. The supernatant was applied to a glutathione affinity column (Sigma-Aldrich; St Louis, Missouri) and washed with PBS7.4. The fusion protein was eluted with a freshly prepared buffer (2.5 mM GSH in 50 mM Tris buffer at pH 8). The GSH was subsequently removed by serial dialysis, 2h of 2 L followed by 4 L PBS7.4 overnight. The fusion protein was concentrated to 2 mg/mL. Thrombin (Tb), with a ratio of 1 unit per mg of protein, was added and incubated at 37 ºC for 1 h for *Ba*PurE and *Yp*PurE and 3 h for *Ft*PurE. Phenylmethylsulfonyl fluoride (PMSF) (Pierce; Dallas, Texas) was added (1 L of 10 mM PMSF per 10 units of Tb). The mixture was put on ice, before it was applied to the affinity column to remove the GST tag. *Ba*PurE, *Ft*PurE, or *Yp*PurE was eluted with PBS7.4, and concentrated to an absorbance at 280 nm (A_{280}) ~ 2 mg/mL. If the protein sample was not used immediately, it was frozen drop-wise (20 µL each drop) in liquid nitrogen and stored at -80 ºC.

4.2.4. Buffers

The following buffers were used. 5 mM phosphate with 0, 25, or 150 mM NaCl at pH 7.4 were prepared and the conductivity measured, using a Yellow Spring model 31 conductivity meter (Yellow Spring Instrument Co; Yellow Spring, Ohio). Also, we prepared 25 mM Tris buffer with 0, 25 or 150 mM NaCl and the conductivity measured.

4.2.5. Protein Thermal Unfolding

4.2.5.1. Secondary Structural Element Unfolding

Each frozen protein sample was thawed and dialyzed overnight in a desired buffer, and the concentration was adjusted to 30 μM (~500 μg/mL). The sample (150 μL) was loaded to a quartz circular dichroism (CD) cuvette for a CD spectrum measurement at 200-250 nm region at room temperature with a CD spectrometer (JASCO J-810 equipped with a Peltier temperature Controller). Then the wavelength was set to 222 nm and the temperature set to higher temperature at a rate of 1 ºC/m. The CD intensity was recorded at each temperature of 0.2 ºC interval, and stopped at 100 ºC.

4.2.5.2. Tertiary Structure Unfolding

SYPRO Orange (SO) (Invitrogen; Carlsbad, California) is a dye with a well-documented sensitivity to its hydrophobic environment (Lo *et al.*, 2004), and was used to access exposed hydrophobic residues by measuring the fluorescence intensity of bounded SO. Protein sample (25 μM) was mixed with 5X SO (the exact concentration was not provided by the supplier, but as 5000X), and the fluorescence intensity was recorded with Jasco FP-6200 spectrofluorometer with excitation at 472 nm and an emission at 570 nm. When the protein molecule was folded, little SO binding, and thus little fluorescence intensity. As the protein was unfolded thermally, more SO molecules were bound to the exposed hydrophobic pockets, and thus more fluorescence intensity was observed.

4.2.6. Protein Hydrodynamic Mass

The hydrodynamic mass of the three proteins were obtained using gel filtration column chromatographic methods with a Superdex 200 column. The 10/30 GL column connected to a fast performance liquid chromatography (FPLC) (AKTA Purifier; GE Healthcare; Pittsburgh, Pennsylvania). The system was first equilibrated with an appropriate buffer, such as 5 mM phosphate pH 7.4 with 150 mM NaCl, which was filtered and degassed prior to usage. The protein sample was thawed on ice, centrifuged at 23,000 g for 2 m before being diluted to 25 μM, loaded to the column and eluted at 0.5 mL/m. A calibration curve using high molecular weight standard proteins (Aldolase, Ovalbumin, Ribonuclease, Ferritin, Conalbumin and Ribonuclease; all ~8 μg/mL and were from GE Healthcare) was established in 5 mM phosphate at pH7.4 with 50 mM NaCl (conductivity = 5,300 MHO) or with 150 mM NaCl (13,000 μMHO). Blue dextran (GE Healthcare) was used to measure the void volume (V_o). The elution volume (V_e) of each sample was then used to calculate the partition coefficient K_{AV} $(V_e - V_o)/(V_t - V_o)$ where V_t was the total volume of the column.

4.2.7. Enzyme Activity

The activity of PurE was monitored by the disappearance of the substrate (CAIR) in the conversion of CAIR to N^5-CAIR (Meyer *et al.,* 1992; Kim *et al.*, 2015). CAIR was synthesized in our lab following the published method (Sullivian *et al.*, 2014). Enzyme (10 nM) and CAIR (30 μM) in 350 μL of a specific buffer were mixed, and the UV absorbance at 260 nm was followed for 90 second. To determine the protein concentrations, the following extinction coefficients were

used: 11460 $M^{-1}cm^{-1}$ for *Ba*PurE, 8605 $M^{-1}cm^{-1}$ for *Ft*PurE and 13980 $M^{-1}cm^{-1}$ for *Yp*PurE and ~9,000 $M^{-1}cm^{-1}$ for CAIR (Meyer *et al.,* 1992).

4.2.8. Kinetics Parameters, Km and K_{cat}

Ten substrate concentrations, from 1 to 100 μM, were used in each buffer system for the enzyme activity measurement. The enzyme activities were plotted as a function of substrate concentration to determine whether the enzyme followed a Michaelis-Menten kinetics. If it did, the double reciprocal plots of activity vs. concentration were obtained. The Y-intercept was recorded as 1/Vmax and the X-intercept was recorded as -1/Km. The catalytic efficiency (K_{cat}) was obtained by dividing V_{max} by the total enzyme concentration. The catalytic efficiency (Km/K_{cat}) was also obtained.

4.2.9. Surface Hydrophobicity Assessment

SYPRO Orange (a final concentration of 5X) was added to the protein samples (*Ba*PurE, *Ft*PurE and *Yp*PurE, each at 25 μM) in a specific buffer system. The fluorescence signal intensities at room temperature were recorded as described in Section 4.2.5.2. The hydrophobic residues on the surface of each protein were also visualized by Chimera 1.12 by selecting hydrophobicity surface from the “presets” menus, using x-ray structures as inputs (1XMP for *Ba*PurE, 3OOW for *Ft*PurE and 3KUU for *Yp*PurE).

4.3. Results

4.3.1. PurE from *B. anthracis*, *Francisella tularensis* and *Yersinia pestis*

*Ba*PurE consisted of 1 tryptophan and 4 tyrosine residues (Figure 4.1) with an extinction coefficient of 11,460 $M^{-1}cm^{-1}$. It had 164 residues, 20 of which are negatively charged and 15 positively charged. The molar mass was 17.3 kDa and the isoelectric point (PI) was 5.3. *Ft*PurE consisted of 1 tryptophan and 2 tyrosine residues with an extinction coefficient of 8,605 $M^{-1}cm^{-1}$. It had 166 residues, 17 of which are negatively charged and 14 positively charged. The molar mass was 17.4 kDa and the PI of 5.8. *Yp*PurE consisted of 2 tryptophan and 2 tyrosine residues with an extinction coefficient of 13.980 $M^{-1}cm^{-1}$. It had 177 residues, 15 were negatively charged and 10 positively charged. The molar mass was 18.2 kDa and the PI 5.6 (TABLE VIII). *Ba*PurE was shown to have 71% sequence similarity to *Ft*PurE, and 62% similarity to *Yp*PurE. *Ft*PurE and *Yp*PurE were shown to have 70% similarity (TABLE VIII). Sequence alignment (Figure 4.1) showed that 81 residues in all 3 enzymes were conserved.

TABLE VIII: SEQUENCE-RELATED PROPERTIES OF *BA*PURE, *FT*PURE, AND *YP*PURE

	*Ba*PurE[a]	*Ft*PurE[b]	*Yp*PurE[c]
# Tryptophan	1	1	2
# Tyrosine	4	2	2
Extension coefficient (M^{-1} cm^{-1})[d]	11460	8605	13980
# Negative residues	20	17	15
# Positive residues	15	14	10
# Total residues[e]	164	166	177
Molecular mass (Da)	17322.9	17477.1	18232.8
pI[d]	5.3	5.8	5.6
Sequence similarity (%)[f]	*Ba* and *Ft*: 71	*Ft* and Yp: 70	*Yp* and *Ba*: 62

[a] *Ba*PurE is *Bacillus anthracis* N^5-carboxy-amino-imidazole ribonucleotide mutase.

[b] *Ft* is *Francisella tularensis*.

[c] *Yp* is *Yersinia pestis*.

[d] Calculated with the program ExPASy ProtParam (https://web.expasy.org/cgi-bin/protparam/protparam).

[e] residues in the full-length protein plus residual residues GSH from fusion protein cleavage

[f] Calculated with the program EMBOSS Needle (https://www.ebi.ac.uk/Tools/psa/emboss_needle/)

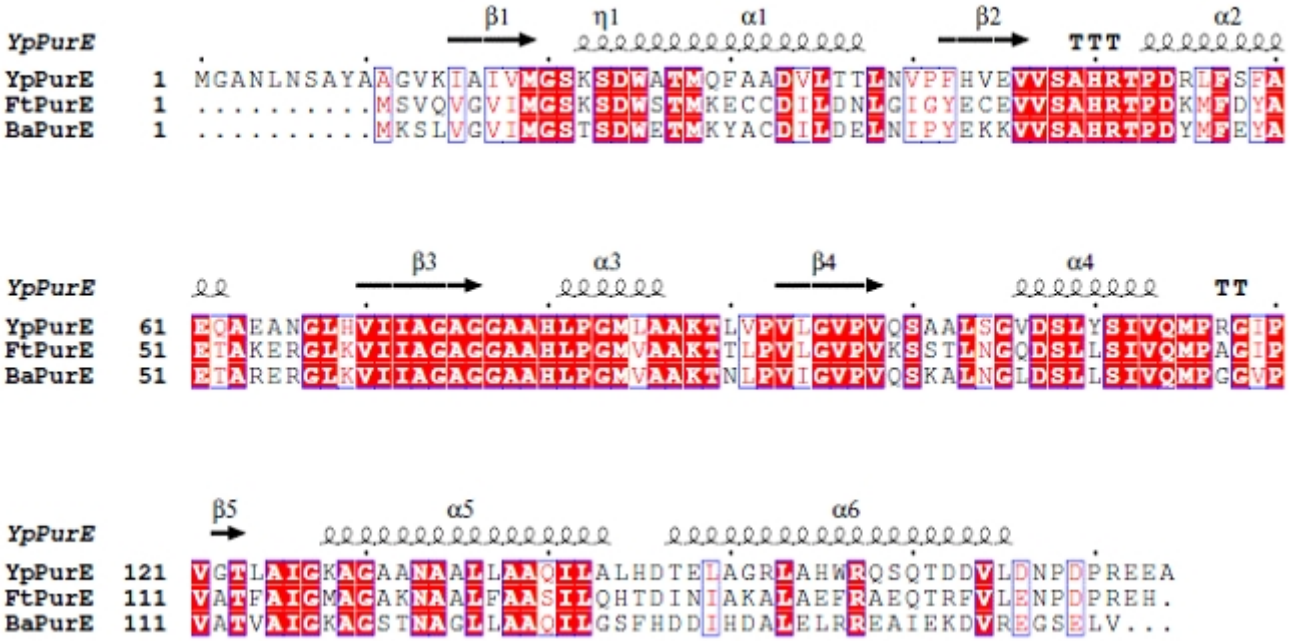

Figure 4.1: Sequence alignment of *Ba*PurE, *Ft*PurE, and *Yp*PurE by clustal omega. (European Bioinformatics Institute, EBI). The conserved residues between the three proteins are highlighted in red. Somewhat conserved residues are boxed in light blue. *Yp, Ft* and *Ba* are the codes representing the organism where the protein is coming from, namely, *Yersinia pestis, Francisella tularensis* and *Bacillus anthracis* in that order. The secondary structural elements (alpha helix α, beta sheet β, TT beta turn, TTT: alpha turn and η 3_{10}-helix) are represented on the top. The alignment was generated by ESPrit. http://espript.ibcp.fr/ESPript/ESPript/.

4.3.2. Buffer Conductivities

The conductivity of 5 mM phosphate with no NaCl (5P-0) was 700 µMHO, 5 mM phosphate with 25 NaCl (5P-25) was of 3,300 µMHO, 5 mM phosphate with 50 NaCl (5P-50) had a conductivity of 5300 µMHO and 5 mM phosphate with 150 NaCl (5P-150) was 13000 µMHO. The conductivity of 25 mM Tris buffer at pH 8 with no NaCl added (25T-0) was 1,300 µMHO, 25Tris with 25 mM NaCl added (25T-25) was 4,000 µMHO, 25Tris with 50 mM NaCl added (25T-50) was 5,400 µMHO and , and 25mM Tris with 150 mM NaCl added (25T-150) was 12500 µMHO (Figure 4.2 ;TABLE IX).

4.3.3. Recombinant Protein Expression and Purification

The plasmids for *Ba*PurE, *Ft*PurE and *Yp*PurE were identical except the PurE gene portion, as confirmed by DNA sequencing results. The whole-cell electrophoresis showed an over-expression of about 43 kDa band of the fusion protein (GST-PurE; sequence mass ~ 45 kDa) (Figure 4.3 A). About 20 mg of fusion protein per liter of culture were obtained for all three proteins, and upon removal of the GST, 7 mg of *Ba*PurE, 5 mg of *Ft*PurE and 3 mg of *Yp*PurE (with similar purity of 80%) were obtained (Figure 4.3 B).

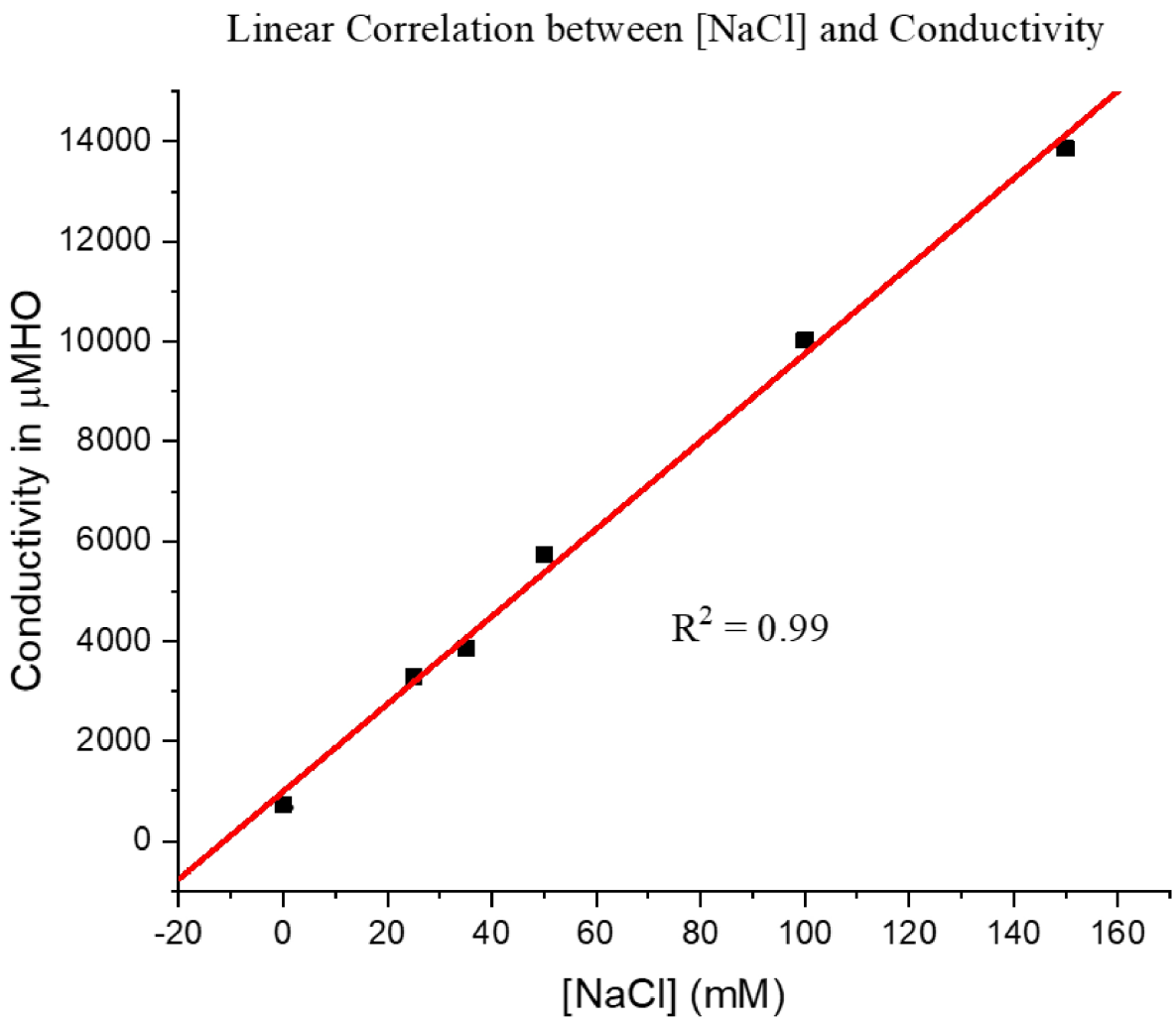

Figure 4.2: Buffer ionic strength as a function of NaCl concentration. A salt concentration ranging from 0-150 mM NaCl yielded a linear correlation with the conductivity, and the R^2 value was 0.99.

TABLE IX: CONDUCTIVITIES OF BUFFERS USED FOR DIFFERENT EXPERIMENTS.

Buffer	5P-0[a]	5P-25	5P-50	5P-150	25T-0[b]	25T-25	25T-50	25T-150
Conductivity (μMHO)	700	3300	5300	13000	1300	4000	5400	12500

[a]5P-0 = 5 mM phosphate with 0 mM NaCl

[b]25T-0 = 25 mM Tris with 0 mM NaCl

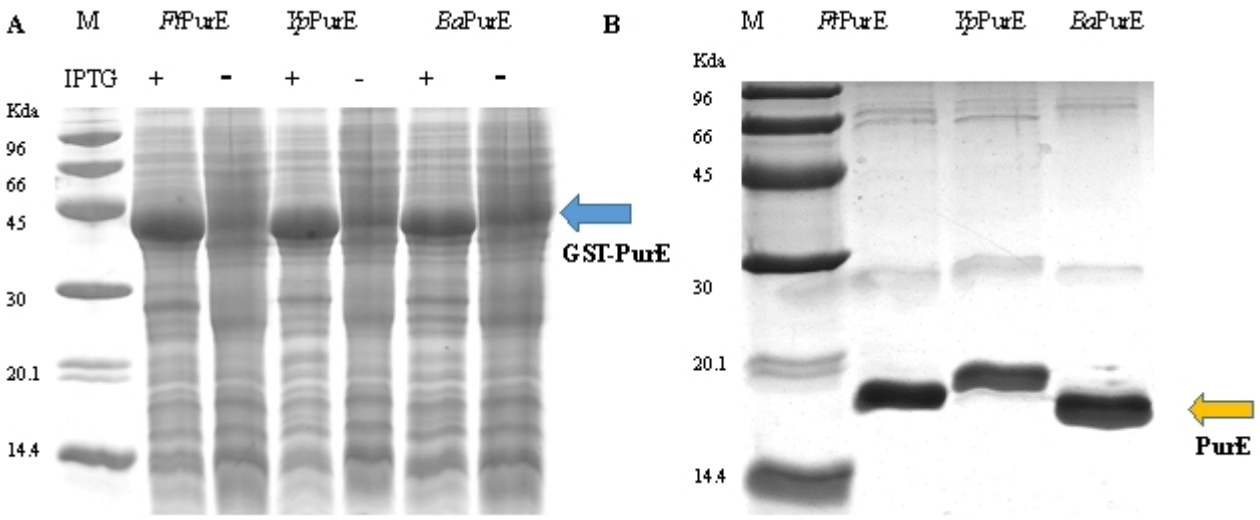

Figure 4.3: 16% SDS-PAGE analysis. A) Whole-cell electrophoresis of cells containing GST-PurE. Each protein was expressed as an N-terminal GST fusion protein in pDEST-15 vector; and the expression was induced with 0.5 mM IPTG. The gel showed the over-expression of the fusion protein in the induced colonies. M: molecular mass marker; (-) no IPTG added; (+) IPTG added. B) Purity assessment (SDS PAGE) of PurE after GST was removed. *Ba*PurE, *Ft*PurE and *Yp*PurE are described in figure 4.1.

4.3.4. Protein Thermal Stability

4.3.4.1. Secondary Structural Elements

A typical unfolding profile of *Ba*PurE exhibited a single transition both in 5 mM phosphate with no or 25 mM NaCl (5P-0; 5P-25) or in 25 mM Tris with no or 25 mM NaCl (25T - 0; 25T-25), and a double transition in both 5 mM phospate with 150 mM NaCl (5P-150) and 25 mM Tris with 150 mM NaCl (25T-150; Figure 4.4 A and D). A single transition was observed in *Ft*PurE in all buffers except in 5P-150 (Figure 4.4 B and E). It should be noted that in 5P-0 and 25T-25 *Ft*PurE exhibited a gradual unfolding even at low temperature. *Yp*PurE exhibited a single transition temperature in all buffers except in 25T-0 where two transition were observed. There were baseline problems in 5P-0 and 5P-25 (Figure 4.4; C and F). The average Tm for *Ba*PurE was 48.6 $\pm$ 0.9 (n = 3) in 5P-0, 50.7 $\pm$ 0.5 (n = 3) in 25T-0, 55.7 $\pm$ 0.9 (n = 4) in 5P-25, 54.7 $\pm$ 0.1 (n = 2) in 25T-25, 62.7 $\pm$ 2.9 (n = 3) in 25 T-150, and 61.5 $\pm$ 0.4 (n = 3) in 5P-150. The Tm for *Ft*PurE 60.3 $\pm$ 0.3 (n = 3) in 5P-0, 59.3 $\pm$ 0.5 (n = 4) in 25T-0, 57.1 $\pm$ 0.1 (n = 2) in 5P-25, 61.5 $\pm$ 2.3 (n = 3) in 25T-25, 63.2 $\pm$ 2.6 (n = 3) in 25 T-150, and 62.5 in 5P-150. The Tm for *Yp*PurE was 61.2$\pm$ 0.0 (n = 2) in 5P-0, 63.7 $\pm$ 0.9 (n = 2) in 25T-0, 62.6 $\pm$ 0.4 (n = 3) in 5P-25, 64.3 $\pm$ 0.1 (n = 2) in 25T-25, 61.3 $\pm$ 1.4 (n = 3) in 25 T-150, and 62.5 $\pm$ 1.1 (n = 2) in 5P-150 (TABLE X-columns with CD_{222nm} heading).

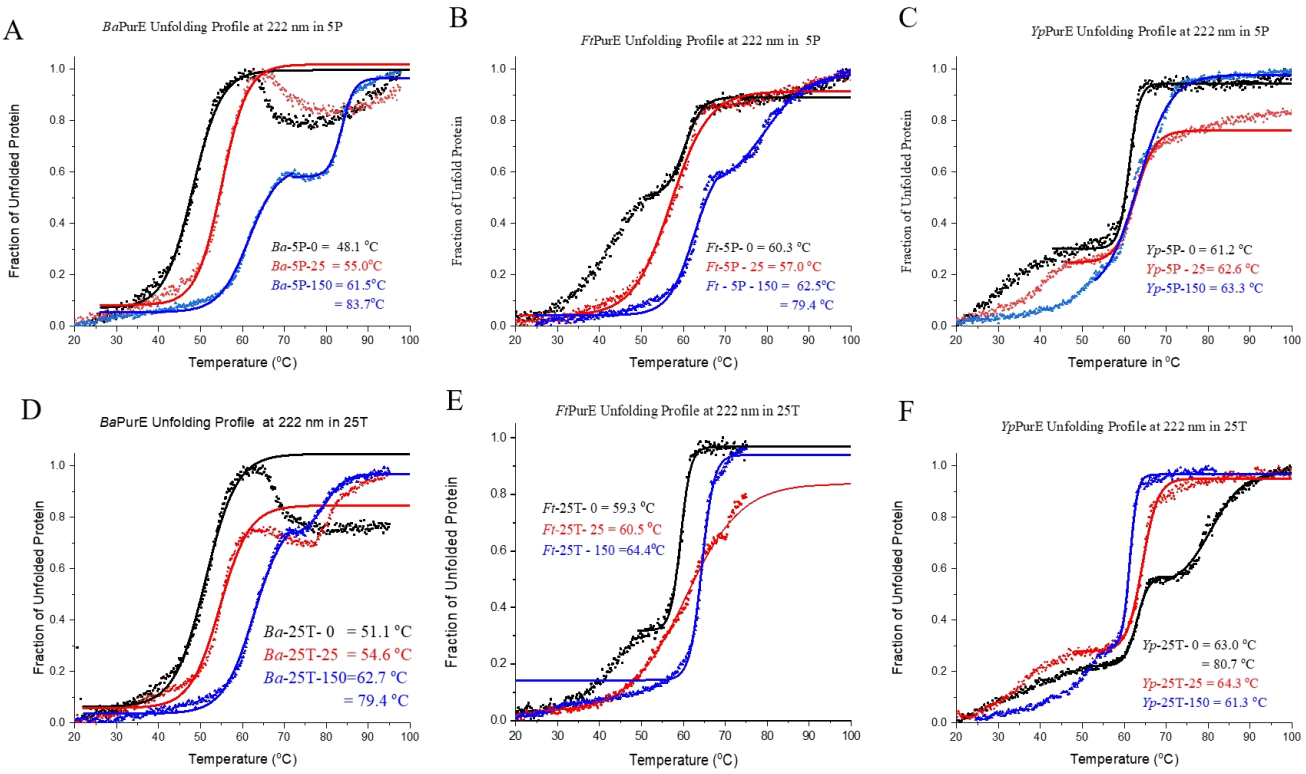

Figure 4.4: Fraction of unfolded protein recorded by CD as a function of temperature. 30 µM sample was heated at a rate of 1°C per minute and the CD signal was recorded at 222 nm. The experimental data are represented by the single points and the fitted line is represented by the solid line and was the Boltzmann fit of the experimental data. A): *Ba*PurE in 5 mM phosphate plus 0-150 mM NaCl. B): *Ft*PurE in 5 mM phosphate plus 0-150 mM NaCl. C): *Yp*PurE in 5 mM phosphate plus 0-150 mM NaCl. D): *Ba*PurE in 25 mM Tris with 0-150 mM NaCl. E): *Ft*PurE in 25 mM Tris with 0-150 mM NaCl. F): *Yp*PurE in 25 mM Tris with 0-150 mM NaCl.

Black (5P-0 or 25T-0), Red (5P-25 or 25T-25), Blue (5P-150 or 25T-150).

TABLE X: AVERAGE T_M VALUES OF THERMAL UNFOLDING OF PURE (30 M) IN BUFFERS WITH DIFFERENT IONIC STRENGTH, MONITORED BY ELLIPTICITY VALUES AT 222 NM WITH CIRCULAR DICHROISM ($CD_{222\ NM}$) METHOD AND WITH FLUORESCENT INTENSITIES (EX = 472 NM; EM = 570 NM) OF ADDED SYPRO ORANGE (5X SYPRO ORANGE) (FL-SO).

Buffer[a]		Conduct[b]	*Ba*PurE		*Ft*PurE		*Yp*PurE	
		µMHO	T_m °C		T_m °C		T_m °C	
	NaCl (mM))		$CD_{222\ nm}$	Fl-SO	$CD_{222\ nm}$	Fl-SO	$CD_{222\ nm}$	Fl-SO
5P	0	700	**48.6** (0.9; 3)[c]	**44.7** (- -; 1)	**60.3** (0.3; 3)	**60.5** (0.9; 4)	**61.2** (0.0; 2)	**60.0** (0.1; 3)
25T	0	1300	**50.7** (0.5; 3)	**49.5** (1.0; 2)	**59.3** (0.5; 4)	**60.8** (0.5; 3)	**63.7**[g] (0.9; 2)	**63.5** (0.4; 2)
5P	25	3300	**55.7** (0.9; 4)	**56.0** (2.7; 4)	**57.1** (0.1; 2)	**60.7** (1.7; 3)	**62.6** (0.4; 3)	**59.8** (0.6; 3)
25T	25	4000	**54.7** (0.1;2)	**53.7** (0.9;2)	**61.5** (2.3;3)	**60.8** (2.8;2)	**64.3** (0.1;2)	**60.3** (0.1;2)
25T	150	12500	**62.7**[d] (2.9; 3)	**63.4** (0.2; 2)	**63.2** (2.6; 3)	**65.0** (0.6; 3)	**61.3** (1.4; 3)	**60.8** (0.2; 2)
5P	150	13000	**61.5**[e] (0.4; 3)	**62.6** (- -; 1)	**62.5**[f] (- -; 1)	**65.1** (- -; 1)	**62.5** (1.1;2)	**58.8** (0.3; 2)

[a]Buffer - 5P for 5 mM phosphate buffer at pH 7.4 and 25T for 25 mM Tris buffer at pH 8.

[b]Cond is the conductivity of the buffer.

[c]The values in the parentheses below each average value are those of the standard deviation and of the number of runs.

[d]A second transition was observed with Tm = 87.2 $\pm$ 1.1 ºC; [e]A second transition was observed with Tm = 83.9 $\pm$ 0.2 ºC (n = 4).

[f]A second transition was observed with Tm = 80.7 ºC. No values are given for those with a single run.

[g]A second transition was observed with Tm = 79.4 ºC.

4.3.4.2. Tertiary Structure Thermal Unfolding

All the proteins exhibited a single transition in all buffer conditions (Figure 4.5). The Tm for *Ba*PurE was 44.7 (n = 1) in 5P-0, 49.5 $\pm$ 1.0 (n = 2) in 25T-0, 56.0 $\pm$ 2.7 (n = 4) in 5P-25, 53.7 $\pm$ 0.9 (n = 2) in 25T- 25, 63.4 $\pm$ 0.2 (n = 2) in 25T-150 and 62.6 (n = 1) in 5P -150. The Tm for *Ft*PurE was 60.5 + 0.9 (n = 4) in 5P-0, 60.8 $\pm$ 0.5 (n = 3) in 25T-0, 60.7 $\pm$ 1.7 (n = 3) in 5P-25, 60.8 $\pm$ 2.8 (n = 2) in 25T- 25, 65.0 + 0.6 (n = 3) in 25T-150 and 65.1 (n = 1) in 5P -150. The Tm for *Yp*PurE, was 60.0 + 0.1 (n = 3) in 5P-0, 63.5 $\pm$ 0.4 (n = 2) in 25T-0, 59.8 $\pm$ 0.6 (n = 3) in 5P-25, 60.3 $\pm$ 0.1 (n = 2) in 25T- 25, 60.8 + 0.2 (n = 2) in 25T-150 and 58.8 + 0.3 (n = 2) in 5P -150 (TABLE X columns with "Fl-S.O" heading).

4.3.5. Protein Homogeneity Assessment by Size Exclusion Chromatography

The plot of K_{AV} versus the molecular mass (13.7 to 440 kDa) of proteins used for calibration was linear with a correlation coefficient of 0.99 (Figure 4.6 A). The elution profile showed single or double peaks (Figure 4.6 B). *Ba*PurE in solution was found to have two components in equilibrium with K_{AV} of 0.29 and 0.43 in 5P-0, and 0.42 and 0.55 in 5P- 25, but with only one component with a K_{AV} of 0.50 in 5P-150 (Figure 4.6 C). *Ft*PurE showed a major component with a K_{AV} of 0.30 in 5P-0, 0.44 in 5P-25, and 0.51in 5P-150 (Figure 4.6 D). *Yp*PurE also eluded as a single component with a K_{AV} of 0.28 in 5P-0, 0.42 in 5P-25 and 0.50 in 5P-150 (Figure 4.6 E; TABLE XI).

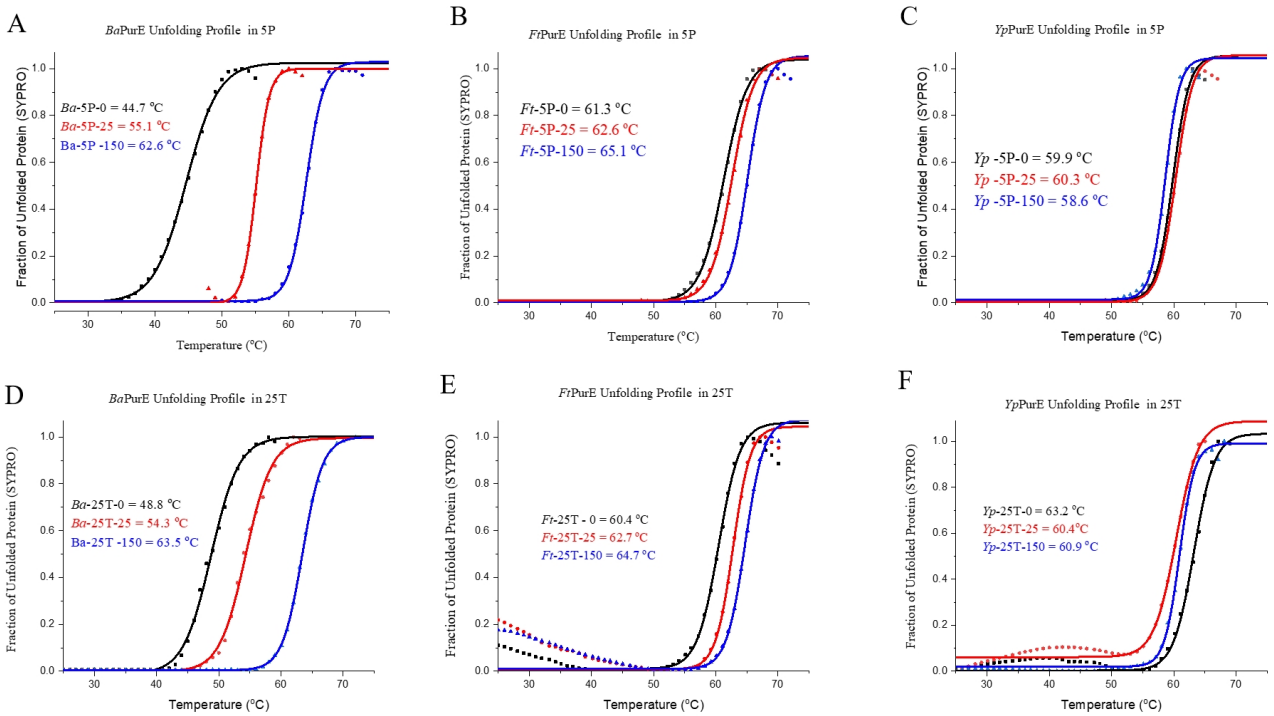

Figure 4.5: Thermal stability of *Ba*PurE (25 µM), *Ft*PurE and *Yp*PurE in buffer with different salt concentration. A): *Ba*PurE in 5 mM phosphate plus 0-150 mM NaCl. B): *Ft*PurE in 5 mM phosphate plus 0-150 mM NaCl. C): *Yp*PurE in 5 mM phosphate plus 0-150 mM NaCl. D): *Ba*PurE in 25 mM Tris with 0-150 mM NaCl. E): *Ft*PurE in 25 mM Tris with 0-150 mM NaCl. F): *Yp*PurE in 25 mM Tris with 0-150 mM NaCl. Black symbols: samples in 5 mM phosphate or 25 mM Tris with no salt added to the buffer; Red symbols: samples in 5 mM phosphate or 25 mM Tris with 25 mM NaCl added to the buffer; Blue symbols: samples in 5 mM phosphate or 25 mM Tris with 150 mM NaCl added to the buffer. The fraction of unfolded protein was obtained by recording the fluorescence intensity of the SYPRO Orange dye.

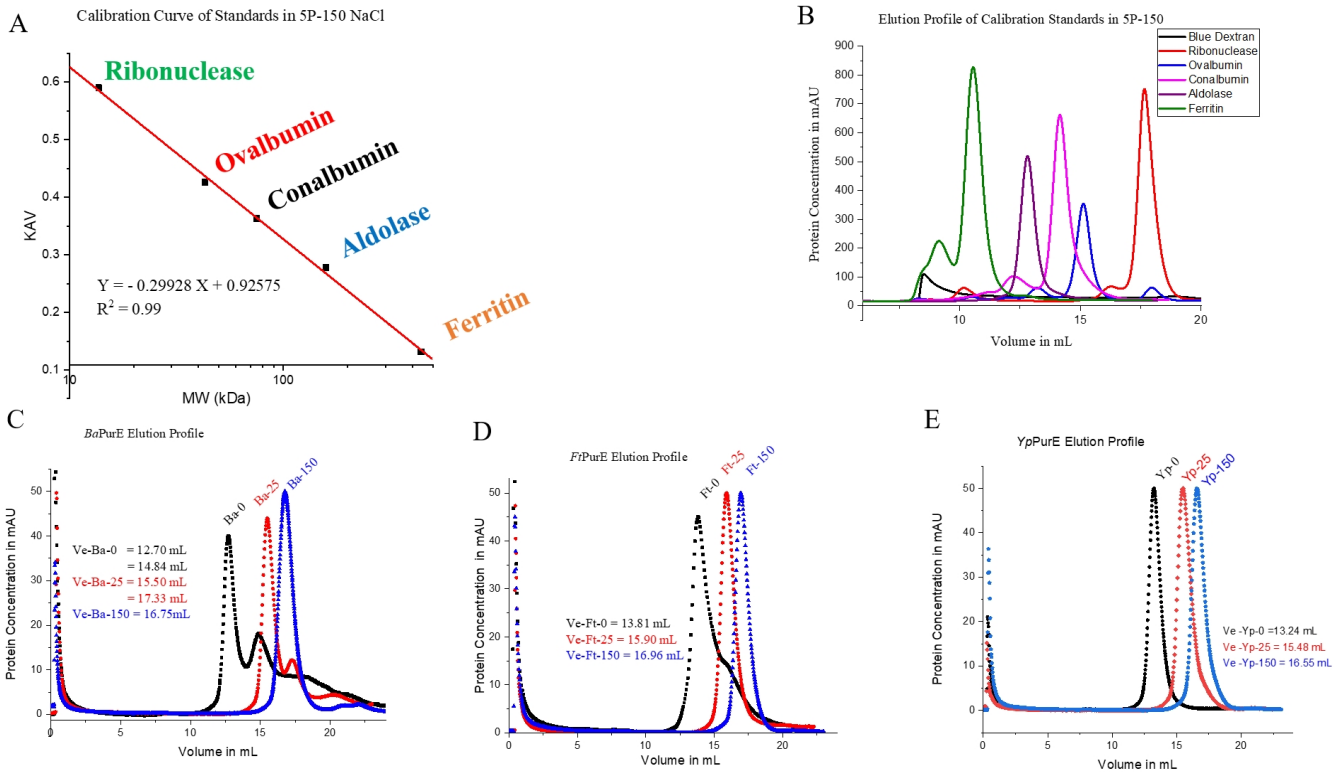

Figure 4.6: Elution profile of *Ba*PurE, *Ft*PurE and *Yp*PurE in 5 mM phosphate using size exclusion with fast performance liquid chromatography (FPLC). 25 µM of the PurE sample was prepared and 150 µL was loaded to the column. A): Calibration curve in 5 mM phosphate buffer at pH7.4 with 150 mM NaCl. B): elution profile of the standard proteins. C): Elution profile of *Ba*PurE in 5 mM phosphate plus 0-150 mM NaCl. D): Elution profile of *Ft*PurE in 5 mM phosphate plus 0-150 mM NaCl. E): Elution profile of *Yp*PurE in 5 mM phosphate plus 0-150 mM NaCl. Samples with no salt added are in black circles; Samples with 25 mM NaCl added are represented in red squares, and the samples with 150 mM salt added are in blue triangles. All samples were run on a Superdex 200 with a flow rate of 0.5 mL/m.

TABLE XI: CALCULATED PARTITION COEFFICIENT (K_{AV}) OF THE ELUTION PEAKS IN THE DIFFERENT BUFFER CONDITIONS. THE K_{AV} WAS OBTAINED FROM N DIFFERENT INDEPENDENT ELUTION PROFILES AND THE VARIATION BETWEEN RUNS ARE REPORTED AS A STANDARD DEVIATION (STD).

Buffer		Conduct. (MHO)	*Ba*PurE						*Ft*PurE			*Yp*PurE		
	[NaCl]		K_{AV} 1[a]	STD	n	K_{AV} 2[b]	STD	n	K_{AV}	STD	n	K_{AV}	STD	n
5P	0	700	0.29	0.01	6	0.43	0.03	6	0.30	0.01	6	0.28	0.01	4
5P	25	3300	0.42	0.00	4	0.55	0.01	4	0.44	0.01	3	0.42	0.00	3
5P	150	13000	0.50	0.01	4				0.51	0.01	4	0.50	0.00	5

[a]K_{AV} 1 = K_{AV} of the first species in the sample

[b]K_{AV} 2 = K_{AV} of the second species in the same sample.

4.3.6. PurE Enzyme Activity

All three enzymes exhibited a Michaelis-Menten kinetics, as shown in the activities versus substrate concentration plot (Figure 4.7).

For *Ba*PurE, the specific activity ($mol.min^{-1}.mg^{-1}$) was found to be 11.2 $\pm$ 2.6 (n = 8) in 25T-0, 19.0 in 5P-25, 23.8 in 25T-25 and 13.5 $\pm$ 3.7 (n = 5) in 5P-150. For *Ft*PurE, the specific activity was 4.0 $\pm$ 2.4 (n = 10) in 25T-0, 10.7 in 5P-25, 16.8 in 25T-25 and 9.9 $\pm$ 1.2 (n = 2) in 5P-150. For *Yp*PurE, the specific activity was 8.3 $\pm$ 1.6 (n = 8) in 25T-0, 16. 9 in 5P-25, 15.3 in 25T-25 and 8.7 $\pm$ 2.2 (n = 6) in 5P-150 (TABLE XII).

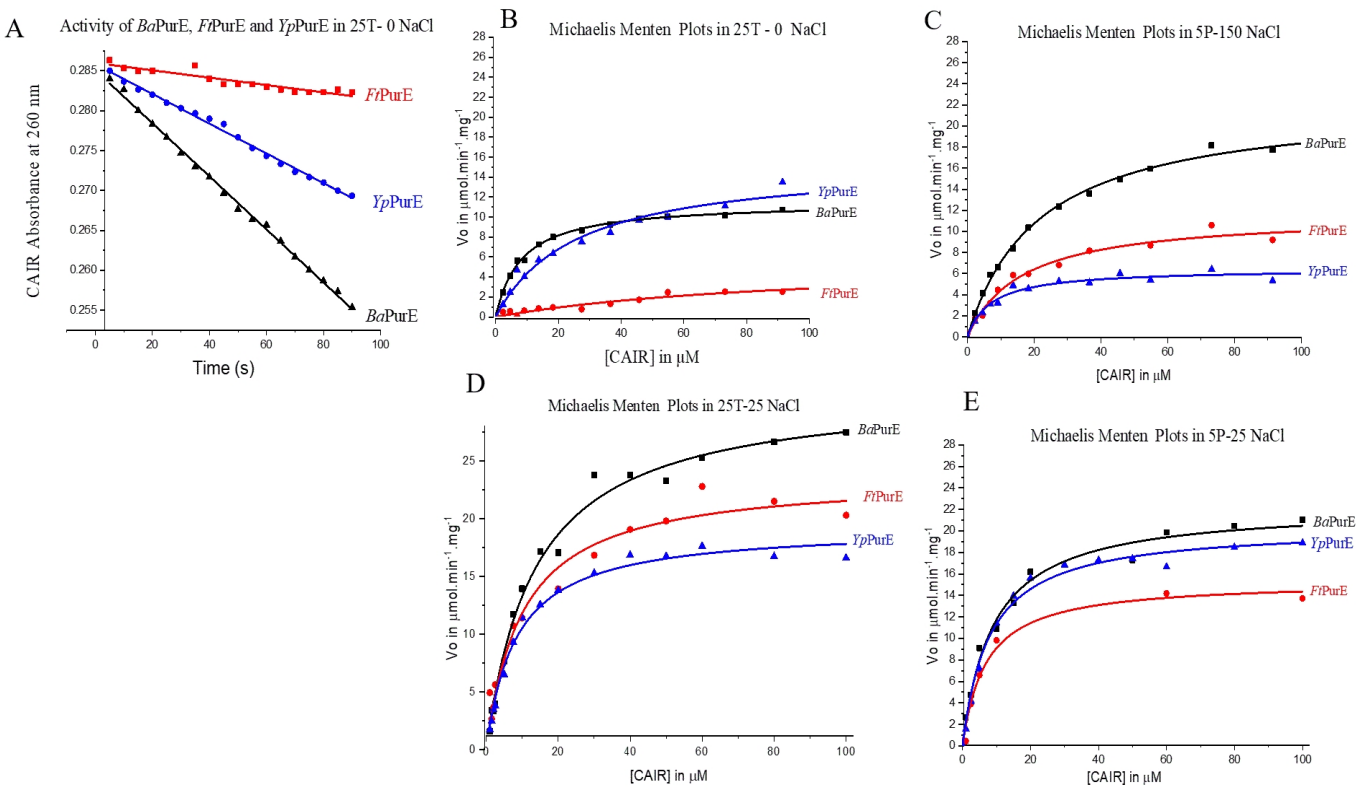

Figure 4.7: A): Time dependent *Ba*PurE, *Ft*PurE and *Yp*PurE activity assay in 25 mM Tris buffer at pH 8. The PurE activity is represented by the decrease of the substrate CAIR absorbance per unit time. The enzymatic assay was carried out using 30 µM of CAIR and 10 nM enzyme. The absorbance of CAIR was recorded at 260 nm every 5s for 90s. B): Michaelis-Menten plots of *Ba*PurE, *Ft*PurE and *Yp*PurE in 25 mM Tris and 25 mM NaCl. C): Michaelis-Menten plots of *Ba*PurE, *Ft*PurE and *Yp*PurE 5 mM phosphate buffer at pH 7.4 with 150 mM NaCl. D): Michaelis-Menten plots of *Ba*PurE, *Ft*PurE and *Yp*PurE 25 mM tris and 25 mM NaCl. E): Michaelis-Menten plots of *Ba*PurE, *Ft*PurE and *Yp*PurE 5 mM phosphate and 25 mM NaCl.

4.3.7. K_m and K_{cat}

For *Ba*PurE, the K_m was 10.8 $\pm$ 3.2 μM (n = 7) in 25T-0, 9.1 μM in 5P-50, 20.9 μM in 25 T-50 and 16.0 $\pm$ 4.5 (n = 2) in 5P-150 (Figure 4.8 A, Figure 4.8 B and TABLE XII). For *Ft*PurE, the K_m was 6.2 μM in 5P-50, 11.2 μM in 25T-50 and 11.2 $\pm$ 0.5 μM (n = 2) in 5P-150. The K_m was not determined in 25T-0 due to low activity. *For Yp*PurE the K_m was 16.4 $\pm$ 5.3 μM (n = 3) in 25T-0, 16.6 μM in 5P-50, 11.3 in 25T-50 and 10.1 μM in 5P-150 (Figure 4.8A and Figure 4.8 B). K_m in 5P-50 and 25T-50 were determined once.

4.3.8. Salt Effect on Enzyme Activity

The specific activity of *Ba*PurE was shown to be 9.9 μmol. min^{-1}. mg^{-1} in low ionic strength buffer (conductivity = 700 μMHO) and increases to 26.5 μmol. min^{-1}. mg^{-1} in a medium low ionic strength buffer (conductivity = 5300 μMHO) and decreases again to 15.1 μmol. min^{-1}. mg^{-1} in high ionic strength buffer (conductivity = 13000 μMHO). The specific activity of *Ft*PurE displayed the same variation and was shown to be 4.2 μmol. min^{-1}. mg^{-1} in low ionic strength buffer and increases to 21.8 μmol. min^{-1}. mg^{-1} in a medium ionic strength buffer and decreases again to 15.1 μmol. min^{-1}. mg^{-1} in high ionic strength buffer . For *Yp*PurE the specific activity of was shown to be 12.2 μmol. min^{-1}. mg^{-1} in low ionic strength buffer and increases to 27.4 μmol. min^{-1}. mg^{-1} in a medium ionic strength buffer and decreases again to 13.2 μmol.min^{-1}. mg^{-1} in high ionic strength buffer (TABLE XII; Figure 4.9).

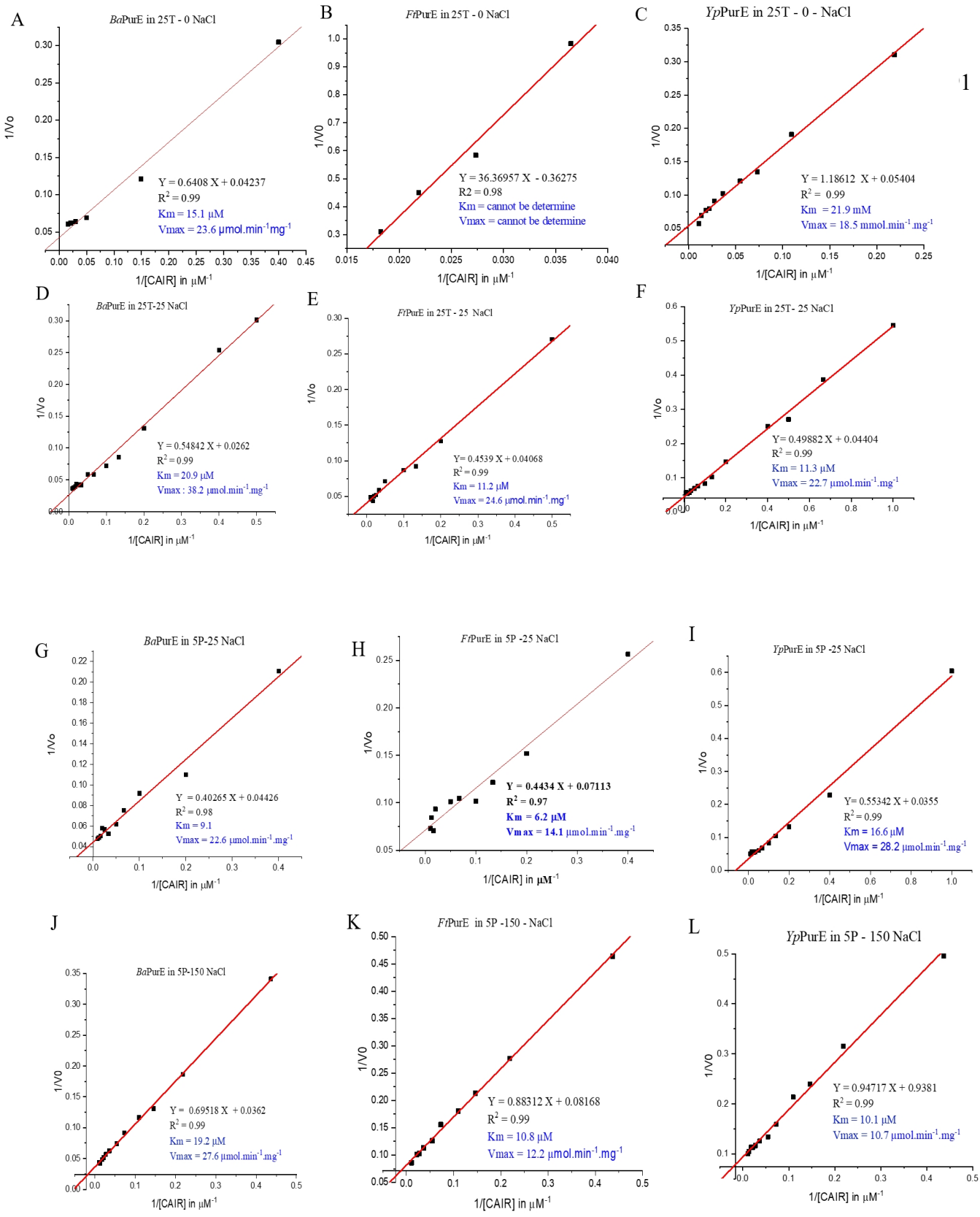
A
BaPurE in 25T - 0 NaCl
Y = 0.6408 X + 0.04237
R2 = 0.99
Km = 15.1 µM
Vmax = 23.6 µmol.min-1mg-1
1/Vo
1/[CAIR] in µM-1
B
FtPurE in 25T - 0 NaCl
Y = 36.36957 X - 0.36275
R2 = 0.98
Km = cannot be determine
Vmax = cannot be determine
1/V0
1/[CAIR] in µM-1
C
YpPurE in 25T - 0 - NaCl
Y = 1.18612 X + 0.05404
R2 = 0.99
Km = 21.9 mM
Vmax = 18.5 mmol.min-1.mg-1
1/V0
1/[CAIR] in µM-1
D
BaPurE in 25T-25 NaCl
Y = 0.54842 X + 0.0262
R2 = 0.99
Km = 20.9 µM
Vmax : 38.2 µmol.min-1.mg-1
1/Vo
1/[CAIR] in µM-1
E
FtPurE in 25T - 25 NaCl
Y= 0.4539 X + 0.04068
R2 = 0.99
Km = 11.2 µM
Vmax = 24.6 µmol.min-1.mg-1
1/Vo
1/[CAIR] in µM-1
F
YpPurE in 25T- 25 NaCl
Y= 0.49882 X + 0.04404
R2 = 0.99
Km = 11.3 µM
Vmax = 22.7 µmol.min-1.mg-1
1/Vo
1/[CAIR] in µM-1
G
BaPurE in 5P-25 NaCl
Y = 0.40265 X + 0.04426
R2 = 0.98
Km = 9.1
Vmax = 22.6 µmol.min-1.mg-1
1/Vo
1/[CAIR] in µM-1
H
FtPurE in 5P -25 NaCl
Y = 0.4434 X + 0.07113
R2 = 0.97
Km = 6.2 µM
Vmax = 14.1 µmol.min-1.mg-1
1/Vo
1/[CAIR] in µM-1
I
YpPurE in 5P -25 NaCl
Y= 0.55342 X + 0.0355
R2 = 0.99
Km = 16.6 µM
Vmax = 28.2 µmol.min-1.mg-1
1/Vo
1/[CAIR] in µM-1
J
BaPurE in 5P-150 NaCl
Y = 0.69518 X + 0.0362
R2 = 0.99
Km = 19.2 µM
Vmax = 27.6 µmol.min-1.mg-1
1/V0
1/[CAIR] in µM-1
K
FtPurE in 5P -150 - NaCl
Y = 0.88312 X + 0.08168
R2 = 0.99
Km = 10.8 µM
Vmax = 12.2 µmol.min-1.mg-1
1/V0
1/[CAIR] in µM-1
L
YpPurE in 5P - 150 NaCl
Y = 0.94717 X + 0.9381
R2 = 0.99
Km = 10.1 µM
Vmax = 10.7 µmol.min-1.mg-1
1/V0
1/[CAIR] in µM-1

Figure 4.8: Double reciprocal linear regression (Lineweaver Burk plot). The K_m and Vmax were obtained from the linear regression. Vmax was calculated as 1/ V_o-intercept and K_m as -1/[CAIR]-intercept. The correlation coefficient (R^2) was used to access the reliability of the data. A): *Ba*PurE in 25 mM Tris, 0 mM NaCl; B): *Ft*PurE in 25 mM Tris, 0 mM NaCl; C): *Yp*PurE in 25 mM Tris, 0 mM NaCl. D): *Ba*PurE in 25 mM Tris, 25 mM NaCl; E): *Ft*PurE in 25 mM Tris, 25 mM NaCl; F): *Yp*PurE in 25 mM Tris, 25 mM NaCl; G): *Ba*PurE in 5 mM phosphate with 25 mM NaCl; H): *Ft*PurE in 5 mM phosphate with 25 mM NaCl; I): *Yp*PurE in 5 mM phosphate with 25 mM NaCl; J): *Ba*PurE in 5 mM phosphate with 150 mM NaCl; K): *Ft*PurE in 5 mM phosphate with 150 mM NaCl; L): *Yp*PurE in 5 mM phosphate with 150 mM NaCl.

TABLE XII: MICHAELIS-MENTEN CONSTANT (K_M). A MAXIMUM INITIAL RATE (V_{MAX})[A], TURN OVER NUMBER (K_{CAT})[B] AND SPECIFIC ACTIVITY (SA) OF *BA*PURE, *FT*PURE, AND *YP*PURE WITH SUBSTRATE CAIR (30 MM) IN BUFFERS WITH DIFFERENT IONIC STRENGTH (CONDUCTIVITY) AT 21 ^{O}C.

Buffer	Conductivity (µMHO)	PurE	K_m (µM)	V_{max} (µmol min^{-1} mg^{-1})	K_{cat} (min^{-1})	K_{cat} / K_m x 10^7 (M^{-1} min^{-1})	SA 30 µM (µmol mg^{-1} min^{-1})
25T-0	1300	*Ba*	10.8 ± 3.2 (7)[c]	17.6 ± 4.3 (7)	306 ± 75 (7)	2.9 ± 0.3 (7)	11.2 ± 2.6 (8)
		Ft	ND[d]	ND	ND	ND	4.0 ± 2.4 (10)
		Yp	16.4 ± 5.3 (3)	13.2 ± 4.7 (3)	303 ± 133 (3)	1.4 ± 0.4	8.3 ± 1.6 (8)
5P-50	5400	*Ba*	9.1	22.6	391	4.3	19.0
		Ft	6.2	14.1	247	4.0	10.7
		Yp	16.6	28.2	514	3.1	16.9
25T-50	5700	*Ba*	20.9	38.2	661	3.2	23.8
		Ft	11.2	24.6	430	3.8	16.8
		Yp	11.3	22.7	414	3.7	15.3
5P-150	13000	*Ba*	16.0 ± 4.5 (2)	21.8 ± 8.3 (2)	377 ± 143 (2)	2.3 ± 0.2 (2)	13.5 ± 3.7 (5)
		Ft	11.2 ± 0.5 (2)	12.7 ± 0.6 (2)	221 ± 11 (2)	2.0 ± 0.0 (2)	9.9 ± 1.2 (5)
		Yp	10.1	10.7	181 ± 19 (2)	1.6 ± 0.6 (2)	8.7 ± 2.2 (6)

[a] K_m and V_{max} values were obtained from double reciprocal plots.

[b]k_{cat} values were calculated from V_{max} /$[PurE]_{total}$. [PurE] = 10 nM per monomer or 1.23 nM per octomer.

[c]n value is shown in parenthesis.

[d]ND = Activity was too low to be measured.

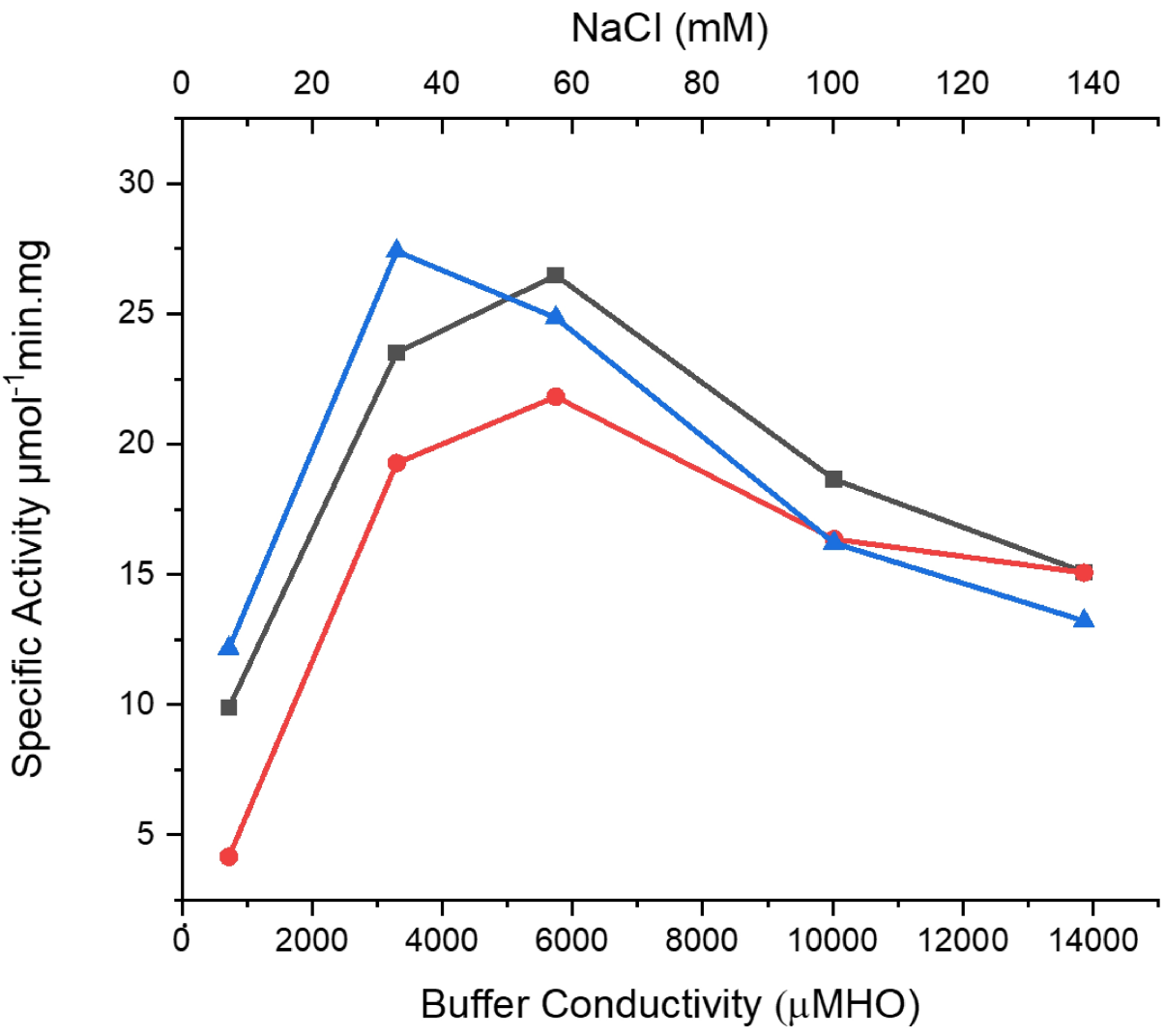

Figure 4.9: The specific activity of enzymes in increasing buffer ionic strength (conductivity) in 5 mM phosphate buffer with variable amount of NaCl added. Black squares represent the specific activity of *Ba*PurE, red circle represent the specific activity of *Ft*PurE and blue triangles represent the specific activity of *Yp*PurE.

4.3.9 Inhibition Study

The activity of *Ft*PurE in 25T-0 was determined with and without LC5. The activity of *Ft*PurE with LC5 was found to be 80% that of the activity of *Ft*PurE without LC5. This 20% inhibition is comparable to that of LC5 on *Ba*PurE (Kim *et al.*, 2015).

4.3.10. Protein Surface Hydrophobicity

The average SYPRO Orange fluorescence intensity for *Ba*PurE (25 μM) samples was 280 $\pm$ 2 au (n = 12), for *Ft*PurE was 107 $\pm$ 2 au (n = 12) and for *Yp*PurE was of 37 $\pm$ 2 au (n = 12) (Figure 4.10). The surface hydrophobicity representation shows the deep orange as highly hydrophobic, light orange as somewhat hydrophobic, white as neutral and blue as hydrophilic. Between the three structures. The qualitative nature of the surface display made it difficult to visualize hydrophobicity quantitatively.

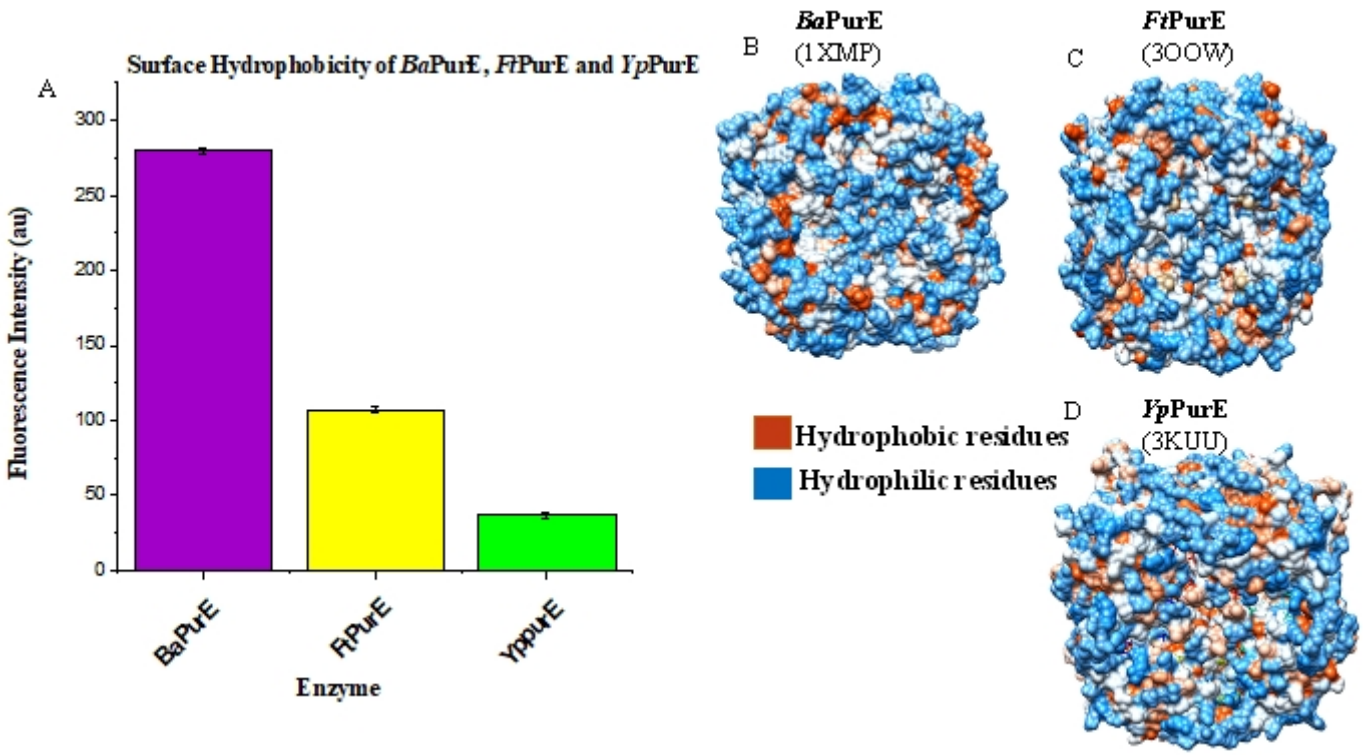

Figure 4.10: Surface hydrophobicity evaluation. Each of the protein was prepared in 5 mM phosphate with 0 mM NaCl or 150 mM NaCl. 25 µM sample was prepared with 5 X SYPRO Orange and the fluorescence intensity was recorded at the excitation of 472 and emission of 570 nm for 3 min at 25 °C. A): Fluorescence intensity of *Ba*PurE, *Ft*PurE and *Yp*PurE. The reported intensities are that of the average of three separate samples. B): Hydrophobic residue on the surface of *Ba*PurE, 1XMP; C): Hydrophobic residue on the surface of *Ft*PurE, 3OOW; D): Hydrophobic residue on the surface of *Yp*PurE, 3KUU. The visual representation was generated by Chimera.

4.4. Discussion

Our goal was to characterize the three homologous (*Ba*PurE, *Ft*PurE and *Yp*PurE) enzymes and identify similarities as well as distinct characteristics that can be exploited in the development of a common inhibitor as well as separate, specific inhibitor for each. With the accessibility of genome sequencing, valid target identification as well are high throughput crystallization is readily available (Anderson *et al.*, 2003). Choosing the optimal condition as well as type of inhibitor for each target still require the full biochemical characterization of the target. The activity of PurE in the *de novo* purine biosynthesis pathway support the growth and the virulence of bacteria like *Bacillus anthracis* and *Yersinia pestis* in murines (Samant *et al.*, 2008; Jenkins *et al.*, 2012) as well as the growth of mycobacterium tuberculosis (Sasseti *et al.*, 2003). Given the importance of PurE in bacterial growth and virulence, finding an inhibitor for this enzyme is necessary.

Our data showed that in a buffer with about 50 mM NaCl to give a conductivity between 5300 to 5400 μMHO, all three enzymes exhibit an optimal activity. Under the same buffer condition, the three enzymes show lower stability as compared with buffers with higher salt concentrations as shown by the secondary and tertiary elements unfolding. The slight difference in structural stability for *Ft*PurE and *Yp*PurE in the different buffer was statistically significant. The homogeneity of *Ba*PurE in solution also dependent on salt content in the buffer.

In general, the three enzymes exhibited similar kinetic as well as structural stability properties in solution. It is thus possible to develop common inhibitors for all 3 enzymes.

However, the surface hydrophobicity showed that *Ba*PurE exhibited almost three times the number of hydrophobic patches on its surface than *Ft*PurE and almost eight times the amount on the

surface of *Yp*PurE in all buffer conditions. Given that the three homologous enzymes are more than 50 percent identical in amino-acid sequence, three to eight times more in surface hydrophobic residues signify a disproportionate preference of the hydrophobic residues on the surface of *Ba*PurE. Thus, we may take advantage of this difference to develop inhibitors that can selectively bind to the *Ba*PurE, but not the other two enzymes, to allow a narrow spectrum antibiotic development.

To our knowledge, this is the first time that PurE for *B. anthracis*, *F. tularensis* and *Y. pestis* have been fully characterized and the molecular information uncovered in this study will be invaluable in the selection of inhibitors.

4.5. Conclusion

Optimization of assay buffer condition and the identification of the appropriate biochemical method are the first essential steps in the long screening process for narrow and broad spectrum antibiotic discovery. PurE has been shown to be a good target for growth and virulence attenuation. To find a potent inhibitor for this enzyme in different species, it is important to find the similarities and differences in the molecular structure that will aid in the selection of the appropriate inhibitors. The data showed a significant difference in the number of hydrophobic residues on the surface of the three proteins that can be explored to select and improve a specific inhibitor. We found that all three enzymes exhibited optimum activity in medium ionic strength buffer with 50 mM NaCl in the buffer, and we found that the homologous enzyme have similar stability in high salt buffer. The structural features uncovered in this study will be useful in the selection of lead compounds.

4.6. Future Directions

The next step is to screen the inhibitors of *Ba*PurE on *Ft*PurE and *Yp*PurE for level of inhibition. It will be important to identify the residues that have the greatest impact on the protein surface hydrophobicity and thus to develop selective inhibitors.

LIST OF REFERENCES

Anderson, C. A. (200.) The Process of Structure-Based Drug Design. *Chem & Bio*. 10, 787-797.

Brugarolas, P., Duguid, M. E., Zhang, W., Poor, B. C. and He, C. (2011). Structural and Biochemical Characterization of N^5-Carboxyaminoimidazole Ribonucleotide Synthetase and N^5-Carboxyaminoimidazole Ribonucleotide Mutase from *Staphylococcus aureus*. *Acta Cryst*. D67, 707- 715.

Chellat, F.M., Raguz, L. and Ried, R. (2016). Targeting Antibiotic Resistance. *Angew. Chem. Int. Ed.* 55, 6600 - 6626.

Chen, Y., Pi, B., Zhou, H., Yu, Y. and Li, L. (2009). Triclosan Resistance in Clinical Isolates of Acinetobacter baumannii. *J. of Med. Microbio*. 58, 1086-1091.

Ciusa, L. M., Furi, L., Knight, D., Decorosi, F., Fondi, M., Raggi, C., Coelho, R. J., Aragones, L., Moce, L., Visa, P., Freitas, T. A., Baldassarri, L., Fani, R., Viti, C., Orefici, G., Martinez, L. J., Morrissey, I. and Oggioni, R. M. (2012). A Novel Resistance Mechanism to Triclosan that Suggests Horizontal Gene Transfer and Demonstrates a Potential Selective Pressure for Reduced Biocide Susceptibility in Clinical Strains of *Staphylococcus aureus*. *Int. J. of Antimicrob. Agents*. 40, 210 - 220.

Cloete, R., Oppon, E., Murungi, E., Schubert, W. and Christoffels, A. (2016). Resistance Related Metabolic Pathways for Drug Target Identification in Mycobacterium tuberculosis. *BMC Bioinfo.* 17, 1-10.

Craig, L. N., (1997). Target Site Selection in Transposition. *Annu. Rev. Biochem*. 66, 437-474.

Davies, J. (2006). Where have all the Antibiotics Gone? *Can. J. Infect. Dis. Med. Microbiol*.17, 287-290.

Fernandes, P. and Martens, E. (2017). Antibiotics in late Clinical Development Biochemical. *Pharmaco.* 133, 152-163.

Freire-Moran, L., Aronssona, B., Manz, C., Gyssens, C. I., So, D. A., Monnete, L. D. and Cars, O. (2011). Critical Shortage of New Antibiotics in Development Against Multidrug-Resistant Bacteria -Time to React is Now. *Drug Resist. Updates.* 14, 118-124.

Galimand, M., Carniel, E. and Courvalin, P. (2006). Resistance of *Yersinia pestis* to Antimicrobial Agents. *Antimicrob. Agent and Chemother*. 50, 3233-3236.

Gerusz, V., Denis, A., Faivre, F., Bonvin, Y., Oxoby, M., Briet, S., LeFralliec, G., Oliveira, C., Desroy, N., Raymond, C., Peltier, L., Moreau., F., Escaich, S., Vongsouthi, V., Floquet, S., Drocourt, E., Walton, A., Prouvensier, L., Saccomani, M., Durant, L., Genevard, J., Sam-Sambo, V. and Soulama-Mouze C. (2012). From Triclosan Toward the Clinic: Discovery of Nonbiocidal, Potent FabI Inhibitors for the Treatment of Resistant Bacteria. *J. Med. Chem*. 55, 9914-9928.

Heath, R. J. and Rock, C.O. (2000). Microbiology: A Triclosan-Resistant Bacterial Enzyme. *Nat*. 406, 145–146.

Hevener, K. E., Mehboob, S., Su, P. C., Truong, K., Boci, T., Deng, J. P., Ghassemi, M., Cook, J. L. and Johnson, M. E. (2012). Discovery of a Novel and Potent Class of Francisella tularensis enoyl-reductase (FabI) Inhibitors by Molecular Shape and Electrostatic Matching. *J. Med. Chem*. 55, 268−279.

Hoskins, A. A., Morar, M., Kappock, T. J., Mathews, I., Zaugg, J. B., Barder, T. E., Peng, P., Okamoto, A., Ealick, S. E. and Stubbe, J. (2007). N -CAIR mutase: Role of CO_2 Binding 5 Site and Substrate Movement in Catalysis. *Biochem*. 46, 2842 - 2855.

Ikaheimo, I., Syjala., H., Karhukorpi, J., Schildt, R. and Koskela, M.(2000). In Vitro Antibiotic Susceptibilityof *Francisella tularensis* Isolated from Human and Animals. *J. of Antimicrob. Chemo. 46*, 287-290.

Jenkins, A., Cote, C., Twenhafel, N., Merkel, T., Bozue, J. and Welkos, S. (2011). Role of Purine Biosynthesis in *Bacillus anthracis* Pathogenesis and Virulence *Infect. and Immun*. 79, 153-166.

Kaur, D., Mathew, S., Nair, C. G. S., Begum, A., Jainanarayan, A. K., Sharma, M. and Samir K. Brahmachari, S. K. (2017). Structure-based Drug Discovery for Designing Leads for the Non-toxic Metabolic Targets in Multi Drug Resistant Mycobacterium tuberculosis. *J. Transl. Med*. 15, 261.

Kim, A., Nina M. Wolf, M. N., Zhu, T., Michael E. Johnson, E. M., Deng, J., Cook, L. J. and Fung, W-M. L. (2015). Identification of *Bacillus anthracis* PurE Inhibitors with Antimicrobial Activity. *Bioorganic & Medicinal Chemistry*. 23, 1492- 1499.

Kohanski, A. M., Dwyer, J. D. and Collins J. J. (2010). How antibiotics kill bacteria: from targets to networks. *Nat. Rev. Microbio*. 8, 423-435.

Kroemer R.T. (2007). Structure-based Drug Design: Docking and Scoring. *Curr Protein Pept Sci*. 8, 312–328.

Lewis, K. (2013). Platforms for antibiotic discovery. *Nat. Rev. Drug Discov*. 12, 371-387.

Lo, M.-C., Aulabaugh, A., Jin, G., Cowling, R., Bard, J., Malamas, M. and Ellestad, G. (2004) Evaluation of Fluorescence-based Thermal Shift Assays for Ht Identification in Drug Discovery. *Anal. Biochem.* 332, 153 - 159.

Mathews, I. I., Kappock, T. J., Stubbe, J. and Ealick, S. E. (1999). Crystal Structure of *Escherichia coli* PurE, an Unusual Mutase in the Purine Biosynthetic Pathway. *Struct.* 7, 1395 - 1406.

McBride, E. M. (1984) Microbial flora of In-Use Soap Products. *App. and Environ. Microbio*. 48, 338-341.

Mesarich, H.C., Rees-George, J., Gardner, P. P., Ghomi, F.A., Gerth, M. L., Andersen, M. T., Rikkerink, H. A. E., Fineran, C. P. and Templeton, D. M. (2017). Transposon Insertion Libraries for the Characterization of Mutants from the Kiwi Fruit Pathogen Pseudomonas syringae pv. actinidiae. *PloS One* 12, e0172790.

Meyer, E., Leonard, N. J., Bhat, B., Stubbe, J., and Smith, J. M. (1992). Purification and Characterization of the PurE, PurK and PurC Gene Products: Identification of a Previously Unrecognized Energy Requirement in the Purine Biosynthetic Pathway. *Biochem*. 31, 5022-5032.

Miles, A. A., Misra, S. S., and Irwin, J.O. (1938). The Estimation of the Bactericidal Power of the Blood. *The J. of Hygiene.* 38, 732-749.

Mistry, L.T., Truong, L., Ghosh, K.A., Johnson, E.M., and Mehboob, S. (2017). Benzimidazole-Based FabI Inhibitors: A Promising Novel Scaffold for Anti-staphylococcal Drug Development. *ACS Infect. Dis*. 3, 54-61.

Nair, D., Memmi, G., Hernandez, D., Bard, J., Beaume, M., S Gill, S., Francois, P., and Cheung, L. A. (2011). Whole-Genome Sequencing of *Staphylococcus aureus* Strain RN4220, a Key Laboratory Strain Used in Virulence Research, Identifies Mutations That Affect Not Only Virulence Factors but Also the Fitness of the Strain. *J. of Bacterio*. 193, 2332-2335

Neggers, J. E., Kwanten, B., Dierckx, T., Noguchi, H., Voet, A., Bral, L., Minner, K., Massant, B., Kint, N., Delforge, M., Vercruysse, T., Baloglu, E., Senapedis, W., Jacquemyn, M., and Daelemans, D. (2018). Target Identification of Small Molecules Using Large-scale CRISPR-Cas Mutagenesis Scanning of Essential Genes. *Nat Com*. 9, 502.

Opijnen, V. T., and Camilli, A. (2013).Transposon Insertion Sequencing:A New Tool for Systems-level Analysis of Microorganisms. *Nat Rev Microbiol*. 11, 1-17.

Price, B. L., Vogler, B., Pearson, T., Busch, D.J., Schupp, M. J. and Keim, P. (2003). In Vitro Selection and Characterization of *Bacillus anthracis* Mutants with High-Level Resistance to Ciprofloxacin. *Antimicrob. Agent and Chemother*. 47, 2362-2365.

Priyadarshi, A., Kim, E.E., and Hwang, Y.K. (2009). Structural Insights into *Staphylococcus aureus* enoyl-ACP Reductase (FabI), in Complex with NADP and Triclosan. *Prot.* 480-486.

Quainoo, S., Coolen, J. P. M., van Hijum, S. A. F. T., Huynen,, M. A., Melchers, W. J. G., van Schaik, W. and Wertheim, H. F. L. (2017). Whole-genome sequencing of bacterial pathogens: the future of nosocomial outbreak analysis. *Clin Microbiol. Rev*. 30, 1015–1063.

Rogers, B. G., Carroll, P. M. And Bruce, D. K. (2012). Enhancing the utility of existing antibiotics by targeting bacterial behaviour? *Brit. J. of Pharmaco*. 165, 845-857.

Samant, S., Lee, H., Ghassemi, M., Chen, J., Cook, J. L., Mankin, A. S., and Neyfakh, A. A. (2008). Nucleotide Biosynthesis is Critical for Growth of Bacteria in Human Blood. *PloS Pathog.* 4, e37.

Sassetti, M. C., Boyd, H. D., and Rubin, J.E. (2003). Genes Required for Mycobacterial Growth Defined by High Density Mutagenesis. *Molecul. Microbio*. 48, 77-84.

Schiebel, J., Chang, A., Lu, H., Baxter, V. M., Tonge, J. P., and Kisker, C. (2012). *Staphylococcus aureus* FabI: Inhibition, Substrate Recognition and Potential Implications for *In Vivo* Essentiality. *Struct.* 20, 802-813.

Skovgaard, S., Nielsen, L. N., Larsen, M. H., Skov, R. L, Ingmer, H. and Westh, H. (2013). *Staphylococcus epidermidis* Isolated in 1965 Are More Susceptible to Triclosan than Current Isolates. *PLoS ONE.* 8, e62197.

Sullivan, K. L., Huma, L., Mullins, E. A., Johnson, M. E., and Kappock, T. J. (2014). Metal Stopping Reagents Facilitate Discontinuous Activity Assays of the *de novo* Purine Biosynthesis Enzyme PurE. *Anal. Biochem*. 452, 43 - 45.

Xu, H., Sullivan, T., Sekiguchi, J., Kirikae, T., Ojima, I., Mao, W., Rock, L.F., Alley, K. R. M. Johnson, F., Walker, G.S., and Tonge, J.P. (2008). Mechanism and Inhibition of *Sa*FabI, the Enoyl Reductase from *Staphylococcus aureus*. *Biochem*. 47, 4228-4236

Zhang, Y., Morar, M., and Ealick, S. E. (2008a). Structural Biology of the Purine Biosynthetic Pathway. *Cell. Mol. Life Sci.* 65, 3699 - 3724.

Zhang, Y., White, R. H., and Ealick, S. E. (2008b). Crystal Structure and Function of 5-Formaminoimidazole-4-Carboxamide Ribonucleotide Synthetase from *Methanocaldococcus jannaschii*. *Biochem.* 47, 205 - 217.

Zheng, X.S., Chan,T., and Zhou, H.H. (2004). Genetic and Genomic Approaches to Identify and Study the Targets of Bioactive Small Molecules. *Chem and Bio.* 11, 609-618.

Zhu, C., Gaoa, Y., Lic, H., Meng, S., Lia, L., S. Franciscoa, S. J, and Zeng, C. X. (2016). Characterizing Hydrophobicity of Amino acid Side Chains in a Protein Environment via Measuring Contact Angle of a Water Nanodroplet on Planar Peptide Network. *Proc. Nat. Acad. Sci.* 113, 12946-12951.

APPENDICES

APPENDIX A

Original Research

An Efficient and Economical Assay to Screen for Triclosan Binding to FabI

Journal of Biomolecular Screening
2016, Vol. 21(4) 391–398

DOI: 10.1177/1087057115615085
jbx.sagepub.com
SAGE

Robel D. Demissie[1], Pauline Kabre[1], Micheal L. Tuntland[1], and Leslie W.-M. Fung[1]

Abstract

Triclosan is an effective inhibitor for enoyl acyl carrier protein reductase (ENR) in fatty acid biosynthesis. Triclosan-resistant mutants of ENR have emerged. Thus, it is important to detect these triclosan-resistant mutations in ENR. Generally, enzyme activity assays on the mutants are used to determine the effect of triclosan on ENR activity. Since the substrates are linked to acyl carrier protein (ACP), the assays are challenging due to the need to prepare the ACP and link it to the substrates. Non-ACP-linked (coenzyme A [CoA]-linked) substrates can be used in some ENR, but not in all. Consequently, screening for triclosan-resistant mutants is also challenging. We have developed a simple thermal shift assay, which does not use ACP-linked substrates, to determine the binding ability of triclosan to the ENR active site, and thus it can be used for screening for triclosan-resistant mutants. *Staphylococcus aureus* FabI enzyme and its mutants were used to demonstrate the binding ability of triclosan with $NADP^+$ to FabI. The direct correlation between the binding ability and enzyme activity was demonstrated with *Francisella tularensis* FabI. This method may also be applied to select effective triclosan analogues that inhibit ENR activity.

Keywords

antibacterial drugs, fluorescence methods, pharmacology, ligand binding, receptor binding, high-content screening, protein chemistry, protein labeling, proteomics

Introduction

Triclosan, 5-chloro-2-(2,4-dichlorophenoxy)phenol or 2,4,4′-trichloro-2′-hydroxydiphenyl ether, has activity against many, but not all, types of Gram-positive and Gram-negative bacteria,[1–3] including methicillin-resistant Gram-positive *Staphylococcus aureus* strains,[4] *Mycobacterium tuberculosis*,[5,6] and *Plasmodium falciparum*.[7] It has also been reported that triclosan is cytotoxic to breast cancer cells.[8] The mode of action of triclosan on bacterial cells is well studied[3,9–12] and it targets enoyl-acyl carrier protein (ACP) reductase (ENR), which is encoded by the gene FabI[11] and catalyzes the final step of the type II (bacterial) fatty acid biosynthesis pathway to reduce the double bond of enoyl-ACP to single-bond acyl-ACP with cofactor NAD(P)H.[13] Triclosan inhibits the enzyme action by forming a stable ternary complex with the oxidized cofactor $NAD(P)^+$ and the side chains of FabI active site residues.[13] The triclosan effect on the human fatty acid synthase study suggests that inhibitors like triclosan may have chemotherapeutic potential.[8]

Due to its usefulness toward inhibiting bacterial growth, triclosan has been widely used,[14] and species resistant to triclosan can arise from mutations in ENR/FabI. For example, *S. aureus* FabI (*Sa*FabI) mutations such as A95V, I193S, and F204S have been identified in selection experiments,[15] suggesting that other mutations in *S. aureus* may also survive triclosan treatment and need to be identified. To determine whether triclosan inhibits certain ENR/FabI mutants, enzymatic activity in the presence of triclosan is commonly measured to determine triclosan inhibition activity. For ENR/FabI enzymes of many species such as *Escherichia coli* and *Francisella tularensis*, it is possible to substitute the substrate enoyl-ACP with coenzyme A (CoA) esters, such as crotonoyl-CoA, as experimental substrates,[16,17] but with much reduced activities.[17] For the ENR/FabI of species where the substrate cannot be substituted with crotonoyl-CoA, such as that of *S. aureus*, substrate enoyl-ACP needs to be used to identify triclosan-resistant mutations or to select effective triclosan analogues as useful antibiotic leads. Obtaining ACP-linked substrates involves the purification of apo-ACP from cellular extract followed by either enzymatic-driven[15,18] or chemically driven[19] linkage of the enoyl chain to the ACP. Consequently, studies that require enoyl-ACP for substrate are laborious. It is speculated that *Sa*FabI diverges from the classical FabI structure and behavior owing to the wealth of branched-chain

[1]University of Illinois at Chicago, Chicago, IL, USA

Received Aug 24, 2015, and in revised form Oct 6, 2015. Accepted for publication Oct 11, 2015.

Corresponding Author:
Leslie W.-M. Fung, Department of Chemistry, University of Illinois at Chicago, 845 West Taylor Chicago, Chicago, IL 60607, USA.
Email: lfung@uic.edu

fatty acids occupying the membranes of *S. aureus*.[20] If so, the traits of *Sa*FabI may be repeated in other organisms with similar membrane compositions, such as the genus *Bacillus*, in which all of the species are with branched fatty acid chains in their membranes.[20,21]

We have developed a thermal shift method to determine whether triclosan binds specifically to the active site of FabI without the use of enoyl-ACP. This thermal shift assay is a sensitive fluorescence-based assay,[22] making it amenable to high-throughput screening. We show that triclosan, together with $NADP^+$, binds to *Sa*FabI wild-type (WT) and triclosan-sensitive mutant M99T, but not to triclosan-resistant mutants A95V, I193S, and F204S. We used the *F. tularensis* FabI (*Ft*FabI) system, WT and a triclosan-resistant mutant, to demonstrate the direct correlation between their thermal shifts and enzyme activities. We also show that the thermal shift is not due to the fluorescent probe used in the assay. We demonstrate that this simple and economical method, without using enoyl-ACP substrate, can be used to screen for triclosan-resistant mutants of ENR/FabI.

Method and Materials

Recombinant Plasmids

The *Sa*FabI gene (NWMN_0881) was amplified from *S. aureus* gDNA and inserted in a pET-15b vector to express recombinant His-tagged *Sa*FabI WT. An AFN-1252-resistant, but triclosan-sensitive M99T mutation[23] and triclosan-resistant mutations A95V, I193S, and F204S[15] were constructed with a site-directed primer mutagenesis method.[24] The *Ft*FabI gene (FTT_0782) was amplified from *F. tularensis* gDNA and inserted in a pET-15b vector to express recombinant His-tagged *Ft*FabI WT. The A92V mutation, a homologous mutation to the *E. coli* FabI (*Ec*FabI) G93V triclosan-resistant mutation,[10] was also constructed using the same method. All resulting gene constructs were sequenced at the University of Illinois at Chicago Research Resource Center (UIC RRC).

Protein Expression and Purification

E. coli competent cells (BL21 CodonPlus(DE3)-RIL; Zymo, Irvine, CA) were used to express both WT and mutant proteins of both *S. aureus* and *F. tularensis*. An overnight culture (100 mL) was added to fresh lysogeny broth medium (1 L in a 2.8 L culture flask). Cells were grown to an optical density at 600 nm of 0.5–0.8 at 37 °C with shaking. Isopropyl β-D-1-thiogalacto-pyranoside was then added to a final concentration of 0.5–1.0 mM to induce protein expression. Cells were grown for an additional 3 h after induction and harvested at 4 °C.

The cells in 50 mM sodium phosphate buffer at pH 8 with 300 mM NaCl (phosphate buffer) plus 10 mM imidazole and 1% Triton X-100 were sonicated for 20 min on ice slurry. The mixture was centrifuged at 35,000 *g* for 30 min to give cell lysate. The lysate was loaded to a nickel affinity column (Qiagen) precquilibrated with the phosphate buffer plus 10 mM imidazole. The His-tagged protein was released from the column with the phosphate buffer plus 300 mM imidazole and dialyzed in 50 mM Tris buffer at pH 8 with 100 mM NaCl (Tris buffer) before concentrating to ~100–300 μM. The protein samples were frozen dropwise (20 μL) in liquid nitrogen and stored at –80 °C until needed. The protein purity was monitored with 16% polyacrylamide gel electrophoresis, and the molecular mass of the proteins was checked with high-resolution mass spectrometry at UIC RRC.

The concentration of each protein was determined from the absorbance at 280 nm and the extinction coefficient derived from its sequence, with 13,410 M^{-1} cm^{-1} for *Sa*FabI WT, A95V, M99T, I193S, and F204S, and 17,420 M^{-1} cm^{-1} for *Ft*FabI WT and A92V.

Enzymatic Assay for FtFabI

The published method for the enzymatic activity of *Ec*FabI WT using crotonyl-CoA as substrate[12] was adapted for that of *Ft*FabI. Briefly, *Ft*FabI WT (450 nM) or A92V (450 nM and 1 μM) in Tris buffer was incubated with 250 μM NADH and 200 μM NAD^+, without and with triclosan (2.5 molar ratio to FabI; triclosan from Sigma, St. Louis, MO, 72779-5G-F), for 5 h at 4 °C.[12] Since triclosan was in DMSO, both samples also consisted of 1% (v/v) DMSO. The relatively long incubation time (5 h) was consistent with the condition used for *Sa*FabI in the thermal shift assay to ensure the complex formation among *Sa*FabI, $NADP^+$, and triclosan. It is known that triclosan exhibits its inhibition activity by forming a tight complex with FabI and $NAD(P)^+$, and it is also known that $NAD(P)^+$ itself exhibits relatively low affinity toward FabI and is in competition for the binding site.[12,20] At the end of the incubation, the mixtures were warmed to 25 °C (in about 10 min), followed by the addition of an experimental substrate, crotonyl-CoA (200 μM final concentration; Sigma, C6146-5MG), to start the reaction. The decrease in NADH concentration, upon oxidation to NAD^+ during the catalytic reaction, was monitored by UV absorption at 340 nm (A_{340}) for ~2.5 min with a plate reader (Victor^3 V; PerkinElmer, Waltham, MA). The slope of a linear fit of A_{340} versus time plot ($\Delta A_{340}/\Delta$min) was converted to a rate of NADH consumed, using the NADH extinction coefficient of 6220 M^{-1} cm^{-1}. Specific activity for *Ft*FabI was calculated as the rate of NADH consumed (μmol/min) per milligram of *Ft*FabI.

Thermal Shift Assay for Binding Triclosan

Samples consisting of *Sa*FabI (7 μM in Tris buffer) and 5× Sypro Orange (Invitrogen, Grand Island, NY) alone (control), or with only triclosan (100 μM) (sample-T), with only

$NADP^+$ (200 μM) (sample-N), or with both triclosan and $NADP^+$ (sample-TN), were prepared side by side, with the same batch of protein, triclosan, and Sypro Orange to reduce sample variability. The control and three samples (sample-T, sample-N, and sample-TN) also included 1% (v/v) DMSO since both Sypro Orange and triclosan stock solutions were in DMSO. Sypro Orange was supplied in DMSO as 5000× stock solution. The mixtures were incubated for 5 h at 4 °C, as in the activity studies. Some samples were incubated for only 30 min. In the *Ft*FabI samples, instead of $NADP^+$, NAD^+ was used.

The fluorescence intensity of Sypro Orange at 570 nm with excitation at 472 nm was monitored with a FP-6200 Jasco (Easton, MD) Spectrofluorometer as a function of temperature in the range of 25–75 °C. The temperature ramp rate was 1.0 °C/min. The intensity values were converted to fractions unfolded.

A Boltzmann sigmoidal fit, modeling a two-state unfolding process, was applied to the data to give transition temperatures measured by Sypro Orange (T_m^{SO}). A difference in the transition temperatures (thermal shift, ΔT_m^{SO}) between control and samples was obtained, and the ΔT_m^{SO} between control and sample-TN was used to indicate a degree of stabilization of FabI upon binding triclosan and $NAD(P)^+$ to the active site of FabI.

Effects of Sypro Orange on Thermal Unfolding

The circular dichroism (CD) ellipticity (θ) signals at 222 nm (with a Jasco J-810 Spectropolarimeter) of *Ft*FabI and *Sa*FabI (15 μM) in the Tris buffer were measured from 25 to 75 °C with a ramp rate of 1.0 °C/min. θ values were converted to fractions of unfolding, with θ at 25 °C as 0 and θ at 75 °C as 1. Again, a Boltzmann fit was applied to the data to give transition temperatures measured by CD (T_m^{CD}). Also measured were FabI samples with 5× Sypro Orange and/or 0.1% (v/v) DMSO. We were not able to do CD measurements in the presence of 1% DMSO (as in the activity assay and thermal shift assay) due to the strong CD signal from 1% DMSO. For the same reason, the CD method was not used to monitor thermal shifts of samples with and without triclosan and $NAD(P)^+$, since the samples included 1% DMSO.

Results

Enzyme Solution Properties

The polyacrylamide gel showed a band around 30 kDa for each of the seven overexpressed proteins, with 80–90% purity. High-resolution mass spectrometry results indicated that the initial methionine in the His-tag was missing in all our proteins, and the masses were within 1 Da of the expected values derived from sequences. For example, for *Sa*FabI WT, the difference between the sequence-derived mass (30,397.4 Da) and experimental mass (30,396.7 Da) was −0.7 Da. For *Sa*FabI M99T, A95V, I193S, and F204S, the sequence-derived masses were 30,367.3, 30,425.3, 30,371.3, and 30,337.3 Da, respectively, and the experimental masses were 30,366.6, 30,424.8, 30,370.6, and 30,336.6 Da, respectively.

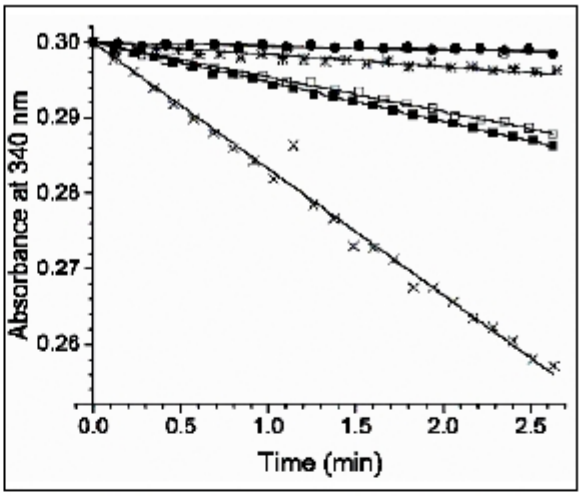

Figure 1. The decrease of 250 μM NADH absorbance upon the addition of 200 μM crotonyl-CoA by 450 nM *Ft*FabI WT with no triclosan (cross) and with 1.125 μM triclosan (asterisk). Also shown are those of 450 nM *Ft*FabI A92V with no triclosan (empty circle) and with 1.125 μM triclosan (filled circle), and an increased concentration of *Ft*FabI A92V (1 μM) with no triclosan (empty square) and with 5 μM triclosan (filled square). The slope of the linear fit of the data points ($\Delta A_{340}/\Delta$min) was converted to a rate of NADH consumed, using the NADH extinction coefficient of 6220 M^{-1} cm^{-1}. Specific activities for *Ft*FabI (WT and A92V) were calculated as the rate of NADH consumed (μmol/min) per milligram of *Ft*FabI. For *Ft*FabI WT, the activity was 0.66 μmol min^{-1} mg^{-1}. See text for details.

The *Ft*FabI WT enzyme exhibited a specific activity of 0.66 μmol min^{-1} mg^{-1} (**Fig. 1**). In the presence of triclosan, the specific activity decreased to 0.06 μmol min^{-1} mg^{-1}, with only 9% activity remaining, clearly demonstrating the inhibitory effect of triclosan on *Ft*FabI. For the A92V mutant at the concentration used for WT measurements (450 nM), the decrease of A_{340} was small, making it difficult to obtain an accurate value for inhibition (**Fig. 1**). However, with the enzyme concentration increased to 1 μM, the decrease in A_{340} as a function of time was more pronounced, and the normalized specific activity value for A92V was 0.09 μmol min^{-1} mg^{-1}. In the presence of triclosan, the specific activity was measured as 0.10 μmol min^{-1} mg^{-1}. Thus, A92V, with much reduced activity compared to that of the WT, was not inhibited by triclosan.

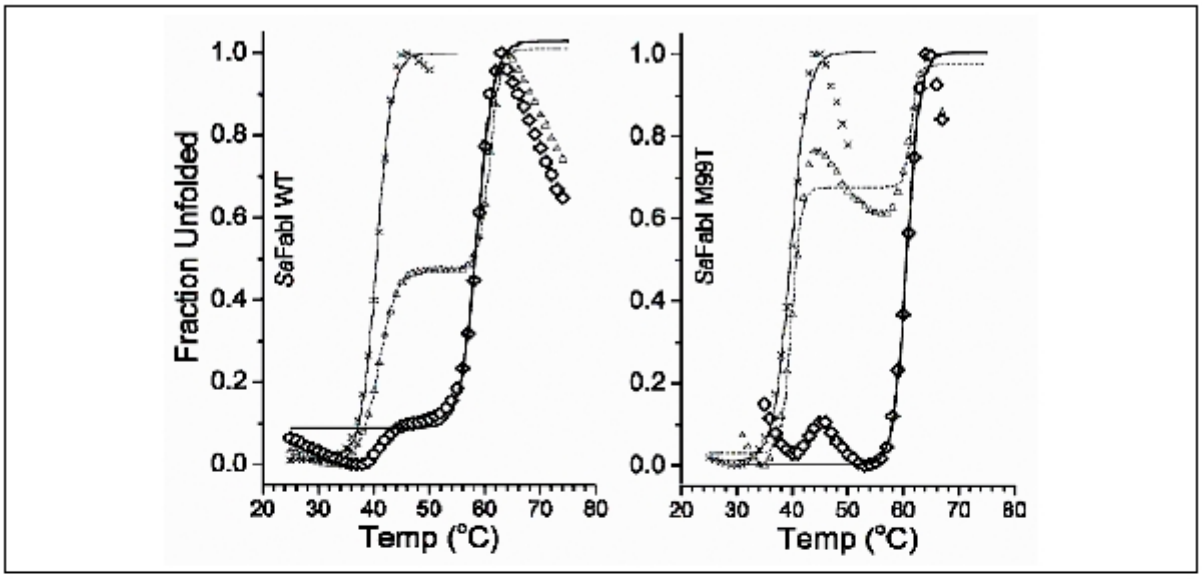

Figure 2. Representative thermal unfolding profiles of *Sa*FabI WT and M99T samples, derived by monitoring the fluorescence emission intensity of Sypro Orange at 570 nm, with excitation at 472 nm. *Sa*FabI WT (cross, left panel), with a T_m^{SO} of 40.5 °C, and *Sa*FabI WT incubated with 100 µM triclosan and 200 µM $NADP^+$ for 5 h (diamond), with a T_m^{SO} of 58.6 °C. We found that incubating triclosan and $NADP^+$ for 30 min (triangle) was not sufficient for *Sa*FabI, and the sample consisted of two populations of *Sa*FabI, one without and one with triclosan/$NADP^+$. The first transition temperature, 40.9 °C, was that of *Sa*FabI without triclosan and $NADP^+$, and the second transition temperature, 60.9 °C, was that of *Sa*FabI with triclosan and $NADP^+$. With 5 h incubation, the transition temperature shifted to 58.6 °C in this typical paired run. *Sa*FabI M99T (cross, right panel), with a T_m^{SO} of 39.7 °C, and *Sa*FabI M99T with 100 µM triclosan and 200 µM $NADP^+$ after 5 h incubation (diamond), with a T_m^{SO} of 60.6 °C. The data from the sample with 30 min incubation (triangle) showed two transitions at 39.8 and 61.4 °C.

The enzyme activity for *Sa*FabI was not measured, as it requires enoyl-ACP as the substrate, as mentioned above.

Thermal Shifts for Triclosan Binding to Active Site

SaFabI. The T_m^{SO} average value from thermal unfolding profiles of *Sa*FabI WT (**Fig. 2**) was 40.5 ± 1.0 °C ($n = 6$). With the addition of just triclosan alone, the average value was 37.6 ± 0.9 °C ($n = 2$), and of just $NADP^+$, the average value was 40.2 ± 1.2 °C ($n = 2$). Neither triclosan nor $NADP^+$ increased the T_m^{SO} values. For *Sa*FabI WT with both triclosan and $NADP^+$ (**Fig. 2**), the average value was 58.8 ± 1.6 °C ($n = 2$). A thermal shift of about 20 °C was observed for *Sa*FabI WT upon addition of both triclosan and $NADP^+$, but no shift upon addition of just triclosan or $NADP^+$. Since the addition of triclosan or $NADP^+$ alone did not stabilize *Sa*FabI, and only when both were added was *Sa*FabI stabilized, the results, together with the knowledge that triclosan and $NADP^+$ bind as a complex to the active site of *Sa*FabI[20], suggest that the observed thermal shift reflects not only binding to *Sa*FabI, but also specific binding to the active site of *Sa*FabI.

The T_m^{SO} average value of *Sa*FabI M99T (**Fig. 2**) was 40.2 ± 0.8 °C ($n = 3$). With the addition of just triclosan alone, the average value was 40.8 ± 0.1 °C ($n = 2$), and of just $NADP^+$, the average value was 41.2 ± 0.1 °C ($n = 2$). For *Sa*FabI M99T with triclosan and NAD^+, the average value was 60.2 ± 1.1 °C ($n = 2$). An approximate 20 °C thermal shift was observed for *Sa*FabI M99T upon binding triclosan and $NADP^+$. It is interesting to note that 30 min incubation allowed some of the triclosan and $NADP^+$ to bind to WT and M99T molecules, but not all, resulting in a thermal shift profile of two transitions (**Fig. 2**). The *Sa*FabI WT sample consisted of two populations, one without and one with triclosan and $NADP^+$; the first transition was at 40.9 °C, representing the thermal transition of the WT without triclosan and $NADP^+$, and the second transition was at 60.9 °C, representing the thermal transition of WT stabilized by triclosan and $NADP^+$. Similarly, for M99T, the triclosan-sensitive mutant, we also found a transition at 39.8 °C and another transition at 61.4 °C (**Fig. 2**).

The T_m^{SO} average value for A95V (**Fig. 3**) without triclosan and $NADP^+$ was 39.4 ± 0.2 °C ($n = 3$), quite similar to that of the WT (**Fig. 2**), and with triclosan and $NADP^+$, it was 40.3 ± 0.1 °C ($n = 2$). No thermal shift was observed for

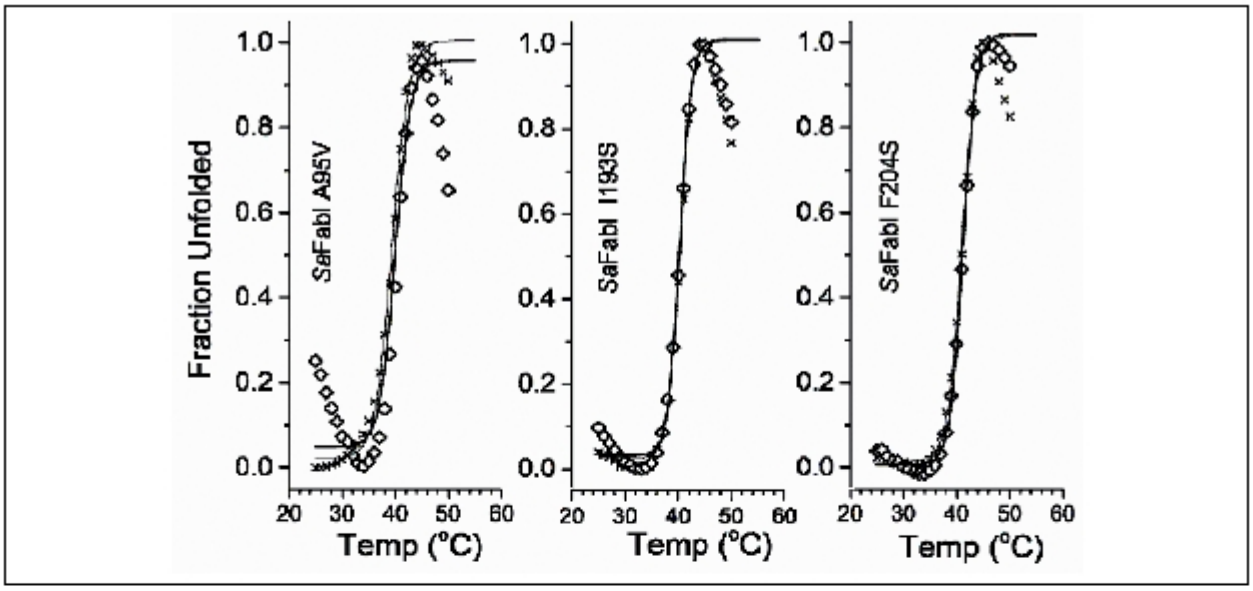

Figure 3. Representative thermal unfolding profiles of *Sa*FabI A95V, I193S, and F204S samples, derived by monitoring the fluorescence emission intensity of Sypro Orange at 570 nm, with excitation at 472 nm. *Sa*FabI A95V (cross, left panel), with a T_m^{SO} of 39.3 °C, and *Sa*FabI A95V incubated for 5 h with 100 μM triclosan and 200 μM $NADP^+$ (open diamond), with a T_m^{SO} of 40.1 °C. *Sa*FabI I193S (cross, middle panel), with a T_m^{SO} of 40.3 °C, and *Sa*FabI I193S incubated for 5 h with 100 μM triclosan and 200 μM $NADP^+$ (open diamond), with a T_m^{SO} of 40.3 °C. *Sa*FabI F204S (cross, right panel), with a T_m^{SO} of 41.2 °C, and *Sa*FabI F204S incubated for 5 h with 100 μM triclosan and 200 μM $NADP^+$ (open diamond), with a T_m^{SO} of 41.0 °C. No thermal shift was observed for *Sa*FabI A95V, I193S, or F204S mutants.

*Sa*FabI A95V. Similarly, the average value for I193S (**Fig. 3**) without triclosan and $NADP^+$ was 40.3 ± 0.0 °C ($n = 2$), and with triclosan and $NADP^+$, it was 40.2 ± 0.1 °C ($n = 2$). No thermal shift was observed for *Sa*FabI I193S. The average value for F204S (**Fig. 3**) without triclosan and $NADP^+$ was 41.1 ± 0.1 °C ($n - 2$), and with triclosan and $NADP^+$, it was 41.2 ± 0.1 °C ($n = 2$). No thermal shift was observed. Our results showed no binding of triclosan and $NADP^+$ to *Sa*FabI mutants A95V, I193S, and F204S.

FtFabI. The T_m^{SO} average value for *Ft*FabI WT (**Fig. 4**) was 53.2 ± 0.4 °C ($n = 4$). With the addition of just triclosan alone, the average T_m^{SO} was 52.3 ± 0.0 °C ($n = 2$), and of just NAD^+, the average T_m^{SO} was 52.4 ± 0.9 °C ($n = 2$). For *Ft*FabI WT with triclosan and NAD^+, the average T_m^{SO} was 60.2 ± 3.4 °C ($n = 2$). About a 7 °C thermal shift was observed for *Ft*FabI. A similar thermal shift was observed (60.8 ± 0.5 °C; $n = 3$) for samples incubated for 30 min. The average value for A92V without triclosan and NAD^+ was 51.7 ± 0.5 °C ($n = 3$), and with triclosan and NAD^+, it was 52.1 ± 0.1 °C ($n = 2$). No thermal shift was observed for *Ft*FabI A92V. Together with the enzyme activity values (**Fig. 1**), we showed that, using the *Ft*FabI system, the thermal shifts and the activity decreases upon addition of triclosan and NAD^+ are well correlated. Triclosan and NAD^+ together stabilized *Ft*FabI WT to increase the thermal transition temperature by 7 °C, and inhibited the enzymatic activity by 91%. For *Ft*FabI A92V, no thermal shift was observed, and there was no change in the residual enzymatic activity in the presence of triclosan and NAD^+. It was interesting to note that, unlike in the *Sa*FabI system, 30 min incubation of triclosan and NAD^+ with *Ft*FabI was sufficient to fully stabilize *Ft*FabI WT (**Fig. 4**).

Sypro Orange Effect on FabI Stability

Since we used Sypro Orange to report the thermal unfolding, we investigated whether Sypro Orange in DMSO affected the thermal unfolding by using CD to monitor the unfolding of FabI with and without 5× Sypro Orange in DMSO (0.1%, v/v). Due to a large CD signal for DMSO, we used only 0.1% DMSO, rather than 1%, as used in the T_m^{SO} studies. Enzyme activities with and without 1% DMSO were about the same. *Ft*FabI WT without DMSO, with 0.1% DMSO, or with 0.1% DMSO and 5× Sypro Orange revealed similar thermal unfolding profiles of secondary structures (**Fig. 5**). The T_m^{CD} average values for samples without ($n - 3$) and with ($n - 2$) DMSO (0.1%) were both 57.7 ± 0.1 °C, and for samples with 0.1% DMSO and 5× Sypro Orange, the value was 56.4 ± 0.2 ($n - 2$).

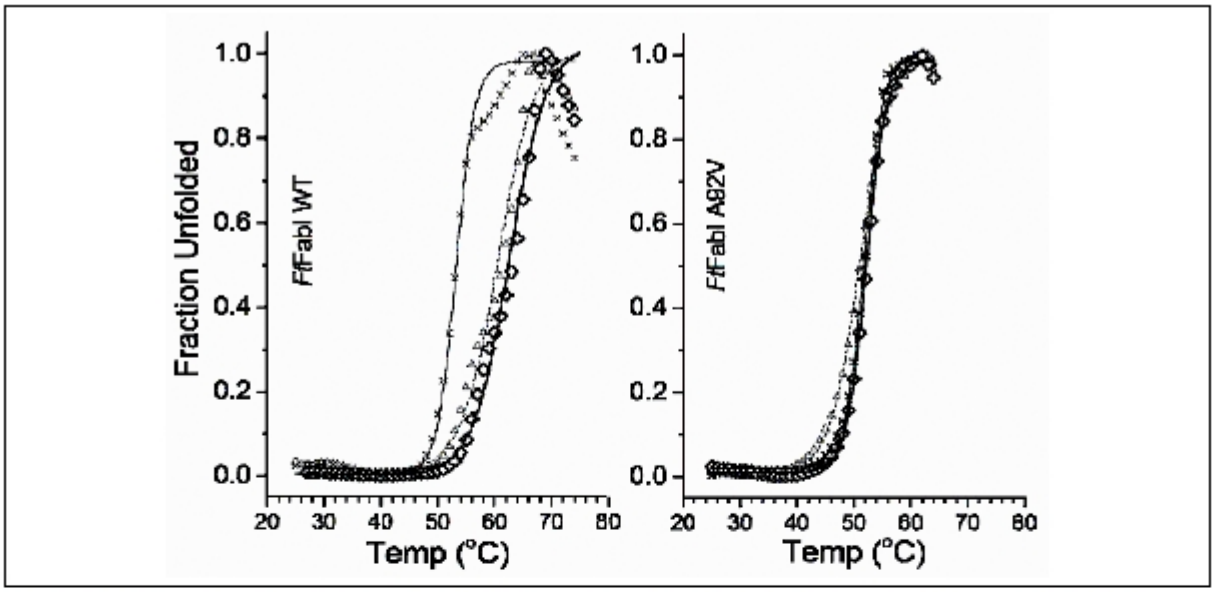

Figure 4. Representative thermal unfolding profiles of *Ft*FabI WT and A92V samples, derived by monitoring the fluorescence emission intensity of Sypro Orange at 570 nm, with excitation at 472 nm. The T_m^{SO} of *Ft*FabI WT (cross, left panel) was 53.2 °C, and of *Ft*FabI WT with 100 µM triclosan and 200 µM NAD^+ after 30 min incubation (triangle), it was 60.3 °C, and after 5 h (diamond), 62.6 °C. For A92V *Ft*FabI (cross, right panel), the T_m^{SO} was 51.8 °C, and for A92V *Ft*FabI with 100 µM triclosan and 200 µM NAD^+ after 30 min (triangle), it was 51.0 °C, and after 5 h (diamond), 52.1 °C.

Similar profiles, except shifted to lower temperatures, were observed for *Sa*FabI WT, with a T_m^{CD} of 43.7 ± 0.0 °C (n = 2). For *Sa*FabI WT in 0.1% DMSO, the T_m^{CD} was 43.6 ± 0.0 (n = 2), and in 0.1% DMSO and 5× Sypro Orange, the T_m^{CD} was 42.7 ± 0.0 (n − 2). Little DMSO or 5× Sypro Orange effect was observed.

The T_m^{CD} and T_m^{SO} values of the same sample differed slightly since the two methods measured slightly different unfolding events, with the CD reporting the unfolding of the secondary structures and the SO reporting the exposed hydrophobic moieties during unfolding.

Discussion

When Sypro Orange is added to intact protein in solution, which has little hydrophobic moieties, it exhibits little fluorescence intensity. However, when protein is thermally unfolded to expose hydrophobic moieties, Sypro Orange molecules around these moieties exhibit fluorescence intensity.[25] By following Sypro Orange fluorescence intensity in a protein sample as a function of temperature, protein unfolding profiles with characteristic transition temperatures are obtained. Since compounds binding to a protein molecule lower the free energy of the system,[26] Sypro Orange has been widely used to track the stabilization of a protein molecule due to compound binding.[22,27,28]

We showed that we may use this principle to determine whether triclosan and $NAD(P)^+$ bind to FabI mutants. The characteristic transition temperature in thermal unfolding of *Sa*FabI WT in Tris buffer was about 40 °C. The temperature did not change upon addition of just triclosan or just $NADP^+$. However, *Sa*FabI WT and M99T were stabilized by the triclosan and $NADP^+$ with the transition temperature shifted about 20 °C. For known triclosan-resistant mutants, A95V, I193S, and F204S, no thermal shift was observed upon addition of triclosan and $NADP^+$. It should also be noted that all *Sa*FabI samples, WT and the mutants, exhibited similar transition temperatures (~40 °C) in the absence of triclosan and $NADP^+$. Since the thermal shifts were observed only when both triclosan and $NADP^+$ were present, but not when only one was present, we suggest that the binding we observed was the active site binding observed previously.[20]

To demonstrate that the active site bindings indicated by thermal shifts are related to enzyme activities, we used the *Ft*FabI system. The transition temperature for *Ft*FabI in Tris buffer was about 53 °C, but shifted to 60 °C upon addition of triclosan and NAD^+. We also showed that the specific activity for *Ft*FabI was inhibited by triclosan and NAD^+. We further showed that a *Ft*FabI triclosan-resistant mutant, A92V, with much reduced specific activity compared with that of the WT, was not further reduced upon addition of

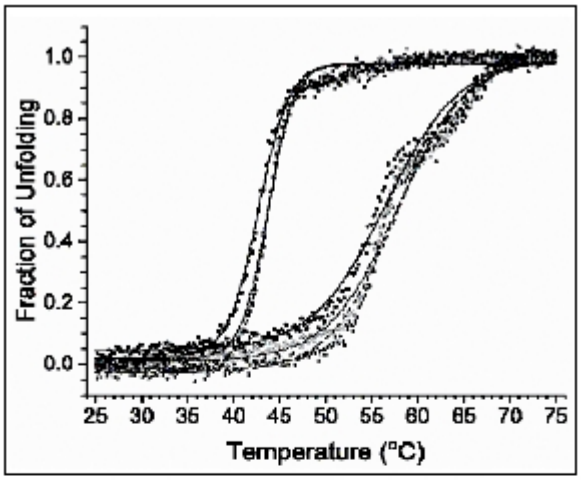

Figure 5. Representative thermal unfolding profiles and T_m values derived by monitoring the CD signal at 222 nm from 25 to 75 °C of 15 µM *Ft*FabI WT with no DMSO (empty circle), T_m = 57.7 ± 0.1 °C; with 0.1% DMSO (half-filled circle), T_m = 57.7 ± 0.1 °C; and with 0.1% DMSO and Sypro Orange (filled circle), T_m = 56.4 ± 0.2 °C; and 15 µM *Sa*FabI WT with no DMSO (empty square), T_m = 43.7 ± 0.0 °C; with 0.1% DMSO (half-filled square), T_m = 43.6 ± 0.0 °C; and with 0.1% DMSO and Sypro Orange (filled square), T_m = 42.7 ± 0.0 °C. These results show little DMSO (0.1%) or Sypro Orange effect on the thermal unfolding of either *Ft*FabI or *Sa*FabI.

triclosan and NAD^+. This mutant exhibited little thermal shift upon addition of triclosan/NAD^+ in its thermal unfolding profile.

It was interesting to note that a 30 min incubation period was sufficient to fully stabilize *Ft*FabI WT with triclosan and NAD^+. However, the unfolding profiles of *Sa*FabI WT and M99T samples with 30 min incubation clearly showed incomplete stabilization compared with those of 5 h incubation. These results suggest different binding kinetics, implying that this method may also provide kinetic information on active site binding of triclosan and $NAD(P)^+$.

In this study, we used Sypro Orange thermal shift on purified protein. With the recent development of cellular thermal shift assay,[29,30] it is certainly possible, using the principles discussed in this work, to apply cellular thermal shift assay on cells to screen for triclosan-resistant ENR/FabI mutants of species requiring enoyl-ACP-linked substrate. This method may also be used to select effective triclosan analogues that, together with $NAD(P)^+$, bind to the active site of ENR/FabI to inhibit the enzymatic activity, and thus inhibit cell growth.

In summary, we have shown that the Sypro Orange–based thermal shift binding assay, with fluorescence sensitivity, can be used easily and reliably to show the binding of the antibiotic triclosan in the presence of $NAD(P)^+$ to the active site of ENR/FabI enzymes, but not to a triclosan-resistant mutant. Thus, the method can be applied to FabI systems that require ACP-linked substrates without the need for the substrate to assay for activities. We have shown the lack of a thermal shift in a triclosan-resistant mutant. This approach offers a quick and convenient method to screen for triclosan-resistant mutations in ENR/FabI. This approach may also be applied to other antibiotics. In addition, it may also provide mechanistic insights into inhibition by studying the kinetics of the binding of triclosan to ENR/FabI.

Acknowledgments

We would like to thank Shahila Mehboob and Michael Johnson at the UIC Center of Pharmaceutical Biotechnology for the *Ft*FabI and *Sa*FabI WT plasmids and Marta Witek for the *Ft*FabI A92V plasmid.

Declaration of Conflicting Interests

The authors declared no potential conflicts of interest with respect to the research, authorship, and/or publication of this article.

Funding

The authors disclosed receipt of the following financial support for the research, authorship, and/or publication of this article: Proteomics and informatics services were provided by the Chicago Biomedical Consortium (CBC)—UIC Research Resources Center Mass Spectrometry, Metabolomics and Proteomics Facility, which was established in part by a grant from the Searle Funds at the Chicago Community Trust to the CBC. R.D.D. is an awardee of the Bridge to the Doctorate Fellowship at UIC. The work was supported by a grant from the National Institutes of Health (U01 AI-077949).

References

1. Russell, A. D. Whither Triclosan. *J. Antimicrob. Chemother.* **2004**, *53*, 693–695.
2. Wang, Y.; Shutao, M. Recent Advances in Inhibitors of Bacterial Fatty Acid Synthesis Type II (FASII) System Enzymes as Potential Antibacterial Agents. *ChemMedChem* **2013**, *8*, 1589–1608.
3. Sivaraman, S.; Sullivan, T. J.; Johnson, F.; et al. Inhibition of the Bacterial Enoyl Reductase fabI by Triclosan: A Structure-Reactivity Analysis of fabI Inhibition of Triclosan Analogues. *J. Med. Chem.* **2004**, *47*, 509–518.
4. Suller, M. T. E.; Russell, A. D. Triclosan and Antibiotic Resistance in *Staphylococcus aureus*. *J. Antimicrob. Chemother.* **2000**, *46*, 11–18.
5. McMurry, L. M.; McDermott, P. F.; Levy, S. B. Genetic Evidence that inhA of *Mycobacterium smegmatis* is a Target for triclosan. *Antimicrob. Agents Chemother.* **1999**, *43*, 711–713.
6. Marrakchi, H.; Lanéelle, G.; Quémard, A. InhA, a Target of the Antituberculosis Drug Isoniazid, Is Involved in a Mycobacterial Fatty Acid Elongation System, fas-II. *Microbiology* **2000**, *146*, 289–296.

7. Kapoor, M.; Gopalakrishnapai, J.; Surolia, N.; et al. Mutational Analysis of the Triclosan-Binding Region of Enoyl-ACP (Acyl-Carrier Protein) Reductase from *Plasmodium falciparum*. *Biochem. J.* **2004**, *381*, 735–741.
8. Liu, B.; Wang, Y.; Fillgrove, K. L.; et al. Triclosan Inhibits Enoyl-Reductase of Type I Fatty Acid Synthase In Vitro and Is Cytotoxic to MCF-7 and SKBr-3 Breast Cancer Cells. *Cancer Chemother. Pharmacol.* **2002**, *49*, 187–193.
9. McMurry, L. M.; Oethinger, M.; Levy, S. B. Triclosan Targets Lipid Synthesis. *Nature* **1998**, *394*, 531–532.
10. Levy, C. W.; Roujeinikova, A.; Sedelnikova, S.; et al. Molecular Basis of Triclosan Activity. *Nature* **1999**, *398*, 383–384.
11. Heath, R. J.; Li, J.; Roland, G. E.; et al. Inhibition of the *Staphylococcus aureus* NADPH-Dependent Enoyl-Acyl Carrier Protein Reductase by Triclosan and Hexachlorophene. *J. Biol. Chem.* **2000**, *275*, 4654–4659.
12. Ward, W. H. J.; Holdgate, G. A.; Rowsell, S.; et al. Kinetic and Structural Characteristics of the Inhibition of Enoyl (Acyl Carrier Protein) Reductase by Triclosan. *Biochemistry* **1999**, *38*, 12514–12525.
13. Rock, C. O.; Jackowski, S. Forty Years of Bacterial Fatty Acid Synthesis. *Biochem. Biophys. Res. Commun.* **2002**, *292*, 1155–1166.
14. Lowy, F. D. Antimicrobial Resistance: The Example of *Staphylococcus aureus*. *J. Clin. Invest.* **2003**, *111*, 1265–1273.
15. Xu, H.; Sullivan, T. J.; Sekiguchi, J. I.; et al. Mechanism and Inhibition of *Sa*FabI, the Enoyl Reductase from *Staphylococcus aureus*. *Biochemistry* **2008**, *47*, 4228–4236.
16. Majerus, P. W.; Alberts, A. W.; Vagelos, P. R. The Acyl Carrier Protein of Fatty Acid Synthesis: Purification, Physical Properties, and Substrate Binding Site. *Proc. Natl. Acad. Sci. USA* **1964**, *51*, 1231–1238.
17. Slabas, A. R.; Sidebottom, C. M.; Hellyer, A.; et al. Induction, Purification and Characterization of NADH-Specific Enoyl Acyl Carrier Protein Reductase from Developing Seeds of Oil Seed Rape. *Biochim. Biophys. Acta*. **1986**, *877*, 271–280.
18. Rafi, S.; Novichenok, P.; Kolappan, S.; et al. Structure of Acyl Carrier Protein Bound to the FabI, the FASII Enoyl Reductase from *Escherichia coli*. *J. Biol. Chem.* **2006**, *281*, 39285–39293.
19. Shimakata, T.; Stumpf, P. K. The Procaryotic Nature of the Fatty Acid Synthetase of Developing *Carthamus tinctorius L.* (Safflower) Seeds. *Arch. Biochem. Biophys.* **1982**, *217*, 144–154.
20. Shiebel, J.; Chang, A.; Lu, H.; et al. *Staphylococcus aureus* FabI: Inhibition, Substrate Recognition, and Potential Implications for In Vivo Essentiality. *Structure* **2012**, *20*, 802–813.
21. Kaneda, T. Iso- and Anteiso-Fatty Acids in Bacteria: Biosynthesis, Function, and Taxonomic Significance. *Microbiol. Rev.* **1991**, *55*, 288–302.
22. Niedziela-Majka, A.; Kan, E.; Weissburg, P.; et al. High-Throughput Screening of Formulations to Optimize the Thermal Stability of a Therapeutic Monoclonal Antibody. *J. Biomol. Screening* **2015**, *20*, 552–559.
23. Yao, J.; Maxwell, J. B.; Rock, C. O. Resistance to AFN-1253 Arises from Missense Mutations in *Staphylococcus aureus* Enoyl-Acyl Carrier Protein Reductase (FabI). *J. Biol. Chem.* **2013**, *288*, 36261–36271.
24. Witek, M. A.; Fung, L. W.-M. Quantitative Studies of Caspase-3 Catalyzed αII-Spectrin Breakdown. *Brain Res.* **2013**, *1533*, 1–15.
25. Lo, M. C.; Aulabaugh, A.; Jin, G.; et al. Evaluation of Fluorescence-Based Thermal Shift Assays for Hit Identification in Drug Discovery. *Anal. Biochem.* **2004**, *332*, 153–159.
26. Pantoliano, M. W.; Petrella, E. C.; Kwasnoski, J. D.; et al. High-Density Miniaturized Thermal Shift Assays as a General Strategy for Drug Discovery. *J. Biomol. Screening* **2001**, *6*, 429–440.
27. Niesen, F. H.; Berglund, H.; Vedadi, M. The Use of Differential Scanning Fluorimetry to Detect Ligand Interactions That Promote Protein Stability. *Nat. Protoc.* **2007**, *2*, 2212–2221.
28. Kim, A.; Wolf, N. M.; Zhu, T.; et al. Identification of *Bacillus anthracis* PurE Inhibitors with Antimicrobial Activity. *Bioorg. Med. Chem.* **2015**, *23*, 1492–1499.
29. Molina, D. M.; Jafari, R.; Ignatuschchenko, M.; et al. Monitoring Drug Target Engagement in Cells and Tissues Using the Cellular Thermal Shift Assay. *Science* **2013**, *341*, 84–87.
30. Jafari, R.; Almqvist, H.; Axelsson, H.; et al. The Cellular Thermal Shift Assay for Evaluating Drug Target Interactions in Cells. *Nat. Protoc.* **2014**, *9*, 2100–2122.

APPENDIX B

Bioorganic & Medicinal Chemistry 23 (2015) 1492–1499

Contents lists available at ScienceDirect

Bioorganic & Medicinal Chemistry

journal homepage: www.elsevier.com/locate/bmc

Identification of *Bacillus anthracis* PurE inhibitors with antimicrobial activity

Anna Kim [a,†], Nina M. Wolf [a,†], Tian Zhu [b], Michael E. Johnson [b], Jiangping Deng [c], James L. Cook [c], Leslie W.-M. Fung [a,*]

[a] Department of Chemistry, University of Illinois at Chicago, 845 W. Taylor Street, Chicago, IL 60607, United States
[b] Center for Pharmaceutical Biotechnology, University of Illinois at Chicago, Chicago, IL 60607, United States
[c] Loyola University Medical Center, Maywood, IL 60153, United States

ARTICLE INFO

Article history:
Received 12 December 2014
Revised 28 January 2015
Accepted 6 February 2015
Available online 16 February 2015

Keywords:
High-throughput screening
De novo purine biosynthesis
PurE
Thermal shift assay
Sypro Orange
2-Carboxamido-1,3,4-oxadiazole

ABSTRACT

N^5-carboxy-amino-imidazole ribonucleotide (N^5-CAIR) mutase (PurE), a bacterial enzyme in the *de novo* purine biosynthetic pathway, has been suggested to be a target for antimicrobial agent development. We have optimized a thermal shift method for high-throughput screening of compounds binding to *Bacillus anthracis* PurE. We used a low ionic strength buffer condition to accentuate the thermal shift stabilization induced by compound binding to *Bacillus anthracis* PurE. The compounds identified were then subjected to computational docking to the active site to further select compounds likely to be inhibitors. A UV-based enzymatic activity assay was then used to select inhibitory compounds. Minimum inhibitory concentration (MIC) values were subsequently obtained for the inhibitory compounds against *Bacillus anthracis* (ΔANR strain), *Escherichia coli* (BW25113 strain, wild-type and Δ*TolC*), *Francisella tularensis*, *Staphylococcus aureus* (both methicillin susceptible and methicillin-resistant strains) and *Yersinia pestis*. Several compounds exhibited excellent (0.05–0.15 μg/mL) MIC values against *Bacillus anthracis*. A common core structure was identified for the compounds exhibiting low MIC values. The difference in concentrations for inhibition and MIC suggest that another enzyme(s) is also targeted by the compounds that we identified.

1. Introduction

Among bacterial pathogens, an increased concern exists for organisms that can be used for bioterrorism, such as *Bacillus anthracis* (*B. anthracis*), which causes anthrax infection. Due to constant bacterial mutations, with some mutations leading to drug resistance, new antibiotics are urgently and constantly needed.

In many bacterial species (including *B. anthracis*) the *de novo* purine biosynthesis pathway enzyme PurK (also known as N^5-carboxy-amino-imidazole ribonucleotide (N^5-CAIR) synthetase) converts 5-amino-imidazole ribonucleotide (AIR) to N^5-CAIR. PurE (N^5-CAIR mutase) then converts N^5-CAIR to 4-carboxy-amino-imidazole ribonucleotide (CAIR).[1,2] Figure 1 in Ref. 1 and Figures 1 and 2 in Ref. 2 show the pathway and structures of molecules involved. In humans, the enzyme in Step 6 of the pathway (*h*Pur6, also known as AIR carboxylase or PurE II,[2] or phosphoribosylaminoimidazole carboxylase;[3] an enzyme containing a PurE domain) converts AIR and CO_2 to CAIR directly.[3] The architecture of the active sites of bacterial PurE and the PurE domain in *h*Pur6 are nearly superimposable, and yet despite these conserved features, biochemical studies have shown that both enzymes are highly specific.[4] Subsequent studies have shown that bacterial PurE has the potential to be a target for new antibiotic development.[5]

Abbreviations: A_{260}, UV absorbance at 260 nm; AIR, 5-amino-imidazole ribonucleotide; *Ba*, *Bacillus anthracis* (ΔANR strain); CAIR, 4-carboxy-amino-imidazole ribonucleotide; CD, circular dichroism; DMSO, dimethyl sulfoxide; *E. coli* Δ*TolC*, *E. coli* efflux pump knockout strain; GST, glutathione-S-transferase; *h*Pur6, human enzyme containing a PurE domain, also known as AIR carboxylase; HTS, high-throughput screening; LC1–6, compound names; MBC, minimum bactericidal concentration; MIC, minimum inhibitory concentration; MRSA, methicillin-resistant *Staphylococcus aureus*; MSSA, methicillin-susceptible *Staphylococcus aureus*; N^5-CAIR, N^5-carboxy-amino-imidazole ribonucleotide; NAIR, 4-nitro-5-amino-imidazole ribonucleotide; PBS, 5 mM phosphate buffer with 150 mM NaCl at pH 7.4; RRC, Research Resource Center; PurE, N^5-carboxy-amino-imidazole ribonucleotide mutase; T_m, Boltzmann transition temperature in thermal unfolding; $T_m^{\bar{x}}$, the average T_m value of *Ba*PurE; T_m^{Rx}, the average T_m value of replicate runs of *Ba*PurE with a particular compound added; ΔT_m, $T_m^{Rx} - T_m^{\bar{x}}$; Tris-25, 25 mM Tris buffer at pH 8; Tris-50, 50 mM Tris buffer at pH 8; UIC, University of Illinois at Chicago.

* Corresponding author. Tel.: +1 312 355 5516.
E-mail address: lfung@uic.edu (L.W.-M. Fung).
† These two authors contributed equally in this work.

http://dx.doi.org/10.1016/j.bmc.2015.02.016
0968-0896/

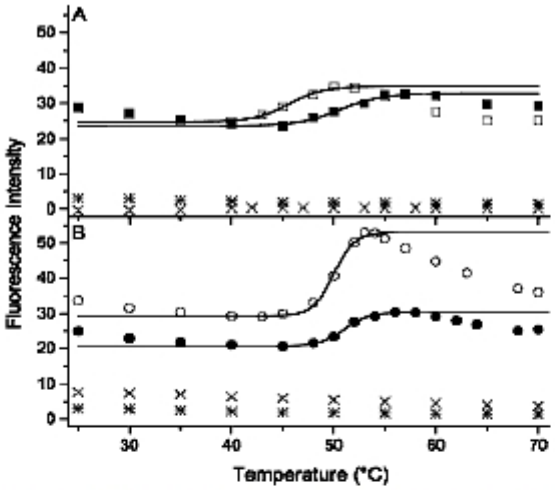

Figure 1. A typical run of thermal unfolding of *Ba*PurE (10 μM) in paired samples (with 100 μM NAIR—filled symbols, or without—empty symbols), monitored by fluorescence intensity of Sypro Orange (5× final concentration) at 563 nm (excitation at 490 nm), shows a 5.0 °C difference in the transition temperatures, ΔT_m, in Tris-25 (25 mM Tris at pH 8.0) (A). The individual T_m values were obtaining from fitting a 2-state unfolding model (solid lines), using only results where fluorescence intensities were increasing with increasing temperatures. It is an indication of protein aggregation when fluorescence intensity decreases as temperature increases.[2,5] The average ΔT_m in Tris-25 was 5.2 °C ($n = 2$). A ΔT_m of 1.0 °C is shown for one sample of NAIR in Tris-50 (50 mM Tris at pH 8.0) (B). The average ΔT_m in Tris-50 was 1.7 °C ($n = 6$). Also shown in the figure are results of samples without *Ba*PurE, but with only 5× Sypro Orange (×), or with 10 mM NAIR and 5× Sypro Orange (*), exhibiting little fluorescence signal. The low ionic strength buffer condition (Tris-25) accentuates the thermal shift of *Ba*PurE upon compound binding.

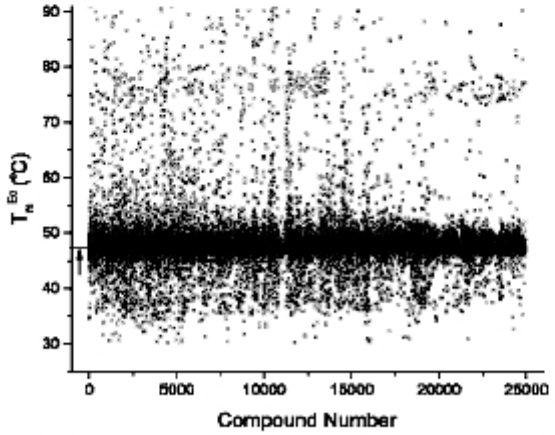

Figure 2. The thermal unfolding transition temperatures of *Ba*PurE in the presence of compounds from an antibacterial focused chemical library (24,917 compounds) (T_m^{Ec}) in Tris-25, of replicate runs (× for run 1 and * for run 2). The T_m value of *Ba*PurE without a compound (T_m^{Ec}) was 47.6 °C ± 0.6 °C ($n = 4878$) and is shown as a short dash on the left (noted with an arrow underneath the dash). Ten thousand and nineteen (10,019) compounds exhibited replicate T_m^{Ec} values that were within 1.0 °C of each other. Five hundred and twenty five (525) compounds with ΔT_m (T_m^{Ec}—47.6) in the range of 1.0–20.0 °C were selected as hits. See text for details.

In this study, a fluorescence-based[5] thermal shift assay[7,8] was applied to *B. anthracis* PurE (*Ba*PurE) for high-throughput screening (HTS) to identify molecules (hits) that bind to *Ba*PurE. In silico docking was used to select those most likely to bind to the active site. The top scoring molecules were then assayed for inhibitory activity toward *Ba*PurE. A few selected inhibitors were used to obtain the minimum inhibition concentration (MIC) against *B. anthracis* (ΔANR strain), *Escherichia coli* (both the wild-type BW25113 strain and a strain with a *TolC* efflux pump knock out—*E. coli* Δ*TolC*[9]), *Francisella tularensis* (*F. tularensis*), *Staphylococcus aureus* (*S. aureus*; both methicillin-susceptible (MSSA) and methicillin-resistant strains (MRSA)), and *Yersinia pestis* (*Y. pestis*). MIC values against *B. anthracis* of 0.5–0.15 μg/mL were obtained for several compounds. A common core structure was identified for compounds with low MIC values. The difference in concentrations for inhibition and MIC suggest that other protein/enzyme molecules are also targeted by the compounds that we identified.

2. Materials and methods

2.1. Chemicals

All materials were purchased from Fisher Scientific (Hampton, NH) unless otherwise noted.

2.2. *Ba*PurE plasmid

The *Ba*PurE gene (BA0288) from *B. anthracis* (ΔANR) cells (GenBank: AE017334.2) was inserted into a Gateway pDEST-15 plasmid (Life Technologies; Grand Island, NY) to express an N-terminal glutathione-*S*-transferase (GST) fusion protein, with a linker between GST and *Ba*PurE. In the linker sequence (PWSNQTSLYKKAGSLVPRGSH), a thrombin cleavage site (the underlined residues) was included. The plasmid was transformed into *E. coli* BL21-CodonPlus (DE3) competent cells (Stratagene; Santa Clara, CA).

2.3. Expression, purification and characterization of *Ba*PurE

Cells were grown in a fermentor (Bioflo 110; New Brunswick Scientific, Enfield, CT) containing Terrific broth (2 L) with ampicillin (0.3 mM) at 37 °C for 3 h and reduced to 25 °C for isopropyl-thio-β-galactoside (1 mM; Gold Biotechnology; St. Louis, MO) induced protein expression for 4 h. The GST-*Ba*PurE fusion protein in 5 mM phosphate buffer with 150 mM NaCl at pH 7.4 (PBS) was purified with a glutathione affinity column (Sigma; St. Louis, MO), following standard procedures.[10,11] Bovine thrombin (Biopharm; Bluffdale, UT) was used to cleave the fusion protein (1 unit thrombin for 1 mg fusion protein). GST and uncleaved fusion protein, if any, in the mixture were removed with the affinity column again, to give *Ba*PurE. An extinction coefficient of 11,460 mol^{-1} cm^{-1}, obtained from the amino acid sequence, was used to determine protein concentration for the monomer. The integrity of the protein was checked with sodium dodecyl sulfate polyacrylamide gel electrophoresis and high-resolution/high-mass mass-spectrometry, using a LTQ-FT spectrometer in the Research Resources Center at the University of Illinois at Chicago (UIC). The *Ba*PurE sample was concentrated to 150 μM (2.6 mg/mL) and frozen dropwise, about 20 μL per drop, in liquid nitrogen for storage at −80 °C.

We selected the GST fusion protein over the commonly used His-tag fusion protein to prepare *Ba*PurE to avoid introducing high concentrations of imidazole, a heterocyclic compound somewhat similar to the substrate, which may be difficult to remove from the protein. Additionally, a His-tag *Ba*PurE protein was initially prepared by standard procedures[12] in 50 mM Tris buffer at pH 7.8 with NaCl and imidazole, 500 mM each. However, following

dialysis of protein (at a concentration of 50–350 μM or 1–7 mg/mL) in 50 mM Tris buffer at pH 7.8 with NaCl and imidazole, 50 mM each, only about 20% protein remained soluble.

The oligomeric state of *Ba*PurE in solution was determined by gel filtration with a Superdex 200 GL column and an FPLC system (AKTApurifier, GE Healthcare Life Sciences; Pittsburgh, PA). A calibration curve of molecular mass and elution volume was obtained with ferritin, aldolase, conalbumin, chymotrypsinogen A, ribonuclease A and blue dextran (GE Healthcare Life Sciences).

The secondary structure of *Ba*PurE (25 μM) in PBS buffer or Tris (25 mM) buffer at pH 8 (Tris-25) at 25 °C was determined from circular dichroism (CD) spectra obtained with a CD spectrometer (Model 810; Jasco; Oklahoma City, OK), and K2D3 software (http://k2d3.ogic.ca;[13]). The secondary structure from the X-ray structure (PDB code: 1XMP,[14]) was obtained for comparison, using PDBsum (http://www.ebi.ac.uk/pdbsum/;[15]).

2.4. Enzyme activity

The published method for assaying PurE[1] was applied to *Ba*PurE. Briefly, the conversion of CAIR to N^5-CAIR in this reversible reaction of PurE was monitored by measuring the UV absorbance at 260 nm (A_{260}) for 1.5 min at 20 °C. CAIR was prepared in house following published methods,[16] involving the use of LiOH to saponify aminoimidazole-4-carboxamide ribonucleotide to give CAIR in high yield (85%) and purity (99%). The K_m value for CAIR in *Ba*PurE was determined as 9.7 μM. The reported K_m value for CAIR in *E. coli* PurE under their experimental condition is reported as 22 μM[17] or 36 μM.[18] The CAIR stock solution (5 mM) was prepared in 50 mM Tris buffer at pH 8.0 (Tris-50) and stored at −80 °C in 100 μL portions, and a working solution of CAIR (60 μM), prepared in Tris-25, was stable with no change in A_{260} for at least 2 h. For the assay sample, equal volumes of *Ba*PurE and CAIR were mixed to give 10 nM *Ba*PurE and 30 μM CAIR in Tris-25. Assay samples consisting of 10 μM CAIR were also prepared. Dimethyl sulfoxide (DMSO, 1%) was included such that the samples were similar to those used in enzyme inhibition assays (Section 2.8). The linear portion of the A_{260} versus time plot was fitted to give a $\Delta A_{260}/\Delta t$ value (the initial rate) (see Fig. 4, for example). CAIR concentration was calculated from a $\Delta\varepsilon_{260}$ of 8930 M^{-1} cm^{-1},[11,18] and was used to determine the specific activity, which was defined[18] as the disappearance of 1 μmol of CAIR in 1 min with 1 mg of PurE (unit/mg). The $\Delta\varepsilon_{260}$ was used since N^5-CAIR in acidic pH is known to undergo auto-decarboxylation to form AIR, but the rate of the decomposition is minimal at pH 8.0.[18]

2.5. Optimization for thermal shift screening

Sypro Orange (Invitrogen; Life Technologies; Carlsbad, CA), used for thermal unfolding,[7] was supplied as a 5000× stock solution in anhydrous DMSO, and stored in a desiccator at 4 °C. The hygroscopic DMSO absorbs moisture during the freeze–thaw process, and when DMSO contains more than 5% water, it does not freeze at 4 °C.[20] Thus, we minimized the number of freeze–thaw cycles of the stock solution, and discarded stock samples when they became liquid at 4 °C.

The initial studies for optimizing the conditions for thermal unfolding of *Ba*PurE to be used for high-throughput assay were monitored with a fluorescence spectrometer (Jasco FP-6200), with Sypro Orange excitation at 490 nm and emission at 563 nm. The buffer conductivity values were measured with a conductivity meter (Yellow Springs model 31; Yellow Springs, OH) to ensure consistency in buffer conditions with different preparations. The conductivity value of Tris-25 was 1200 μMHO; for Tris-50 it was 2600 μMHO; and for PBS it was 13,000 μMHO. The fluorescence emission intensities for samples of *Ba*PurE (10 μM) in different buffers with 5–15× Sypro Orange and 1% DMSO were measured from 25 to 75 °C. A known inhibitor, 4-nitro-5-amino-imidazole ribonucleotide (NAIR),[4] at 100 μM, was used to evaluate whether the compound-binding-induced stability in *Ba*PurE was detectable by the thermal shift method. Samples without *Ba*PurE, but with only Sypro Orange and NAIR, or with only Sypro Orange were also prepared. NAIR, also called NO_2-AIR,[17] was synthesized in house as described.[21] The thermal unfolding data were fitted to a two-state transition model to give Boltzmann transition temperatures.

2.6. High-throughput thermal shift screening

*Ba*PurE samples from different preparations, a total of about 100 mg, were combined and dialyzed in the buffer identified in optimization studies (Tris-25; from Section 3.2). An antibacterial focused chemical library of 24,917 compounds (Life Chemicals; Burlington, Canada)[22] was screened. Compounds (10 mM) in anhydrous DMSO were stored in 384-well plates at −80 °C with desiccation. All components (10 μM *Ba*PurE in Tris-25 with 5× Sypro Orange, a condition determined from the results obtained in optimization studies (from Section 3.2), 100 μM compound and 1% DMSO) were delivered to each well in the 384-well white plates (ABgene SuperPlate, Fisher Thermo Scientific) by a liquid handling system (Freedom Evo, Tecan; Mannedorf, Switzerland). A total of 78 plates were used per run, and replicate runs were done. For each plate, 32 wells were reserved for samples (1) with only Sypro Orange and DMSO (no *Ba*PurE and compound) to monitor the background fluorescence, and (2) with *Ba*PurE, Sypro Orange and 1% DMSO (no compound) to monitor signals from the control samples. For two plates 32 wells were reserved for samples with 100 μM NAIR, as positive control. Plates were covered with plastic film (Applied Biosystems, Foster City, CA) and stored at 4 °C.

The first plate, within 10–30 min after it was prepared, was removed from storage and placed in a RT-PCR instrument (ViiA7 RT-PCR; Applied Biosystems, Carlsbad, CA) for thermal unfolding measurements over a temperature range of 25–95 °C at a rate of 0.075 °C/s. An instrument filter with emission at 586 ± 10 nm and excitation at 470 ± 15 nm was used. The measurements were done continuously. A replicate run followed immediately after the first run. All operations and measurements were done in the Research Resource Center (RRC) at UIC.

The thermal unfolding profiles were analyzed with the Protein Thermal Shift Software (Applied Biosystems) to determine the Boltzmann transition temperature, T_m. Compounds with T_m values in replicate runs that differed by more than 1.0 °C were eliminated, since our standard deviation values for T_m values of *Ba*PurE was 0.6 (n = 4878; from Section 3.3). The average T_m value of the control (*Ba*PurE) (T_m^E) and the average value of replicate runs of compound (T_m^{Ec}) were used to determine thermal shift values ($\Delta T_m = T_m^{Ec} - T_m^E$). Hits were defined as those with 1.0 °C < ΔT_m < 20.0 °C. We used 20.0 °C as the upper cut-off since most of the thermal shift values in the literature are less than 20 °C (e.g.,[23–25]). The thermal shift value for our positive control (NAIR) was 5.6 °C (from Section 3.3). This selection criterion may obviously eliminate a fraction of molecules that bind to *Ba*PurE, but is more time and cost efficient as well as providing more reliable hits.

The Z′-factor[26] used to evaluate the quality of the thermal shift assay was determined from the average T_m values of *Ba*PurE, in the absence (T_m^E) and in the presence of 100 μM NAIR (T_m^{Ec} (NAIR)), and their corresponding standard deviation (SD) values, as 1–3 (T_m^{Ec} (NAIR) + T_m^E)/(SD (NAIR) − SD (*Ba*PurE)).

2.7. Docking to active site

The SMILES strings of hits were converted, using LigPrep (Schrödinger), to their 100 most energetically and structurally

favorable structures. All structures were also clustered and selected with Canvas (Schrödinger) for structural diversity. GOLD v5.0.1 (Cambridge Crystallographic Data Centre; Cambridge, United Kingdom) was used for docking the structures of each compound to PurE. We did not use the published structure of *Ba*PurE (PDB: 1XMP) since it does not contain a ligand, instead we used the structure of *E. coli* PurE with AIR (PDB: 1D7A), with AIR removed. The AIR binding site was assumed to be the active site, or part of the active site, and a binding site sphere with a radius of 10 Å centered on AIR was used. Standard default settings were used for other parameters, such as full solvation, retaining the three top solutions, and no force constraints.

2.8. Enzyme inhibition

Each compound (20 μM) and *Ba*PurE (20 nM) was incubated in Tris-25 for 1.5 min at 20 °C, followed by addition of an equal volume of CAIR to give an assay sample consisting of compound (10 μM), *Ba*PurE (10 nM) and CAIR (30 μM) in Tris-25 with 1% DMSO. A control sample (without the compound) was prepared in parallel. Assay samples with CAIR concentration the same as compound concentration (10 μM) were also tested. A_{260} was measured as a function of time, and *Ba*PurE activity inhibitions were determined as [(activity with compound)/(activity without compound) × 100].

Only compounds with masses validated by mass spectrometry analysis were used. To avoid compound aggregation and stability problems due to freeze–thawing,[27,28] the compounds in DMSO were stored at room temperature under desiccation. We noted that some compounds precipitated out when pipetted into Tris-25; those were eliminated from further study. Compounds in Tris-25 that exhibited increasing or decreasing A_{260} readings as a function of time were also eliminated. No particular actions were taken for those compounds exhibiting a constant A_{260} value since the absorption only added to the baseline. Triton X-100 (0.01–0.1%) was included in some assay solutions to check for compound aggregation induced inhibition. Compound concentration of stock solutions was determined by weight and volume, which may introduce uncertainties.[29]

2.9. Minimum inhibitory concentration (MIC) and minimum bactericidal concentration (MBC)

MIC was determined as in prior work.[30] Briefly, the MICs of compounds were tested against *B. anthracis* (ΔANR strain), *E. coli* (BW25113 strain, WT and Δ*TolC*), *F. tularensis* (BEI/ATCC: UTAH 112), two strains of *S. aureus*, one methicillin-sensitive (ATCC: 29213) and one *mecA*-positive, methicillin-resistant (ATCC: 43300), and *Y. pestis* (BEI/ATCC: A1122). LB medium was added to each well in a row of a sterile 96-well flat bottom tissue culture plate, with 96 μL to the first column and 50 μL to all subsequent wells. The inhibitors to be tested were added to the first column to give a final well volume of 100 μL. Inhibitors were then serially diluted (2-fold) across the columns of wells by pipetting and mixing 50 μL of solution. The extra 50 μL was discarded from the final well. Ciprofloxacin, a commercial antibiotic used for the treatment of a number of bacterial infections, was used as positive control in these studies. Prior to setting up the MIC plates, the appropriate bacterial cultures were grown to mid-log phase and subsequently diluted to an optical density reading at 600 nm of 0.004 with fresh LB medium. This bacterial dilution (50 μL) was added to each well of the plate, and the plate was then incubated at 37 °C overnight without shaking. For each inhibitor the first clear well with no signs of visible growth was reported as the MIC value. All MIC values were confirmed by at least two independent titrations.

MBC values were estimated using the standard method of testing all negative MIC wells (no visible growth) for evidence of viable bacteria by transferring an aliquot of MIC dilution culture media to antibiotic-free agar plates. Medium (100 μL) from each negative (clear) well in MIC assays was streaked onto LB agar plates, and the plates were incubated for 72 h for detection of bacterial growth. The MBC of an inhibitor was defined as the highest MIC assay dilution that resulted in no growth of bacteria during this subcultivation. Bactericidal activity was defined as an MBC/MIC ratio ≤4. Since the highest compound concentration tested was 12.5 μg/mL, clear statements about bacteriostatic versus bactericidal activity could only be made about inhibitors with MICs ≤3.13 μg/mL.

3. Results

3.1. Protein properties

About 15 g of cells were obtained from 2 L of medium, and about 0.5 mg recombinant *Ba*PurE (>85% pure) was obtained from 1 g of cells with 80–90% purity, as indicated by sodium dodecyl sulfate gel electrophoresis. Mass spectrometry results showed a mass of 17,322.1 Da, with the expected mass from sequence of 17,322.9 Da, confirming the integrity of *Ba*PurE. In PBS, the protein, up to ~1.7 mM (~30 mg/mL), remained soluble in its native form as an octomer, as indicated by the hydrodynamic mass of 149 kDa from gel filtration measurements.

CD spectra of *Ba*PurE in PBS and in Tris-25 at 25 °C showed a secondary structure with about 24% beta sheet and 32% alpha helix, indicating well folded protein samples. Slightly higher helical and lower sheet contents were obtained for buffers with higher salt concentrations (Wolf and Fung, unpublished data). The secondary structure content calculated from the X-ray structure (PDB: 1XMP) is 15% beta sheet and 45% alpha helix.

For enzyme activity, the average $\Delta A_{260}/\Delta t$ value in Tris-25 at 20 °C was 0.0115 ± 0.0012 (n = 21) to give a specific activity of 7.5 ± 0.8 unit/mg. The value varied in other buffers: 10.6 ± 1.6 unit/mg (n = 13) in Tris-50, and 12.4 ± 1.3 unit/mg (n = 24) in PBS. These values differ from those of PurE from other species under different solution conditions.[17–19]

3.2. Optimal condition for thermal shift screening

Sypro Orange at 5× concentration with or without NAIR, but with no *Ba*PurE, exhibited little changes in the fluorescence intensity as a function of temperature in either Tris-25 (Fig. 1A) or Tris-50 (Fig. 1B). In Tris-25, a typical thermal unfolding profile of *Ba*PurE (10 μM), with 5× Sypro Orange and 1% DMSO, showed a prominent thermal transition, with a T_m^E value of 45.6 °C, and was shifted to 50.6 °C in the presence of NAIR (100 μM), to give a change in the T_m value (ΔT_m) of 5.0 °C for this particular run (Fig. 1A). In Tris-50, the T_m^E value was higher (50.0 °C), but was shifted only to 51.0 °C in the presence of NAIR to give a ΔT_m of 1.0 °C in this paired run (Fig. 1B). The average thermal shift for NAIR in Tris-25 was 5.2 ± 0.3 °C (n = 2), and in Tris-50 was 1.7 ± 0.9 °C (n = 6). Thus, *Ba*PurE in Tris-25 exhibited a larger thermal shift than in Tris-50, and Tris-25 was selected for HTS. Three Sypro Orange concentrations, 5×, 10× and 15×, yielded satisfactory thermal unfolding profiles for *Ba*PurE in Tris-25, and the lowest concentration, 5×, was selected for HTS.

3.3. High-throughput thermal shift screening

From the conditions identified above, the high-throughput thermal shift screening samples consisted of *Ba*PurE at 10 μM in Tris-25 with 5× Sypro Orange and 1% DMSO.

From HTS thermal shift measurements, the average T_m^{ff} was found to be 47.8 ± 0.3 °C (n = 32), and the T_m^{Ec} (NAIR) was 53.4 ± 0.5 °C. The Z′-factor was calculated as 0.57, indicating the set-up provided reliable thermal shift results.

The average T_m^{ff} obtained from all the control wells in all plates, was 47.6 ± 0.6 °C (n = 4878) (Fig. 2). For the samples with compounds (24,917 compounds) (Fig. 2), 10,019 samples displayed a difference in T_m^{Ec} < 1.0 °C between replicate runs, and were used for further analysis. The remaining samples (14,898 samples) were eliminated. Based on the T_m selection criteria for hits discussed in Section 2.6 as 1.0 °C < ΔT_m < 20.0 °C, compounds exhibiting ΔT_m ($= T_m^{Ec} - 47.6$) values outside the range of 1–20 °C were not considered. Thus 197 samples with negative ΔT_m, 9257 with less than 1 °C in ΔT_m and 40 with ΔT_m larger than 20 °C were not considered further. The remaining samples (525 compounds) satisfied the selection criteria.

3.4. Active site docking selection

The docking of 525 thermal shift hits to the AIR binding site sphere yielded 79 compounds with GOLD docking scores greater than or equal to 55. Both CAIR and NAIR gave a docking score of 56. Compound diversity selection (discussed in Section 2.7) further narrowed the list to 60 compounds. Two of these compounds are shown in the active site, with AIR in the center of the cavity (Fig. 3). The active site appears to be relatively open and spacious, with ample space for a hit to bind. With one of these hits in the active site, the substrate N^5-CAIR (similar in size to AIR) would be blocked from entering the active site.

3.5. Inhibition activity

Of the 60 selected compounds, 16 compounds, at 10 μM, exhibited 6% to 27% inhibition of the activity of *Ba*PurE (10 nM) in Tris-25 at 20 °C (Tables 1 and 3). We found that the inhibition values did not depend on whether 10 or 30 μM CAIR was used. In a typical paired run under the same condition, the known inhibitor NAIR reduced the activity by 21%, whereas **LC1** inhibited by 30% (Fig. 4).

The inhibition assay results of samples with and without 0.1–0.01% Triton X-100 were generally similar. For example, for **LC3** without Triton the average was 13 ± 4%, and with Triton it was 12 ± 3%; for **LC5** without Triton it was 20 ± 5% and with Triton it was 26 ± 5%; and for **LC6** without Triton it was 15 ± 0 % and with Triton it was 7 ± 4%. These results indicated that the observed inhibitions were not due to compound aggregation induced inhibition.

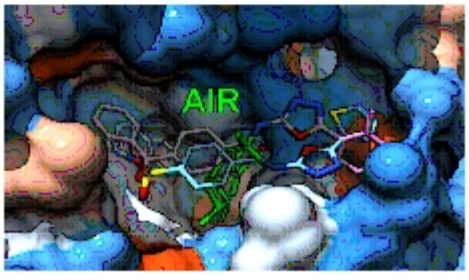

Figure 3. The active site of *Ec*PurE with AIR (PDB: 1O7A, Chain B) is displayed. It is colored by amino acid residue hydrophobicity, with blue for the most hydrophilic, to white, to orange-red for the most hydrophobic. AIR (green color) is deep in the binding-site pocket. The residues on the right are K17 and E158 (blue color) and the residue on the left is A96 (beige color). Two representative compounds (LC1 and LC3) are docked in the active site. The active site appears to be relatively open and spacious, with ample space for the compounds. With any of these compounds in the active site, molecules similar in size to AIR would be blocked from entering the active site.

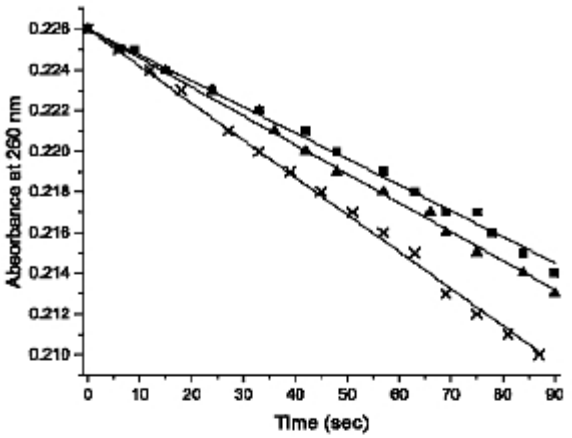

Figure 4. The activity of 10 nM *Ba*PurE in Tris-25 (×) was monitored by the absorbance at 260 nm of 30 μM CAIR. To measure the inhibition activity, LC1 or NAIR (20 μM) and *Ba*PurE (20 nM) was incubated in Tris-25 for 1.5 min at 20 °C, following by addition of an equal volume of CAIR to give an assay sample consisting of LC1 or NAIR (10 μM), *Ba*PurE (10 nM) and CAIR (30 μM) in Tris-25 with 1% DMSO. The A_{260} value was monitored for 1.5 min at 20 °C; the linear portion of the plot was fitted to give a $\Delta A_{260}/\Delta t$ value (initial rate). The inhibition activity of LC1 (filled square) was 30% and of NAIR (filled triangle) was 21% in this paired run. The average inhibition activity for LC1 was 27 ± 6% (n = 3), and for NAIR was 21 ± 3%.

3.6. MIC values

MIC assay results (Tables 1 and 3) were highly reproducible. On repeated testing, most were identical, a few differed by twofold, and only 1 differed by fourfold. Five compounds exhibited excellent bacteriostatic antimicrobial activity against *B. anthracis* at a level of 0.05–0.15 μg/mL, which is comparable to the activity of ciprofloxacin (0.11 μg/mL) and better than linezolid (2 μg/mL, from Ref. 31). Higher MIC values were obtained for these compounds when tested against *F. tularensis* than when tested against *B. anthracis*. Thus, four of the compounds had bacteriostatic activity against *F. tularensis* at concentrations ranging from 1.2–6.3 μg/mL, while one compound (**LC3**) had no detectable activity (MIC > 12.5 μg/mL). Two of the compounds (**LC5** and **LC6**) had detectable bacteriostatic activity against *Y. pestis*, with MICs of 3.1 μg/mL, whereas the other three compounds were inactive (MIC > 12.5 μg/mL) (Table 1).

Comparative testing of these compounds against methicillin-susceptible *S. aureus* (MSSA) and methicillin-resistant *S. aureus* (MRSA) revealed three patterns of activity. One of the compounds (**LC3**) was inactive against both MSSA and MRSA (MICs > 12.5 μg/mL). Three of the compounds (**LC1**, **LC5** and **LC6**) had excellent activity against MSSA, with MICs of 0.29, 0.78 and 1.56 μg/mL, respectively. These MICs were in a similar range to that of the positive control antibiotic, ciprofloxacin. These compounds also had activity against MRSA that was similar to their activity against MSSA (within a 1–3 fold difference), with anti-MRSA MICs of 0.39, 1.95 and 3.13 μg/mL, respectively. The fifth compound (**LC4**) tested against these staphylococcal strains had a unique pattern of activity, when compared with the others. It was highly active against MSSA (MIC = 0.20 μg/mL) but inactive against MRSA (MIC > 12.5 μg/mL).

These compounds were also tested against *E. coli* as a representative Gram-negative pathogen. Initial studies revealed that wild

Table 1
The thermal shift (ΔT_m) of *Ba*PurE induced by compounds (100 μM) and inhibitory activity of compounds (10 μM) toward *Ba*PurE in 25 mM Tris buffer

Compound	ΔT_m[a] (°C)	Inhibition[b] (%)	MIC (μg/mL)					
	*Ba*PurE	*Ba*PurE	*Ba*[c]	*Ft*[c]	*Yp*[c]	*MSSA*[c]	*MRSA*[c]	*Ec*ΔTolC[c]
LC1	2.0	27	0.15	6.25	>12.5	0.29	0.39	0.29
LC2	7.9	19	0.10	3.1	>12.5	>12.5	6.25	0.39
LC3	1.9	13	0.10	>12.5	>12.5	>12.5	>12.5	>12.5
LC4	2.4	19	0.10	6.3	>12.5	0.2	>12.5	0.02
LC5	1.1	20	0.05	1.6	3.1	0.78	1.95	0.07
LC6	1.4	15	0.78	1.2	3.1	1.56	3.13	0.39
NAIR	5.6	24	ND	ND	ND	ND	ND	ND
Ciprofloxacin	ND[d]	ND	0.11	0.03	0.04	0.35	0.34	0.01
Linezolid	ND	ND	2[e]	32[f]	ND	2[g]	ND	ND

Also listed are the MIC values of the compounds against various bacterial strains.
[a] $\Delta T_m = T_m^{ff} - T_m^{f}$, with the average transition temperature for *Ba*PurE (T_m^{f}) as 47.6 °C from high throughput screening, with $n = 4878$. T_m^{ff} values were average values from replicate runs in high-throughput screening. For NAIR, $n = 32$.
[b] Values were averages, with $n = 2–4$ with the standard deviations ~7%.
[c] *Ba* = *B. anthracis* (ΔANR strain) cells; *Ft* = *F. tularensis* cells; *Yp* = *Y. pestis* cells; *MSSA* = *S. aureus* (methicillin susceptible strain 29213) cells; *MRSA* = *S. aureus* (methicillin-resistant strain 43300) cells; *Ec*ΔTolC = *E. coli* (BW25113 ΔTolC) cells.
[d] ND = not determined.
[e] Ref. 31.
[f] Ref. 40.
[g] Ref. 41.

Table 2
Structures of the inhibitor compounds in Table 1

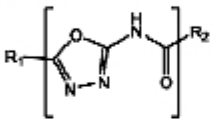

Compound	R_1	R_2
LC1	Thiophene	1-(Toluene-4-sulfonyl)-1,2,3,4-tetrahydro-quinoline
LC2	2,5-Dichlorobenzene	2-Phenylpiperidine
LC3	2,4-Dimethylbenzene	Benzophenone
LC4	2,5-Dimethylbenzene	3-Chlorobenzene
LC5	2,5-Dimethylbenzene	2,5-Chlorothiophene
LC6	4-Bromobenzene	4-Chloroanisole

These compounds include a core structure of 2-carboxamido-1,3,4-oxadiazole, with the R_1 and R_2 groups noted.

type *E. coli* was highly resistant to these compounds (MIC > 12.5 μg/mL). However, four compounds were highly active against *E. coli* ΔTolC, with MICs ranging from 0.02 to 0.4 μg/mL, and one of the compounds (**LC3**) was inactive. Two of the compounds (**LC4** and **LC5**) exhibited activities (MIC of 0.02 and 0.07 μg/mL, respectively) that were comparable to that of ciprofloxacin (MIC of 0.01 μg/mL) against *E. coli* ΔTolC.

The MBC value against *B. anthracis* for **LC4** was 6.3 μg/mL and for **LC5** was 0.8 μg/mL. The values for **LC1**, **LC2**, **LC3**, and **LC6** were >12.5 μg/mL. For all six compounds (**LC1**–**LC6**), the MBC/MIC ratios were >4. Thus these compounds exhibited bacteriostatic activity against *B. anthracis*.

3.7. Core structure identification

Six inhibitors exhibited very low MIC values against *B. anthracis* (0.05–0.78 μg/mL) (Table 1). We found that all six inhibitors contained a common core structure, a 2-carboxamido-1,3,4-oxadiazole (Table 2). The inhibitors that exhibited MIC values >12.5 μg/mL against *B. anthracis*, *F. tularensis* and *Y. pestis* (Table 3) did not have the same core structure and were not tested against *S. aureus* and *E. coli* ΔTolC.

4. Discussion

N^5-carboxy-amino-imidazole ribonucleotide mutase (PurE) is an essential enzyme in the *de novo* purine biosynthesis pathway in *B. anthracis*, *F. tularensis*, *S. aureus*, *Y. pestis*, and many other pathogens, and studies have shown it to be a potential target for a new generation of antibiotics.[5]

The standard enzyme assay for PurE is a UV-based assay,[1,18,19] which is insensitive for high-throughput screening. Thermal shift binding methods have been used to screen for compounds binding

Table 3
The thermal shift (ΔT_m) of *Ba*PurE induced by inhibitors that exhibited large (>12.5 μg/mL) MIC values for *B. anthracis* (ΔANR strain), *F. tularensis*, and *Y. pestis*

Compound	*Ba*PurE		SMILES	MIC (μg/mL)		
	ΔT_m (°C)	Inhibition (%)		*Ba*	*Ft*	*Yp*
LC7	5.2	28	BrC1=CC(=CC=C1OC(=O)OC1=CC=CC=C1)N(C(=O)OC1=CC=CC=C1)S(=O)(=O)C1=CC=C2C=CC=CC2=C1	>12.5	ND[a]	ND
LC8	1.8	20	FC1=CC(Cl)=C(C=C1)C(=O)NC1=CC=C(CC(=O)NCC2=CC=CS2)C=C1	>12.5	>12.5	>12.5
LC9	3.0	17	COC1=C(OC)C(=CC=C1)C(=O)NC1=CC=C(C=C1)C1=CN2C=CSC2=N1	>12.5	>12.5	>12.5
LC10	4.4	17	[Br-].CC1=[N+](CC(O)=O)C2=C(S1)C=CS2	>12.5	>12.5	>12.5
LC11	3.1	14	FC(F)(F)C1=CC=CC(NC(=O)N2CCN(CC2)C2=NN3C=NN=C3C=C2)=C1	>12.5	>12.5	>12.5
LC12	1.5	12	NS(=O)(=O)C1=CC=C(NC(=O)C5C2=NN=C(O2)C2=CC=CC=C2)C=C1	>12.5	ND	ND
LC13	4.7	11	ClC1=CC=C(C=C1)C1=C(CNC(=O)C2=CC=CS2)N2CCSC2=N1	>12.5	>12.5	>12.5
LC14	1.8	7	CCCCC(CC)CNC1=NC2=C(N1CC(O)COC1=CC=C(C)C(C)=C1)C(=O)NC(=O)N2C	ND	>12.5	ND
LC15	1.2	6	COC1=C(OC)C(=CC=C1)C1=NC(CN2N=NC(C(=O)NCC3=CC=C(Cl)C=C3)=C2N)=C(C)O1	>12.5	>12.5	ND

These inhibitors do not have the core structure discussed in the text and shown in Table 2. Samples used both thermal shift and inhibitions were in Tris-25.
[a] ND = not determined.

to proteins. However, in 50 mM Tris buffer at pH 8, a buffer condition used in most PurE activity studies,[1,19] we showed that the thermal shift from a molecule known to bind to PurE, NAIR, was relatively small (1–2 °C). We found that a much larger thermal shift, about 5 °C, was observed for *Ba*PurE in 25 mM Tris buffer at pH 8. With this buffer condition, we identified over 500 compounds in a chemical library of about 25,000 compounds that exhibited 1–20 °C thermal shift and thus as 'binders' to *Ba*PurE. These compounds were further selected as potentially binding to the active site, with docking method. Sixty compounds with high docking scores were selected for enzyme activity inhibition measurement, and 15 compounds found to inhibit *Ba*PurE activity. Several compounds exhibited an inhibition activity comparable to that of NAIR. NAIR has been reported to be a tight-binding inhibitor of *Gallus gallus* PurE with a K_i of 0.34 nM but a steady-state inhibitor of *E. coli* PurE with K_i of 0.5 μM.[32]

Six inhibitors also exhibited low MIC values against *B. anthracis* (ΔANR strain), *E. coli* (*BW25113 strain, ΔTolC*), *F. tularensis*, *S. aureus*, or *Y. pestis*. Two of these inhibitors exhibited activity against 3 of the 6 Category A biowarfare agents (*F. tularensis*, *B. anthracis* and *Y. pestis*, CDC information) at levels comparable to current commercial antibiotics, presumably through a different (novel) mechanism not utilized by any other commercial antibiotic. The precise molecular mechanism awaits future elucidation. It is interesting to note that the MIC values of the compounds were much lower (about 0.1 μM for **LC5**, for example) than the concentration (10 μM) needed to exhibit inhibition toward *Ba*PurE activity. These results suggest that other protein/enzyme molecules are also targeted by these compounds. Clearly additional studies are warranted for further development of these antimicrobial compounds as potential drug molecules.

These 6 compounds exhibiting low MIC values contain a core structure of 2-carboxamido-1,3,4-oxadiazole. A component of the core structure is the 1,3,4-oxadiazole moiety. Compounds containing the 1,3,4-oxadiazole moiety have been identified in several studies (e.g.,[33–37]), and reviewed recently.[38] Four of the five recently identified inhibitors of *trans*-translation contain the core structure,[39] but these four compounds are not the same as the ones identified in this study. As noted previously,[34] 'there are numerous literature examples of the 2,5-disubstituted-1,3,4-oxadiazole system that have shown biological activities including anticancer, anti-inflammatory, antifungal, antiviral, and antibacterial or antimycobacterial activity'. Amongst the compounds with this core structure that have appeared in literature, only one compound described here (**LC5**) has appeared in literature.[34] However, the published studies have not identified detailed mechanism of action of these compounds.

Our studies identified six inhibitors from high-throughput screening with *Ba*PurE that exhibit high-level antimicrobial activity against *B. anthracis* (MIC < 1 μg/mL). The finding supports the approach of screening compounds for enzyme inhibition activity as a means to identify lead agents with antimicrobial activity. Some of the compounds had cross-strain activity against *F. tularensis* and *Y. pestis*, but with MIC values that were ~10 times higher than those for *B. anthracis*. The reduction in activity against these species is perhaps a consequence of limited cell penetration or differential efflux.

Some of the compounds had cross-strain activity against *S. aureus*, in some cases with MICs < 1 μg/mL. These results suggest that these compounds might represent a new class of antimicrobial agents that could be studied and developed for anti-staphylococcal activity. This possibility is much more important for the compounds with anti-MRSA activity (see below), since the clinical options for treating MRSA infections are limited.

Three of the compounds that had anti-Staph (MSSA) activity had nearly comparable activity against MRSA. In contrast, one of the compounds (**LC4**) had high-level bacteriostatic activity against MSSA (MIC = 0.2 μg/mL) but was inactive against MRSA (MIC >12.5 μg/mL). These observations raise interesting questions about the mechanisms of action of the compounds that were active against MRSA and even more interesting questions about the compound structure–function related differences that might explain the high-level resistance of MRSA to **LC4**.

The high-level activity of some of these compounds against the *E. coli* efflux pump knockout strain (*ΔTolC*) (MIC values between 0.02 and 0.39 μg/mL) indicate that the target in some Gram-negative bacteria is sensitive to some of these inhibitors. Further testing of efflux pump competent (wild-type) strains of *E. coli* and of other Gram-negative bacteria will be required to determine the extent of inhibitory activity and the limitations of compound efflux and to consider means of evading efflux-mediated resistance in *E. coli*.

5. Conclusion

Among bacterial pathogens, an increased concern exists for organisms that can be used for bioterrorism, such as *Bacillus anthracis* (*B. anthracis*), which causes anthrax infection. Due to constant bacterial mutations, with some mutations leading to drug resistance, new antibiotics are urgently and constantly needed. We used a low ionic strength buffer condition to accentuate the thermal shift values of *Ba*PurE upon binding compounds from an antibacterial focused chemical library of 24,917 compounds. From the binding compound list, we applied in silico docking to reduce hits to 60 compounds for enzyme activity measurements. 15 inhibitors were identified and six exhibited high-level antimicrobial activity against *B. anthracis* (ΔANR strain) (MIC < 1 μg/mL). These compounds also exhibited low MIC values against *E. coli ΔTolC*, *F. tularensis*, *S. aureus* (*MSSA and MRSA*), and *Y. pestis*. The compounds with low MIC values all contained a core structure of 2-carboxamido-1,3,4-oxadiazole. It should be noted that with the concentrations needed for *Ba*PurE inhibition being much higher than MIC values, our study also suggest that other protein/enzyme molecules are being targeted by these compounds. With the low MIC values, we believe that these compounds are well-suited for further studies on the molecular mechanism of their antimicrobial action and for future synthetic improvement to enhance antimicrobial activities for drug development.

Acknowledgements

This work was supported in part by the Defense Threat Reduction Agency (DTRA) with contract HDTRA1-11-C-0011 (to M.E.J., J.L.C. and L.W.-M.F.), the UIC LAS Award for Faculty in the Natural Science (to L.W.-M.F.) and the UIC Chancellor's Graduate Research Fellowship (to N.M.W.). The authors thank Shahila Mehboob of UIC for the *Ba*PurE gene, Loredana Huma for preparing CAIR and NAIR, and S. Tranchimand and T. Joseph Kappock of Purdue University for initial *Ba*PurE enzyme activity assay. We also thank the RRC staff in the DNA Facility for the assistance with the RT-PCR instrument and the High-Throughput Screening Facility. The mass spectrometry facility at RRC was established in part by a grant from the Searle Funds at the Chicago Community Trust to the Chicago Biomedical Consortium.

References and notes

1. Tranchimand, S.; Starks, C. M.; Mathews, I. I.; Hockings, S. C.; Kappock, J. T. *Biochemistry* **2011**, *50*, 4823.
2. Zhang, Y.; Morar, M.; Ealick, S. E. *Cell. Mol. Life Sci.* **2008**, *65*, 3699.
3. Li, S.-X.; Tong, Y.-P.; Xie, X.-C.; Wang, Q.-H.; Zhou, H.-N.; Han, Y.; Zhang, Z.-Y.; Gao, W.; Li, S.-G.; Zhang, X. C.; Bi, R.-C. *J. Mol. Biol.* **2007**, *365*, 1603.

4. Firestine, S. M.; Wu, W.; Youn, H.; Davisson, V. J. *Bioorg. Med. Chem.* **2009**, *17*, 794.
5. Samant, S.; Lee, H.; Ghassemi, M.; Chen, J.; Cook, J. L.; Mankin, A. S.; Neyfakh, A. A. *PLoS Pathogen* **2008**, *4*, e37.
6. Lo, M.-C.; Aulabaugh, A.; Jin, G.; Cowling, R.; Bard, J.; Malamas, M.; Ellestad, G. *Anal. Biochem.* **2004**, *332*, 153.
7. Kranz, J. K.; Schalk-Hihi, C. *Methods Enzymol.* **2011**, *493*, 277.
8. Pantoliano, M. W.; Petrella, E. C.; Kwasnoski, J. D.; Lobanov, V. S.; Myslik, J.; Graf, E.; Carver, T.; Asel, E.; Springer, B. A.; Lane, P.; Salemme, F. R. *J. Biomol. Screening* **2001**, *6*, 429.
9. Koronakis, V. *FEBS Lett.* **2003**, *555*, 66.
10. Tuntland, M. L.; Johnson, M. E.; Fung, L. W.-M.; Santarsiero, B. D. *Acta Crystallogr., Sect. D* **2011**, *D67*, 870.
11. Tuntland, M. L.; Santarsiero, B. D.; Johnson, M. E.; Fung, L. W.-M. *Acta Crystallogr., Sect. D* **2014**, *D70*, 3057.
12. Wolf, N. M.; Abad-Zapatero, C.; Johnson, M. E.; Fung, L. W.-M. *Acta Crystallogr., Sect. D* **2014**, *D70*, 841. Corrigendum: **2014**, *D70*, 3087.
13. Louis-Jeune, C.; Andrade-Navarro, M. A.; Perez-Iratxeta, C. *Proteins: Struct., Funct., Bioinf.* **2012**, *80*, 374.
14. Boyle, M. P.; Kalliomaa, A. K.; Levdikov, V.; Blagova, E.; Fogg, M. J.; Brannigan, J. A.; Wilson, K. S.; Wilkinson, A. J. *Proteins: Struct., Funct., Bioinf.* **2005**, *61*, 674.
15. Laskowski, R. A. *Nucleic Acids Res.* **2009**, *37*, D355.
16. Sullivan, K. L.; Huma, L. C.; Mullins, E. A.; Johnson, M. E.; Kappock, T. J. *Anal. Biochem.* **2014**, *452*, 43.
17. Hoskins, A. A.; Morar, M.; Kappock, T. J.; Mathews, I. I.; Zaugg, J. B.; Barder, T. E.; Peng, P.; Okamoto, A.; Ealick, S. E.; Stubbe, J. *Biochemistry* **2007**, *46*, 2842.
18. Constantine, C. Z.; Starks, C. M.; Mill, C. P.; Ransome, A. E.; Karpowicz, S. J.; Francois, J. A.; Goodman, R. A.; Kappock, T. J. *Biochemistry* **2006**, *45*, 8193.
19. Meyer, E.; Leonard, N. J.; Bhat, B.; Stubbe, J.; Smith, J. M. *Biochemistry* **1992**, *31*, 5022.
20. Rasmussen, D. H.; MacKenzie, A. P. *Nature* **1968**, *220*, 1315.
21. Firestine, S. M.; Davisson, V. J. *J. Med. Chem.* **1993**, *36*, 3484.
22. Lee, H.; Zhu, T.; Patel, K.; Zhang, Y.-V.; Truong, L.; Hevener, K. E.; Gatuz, J. L.; Subramanya, G.; Jeong, H.-Y.; Uprichard, S. L.; Johnson, M. E. *PLoS ONE* **2013**, *8*, e75144.
23. Ferguson, A. D.; Sheth, P. R.; Basso, A. D.; Paliwal, S.; Gray, K.; Fischmann, T. O.; Le, H. V. *FEBS Lett.* **2011**, *585*, 104.
24. Sainsbury, S.; Bird, L.; Rao, V.; Shepherd, S. M.; Stuart, D. I.; Hunter, W. N.; Owens, R. J.; Ren, J. *J. Mol. Biol.* **2011**, *405*, 173.
25. Sun, F.; Zhou, L.; Zhao, B. C.; Deng, X.; Cho, H.; Yi, C.; Jian, X.; Song, C. X.; Luan, C. H.; Bae, T.; Li, Z.; He, C. *Chem. Biol.* **2011**, *18*, 1032.
26. Zhang, J.-H.; Chung, T. D. Y.; Oldenburg, K. R. *J. Biomol. Screening* **1999**, *4*, 67.
27. Kozikowski, B. A.; Burt, T. M.; Tirey, D. A.; Williams, L. E.; Kuzmak, B. R.; Stanton, D. T.; Morand, K. L.; Nelson, S. L. *J. Biomol. Screening* **2003**, *8*, 205.
28. Cheng, X.; Hochlowski, J.; Tang, H.; Hepp, D.; Beckner, C.; Kantor, S.; Schmitt, R. *J. Biomol. Screening* **2003**, *8*, 292.
29. Popa-Burke, I. G.; Issakova, O.; Arroway, J. D.; Bernasconi, P.; Chen, M.; Coudurier, L.; Galasinski, S.; Jadhav, A. P.; Janzen, W. P.; Lagasca, D.; Liu, D.; Lewis, R. S.; Mohney, R. P.; Sepetov, N.; Sparkman, D. A.; Hodge, C. N. *Anal. Chem.* **2004**, *76*, 7278.
30. Hevener, K. E.; Mehboob, S.; Su, P.-C.; Truong, K.; Boci, T.; Deng, J.; Ghassemi, M.; Cook, J. L.; Johnson, M. E. *J. Med. Chem.* **2012**, *55*, 268.
31. Louie, A.; Heine, H. S.; Kim, K.; Brown, D. L.; VanScoy, B.; Liu, W.; Kinzig-Schippers, M.; Sorgel, F.; Drusano, G. L. *Antimicrob. Agents Chemother.* **2008**, *52*, 2486.
32. Firestine, S. M.; Poon, S.-W.; Mueller, E. J.; Stubbe, J.; Davisson, V. J. *Biochemistry* **1994**, *33*, 11927.
33. Richter, S. G.; Elli, D.; Kim, H. K.; Hendrickx, A. P. A.; Sorg, J. A.; Schneewind, O.; Missiakasa, D. *Proc. Nat. Acad. Sci. U.S.A.* **2013**, *100*, 3531.
34. Reynolds, R. C.; Ananthan, S.; Faaleolea, E.; Hobrath, J. V.; Kwong, C. D.; Maddox, C.; Rasmussen, L.; Sosa, M. I.; Thammasuvimol, E.; White, E. L.; Zhang, W., ; Secrist, J. A., III *Tuberculosis* **2012**, *92*, 72.
35. Hou, Z.; Nakanishi, I.; Kinoshita, T.; Takei, Y.; Yasue, M.; Misu, R.; Suzuki, Y.; Nakamura, S.; Kure, T.; Ohno, H.; Murata, K.; Kitaura, K.; Hirasawa, A.; Tsujimoto, G.; Oishi, S.; Fujii, N. *J. Med. Chem.* **2012**, *55*, 2899.
36. Cheng, T. J. R.; Wu, Y.-T.; Yang, S.-T.; Lo, K.-H.; Chen, S.-K.; Chen, Y.-H.; Huang, W.-I.; Yuan, C.-H.; Guo, C.-W.; Huang, L.-Y.; Chen, K.-T.; Shih, H.-W.; Cheng, Y.-S. E.; Cheng, W.-C.; Wong, C.-H. *Bioorg. Med. Chem.* **2010**, *18*, 8512.
37. Ates, O.; Kocabalkanli, A.; Cesur, N.; Otuk, G. *Il Farmaco* **1998**, *53*, 541.
38. de Oliveira, C. S.; Lira, B. F.; Barbosa-Filho, J. M.; Lorenzo, J. G. F.; de Athayde-Filho, P. F. *Molecules* **2012**, *17*, 10192.
39. Ramadoss, N. S.; Alumasa, J. N.; Cheng, L.; Wang, Y.; Li, S.; Chambers, B. S.; Chang, H.; Chatterjee, A. K.; Brinker, A.; Engels, I. H.; Keiler, K. C. *Proc. Nat. Acad. Sci. U.S.A.* **2013**, *110*, 10282.
40. Kreizinger, Z.; Makrai, L.; Helyes, G.; Magyar, T.; Erdelyi, K.; Gyuranecz, M. *J. Antimicrob. Chemother.* **2013**, *68*, 370.
41. Jones, M. E.; Visser, M. R.; Klootwijk, M.; Heisig, P.; Verhoef, J.; Schmitz, F.-J. *Antimicrob. Agents Chemother.* **1999**, *43*, 421.

APPENDIX C

Copy Right Permission

Licensed Content Publisher John Wiley and Sons Licensed Content Publication

Angewandte Chemie International Edition

Licensed Content Title Targeting Antibiotic Resistance

Licensed Content Author Mathieu F. Chellat,Luka Raguž,Rainer Riedl

Licensed Content Date Mar 22, 2016

Licensed Content Pages 27

Type of use Dissertation/Thesis

Requestor type University/Academic

Format Electronic

Portion Figure/table

Number of figures/tables 2

Original Wiley figure/table number(s) Figure 0

Will you be translating? No

Title of your thesis / dissertation Protein Target Identification and Characterization for Antibiotic Discovery

Expected completion date Jun 2018

Expected size (number of pages) 120

Requestor Location Mrs. Pauline Kabre

7258 S Oglesby

CHICAGO, IL 60649

United States

Attn: Mrs. Pauline Kabre

Publisher Tax ID EU826007151

Total 0.00 USD

This Agreement between Mrs. Pauline Kabre ("You") and John Wiley and Sons ("John Wiley and Sons") consists of your license details and the terms and conditions provided by John Wiley and Sons and Copyright Clearance Center.

License Number 4366581160723

License date Jun 12, 2018

Licensed Content Publisher John Wiley and Sons

Licensed Content Publication Angewandte Chemie International Edition

Licensed Content Title Targeting Antibiotic Resistance

Licensed Content Author Mathieu F. Chellat,Luka Raguž,Rainer Riedl

Licensed Content Date Mars 22, 2016

Licensed Content Pages 27

Type of use Dissertation/Thesis

Requestor type University/Academic

Format Electronic

Portion Figure/table

Number of figures/tables 2

Original Wiley figure/table number(s) Figure 1

Will you be translating? No

Title of your thesis / dissertation Protein Target Identification and Characterization for Antibiotic Discovery

Expected completion date Jun 2018

Expected size (number of pages) 120

Requestor Location Mrs. Pauline Kabre

7258 S Oglesby

CHICAGO, IL 60649

United States

Attn: Mrs. Pauline Kabre

Publisher Tax ID EU826007151

Total0.00 USD

Terms and Conditions

TERMS AND CONDITIONS

This copyrighted material is owned by or exclusively licensed to John Wiley & Sons, Inc. or one of its group companies (each a"Wiley Company") or handled on behalf of a society with which a

VITA

Pauline Kabre
Pkabre2@uic.edu
312-355- 0566

Department of Chemistry
University of Illinois at Chicago
845 W Taylor street
Chicago, IL 60607

EDUCATION

1. Ph.D. in Chemistry/Biochemistry (2011 – Expected Jun 2018)
   University of Illinois at Chicago, Department of Chemistry
   Dissertation Advisor: Dr. L.W.-M. Fung

2. Bachelor of Science in Biochemistry (2010)
   University of Illinois at Chicago

RESEARCH EXPERIENCE

University of Illinois at Chicago, Chicago, IL

Research Student January 2012 - December 2017

Comparing solution properties of homologous enzymes

- Effectively characterized homologous enzymes and carried out enzymatic assay
- Successfully cloned genes into expression vectors for protein expression
- Highly skilled in protein expression, purification, and quantification including FPLC methods
- Determined enzymatic activities and optimized enzymatic assay conditions
- Competent in spectroscopies solution properties assessment of proteins using circular dichroism and fluorescence
- Knowledgeable in protein crystallization screening process and protein crystallography
- Familiar with high throughput screening for inhibitor identification
- Proficient in DNA extraction, purification, size evaluation using DNA gel and UV visualization and gene amplification by PCR
- Proficient in detail record keeping and documentation of data and results

Research Student June 2015 - January 2018

Target identification by mutant selection

- Effectively selected resistant colonies of staphylococcus aureus
- Determine MIC of compounds on various bacterial strains
- Successfully extracted genomic DNA, designed primers and amplified various genes by PCR
- Effectively used checker board assay for synergism and antagonism of compounds with known antibiotics
- Consistently purified genomic DNA for next generation sequencing (NGS)
- Analyzed NGS results, designed primers and amplified target gene from genomic DNA for mutant identification by PCR.
- Assessed cross resistance by MIC of known antibiotics on resistant variants
- Accomplished gene knock out through phage transduction

Research Student October 2015 -Present

Development of a laboratory FabI mutant library

- Developed error prone PCR method to give over 322 mutations in the FabI gene of staphylococcus aureus
- Generated 135 protein expression plasmids with FabI mutants
- Obtained DNA samples for sequencing, and identified mutants from sequencing results

TEACHING EXPERIENCE

Teaching Assistant for Biochemistry I, UIC Spring and Fall 2016 and Fall 2017

- Taught discussion session for 16 to 22 students each semester
- Introduced the concept of biochemistry to students
- Guided students on study methods and retaining techniques
- Reviewed students performance and provided corrective measures when needed
- Provided feedback to students on missed understood subjects

Laboratory Instructor for Biochemistry, UIC Spring 2017

- Guided a group of 12 students on performing current biochemical laboratory techniques
- Directed students on data collection, analysis, and scientific reporting
- Oversaw and instructed students on preparing and presenting oral presentation
- Addressed students concerns about laboratory concept and procedures
- Established laboratory report rubric for grading
- Prepared and graded quizzes, exams and presentations for all sections (60 to 70 students)

General chemistry instructor, UIC Summers 2013 and 2017

- Refined lecture material using power point slides for 15 to 20 students
- prepared and graded homework and quizzes
- Held office hours for groups and individuals
- Prepared quizzes and practice worksheets
- Proctored and graded exams
- Prepared smart views for online grades and course management

Teaching Assistant for general chemistry, UIC 2011 – 2015

- Carried out problem solving session in small group settings (5 to 10 students)
- Instructed and graded introductory and general chemistry laboratories for 3 groups of 22 students
- Guided student on the steps of writing a laboratory report as well as solving chemistry problems
- Prepared practical exams and practice exams

Instructor of chemistry support course, UIC Spring 2018

- Guide international students on requirement for successful course completion
- Generate worksheets for six different levels (83 students)
- Addresses cultural norms in college life
- Answer students questions study tips and on ways to improve their grades

PUBLICATIONS

Demissie R.; **Kabre P.**; Tuntland M.; Fung L.W.-M. An Efficient and Economical Assay to Screen for Triclosan Binding to FabI. J. Biomol. Screening. 2016, 21, 391-398.

Kabre P.; Fung L.W.-M. Comparison of the Solution Properties of N-5 Caboxyaminoimidazole Ribonucleotide Mutase (PurE) from *Francissella tularensis, Yersinia pestis* and *Bacillus anthracis.* (Manuscript in preparation)

Kabre P.; Demissie R.; Fung L.W.-M. The Development of a Laboratory *FabI* mutants Library for Identifying Triclosan Resistant S.aureus. (Manuscript in preparation)

POSTERS PRESENTATIONS

Midwest Enzyme Chemistry Conference 2017 at Loyola University in Chicago
Target identification by mutant selection

Northwestern Black Graduate Student Association 19th Annual Conference 2016 at Northwestern University
A Mutant library of *Staphylococcus aureus FabI* as a mean to detect Triclosan resistant mutants

Midwest Enzyme Chemistry Conference 2016 at University of Illinois in Chicago
Ionic strength effect on the catalytic activity of PurE homologous enzymes
Student Research Forum, University of Illinois in Chicago; Spring 2016
Biochemical characterization of N^5-caboxyaminoimidazole ribonucleotide mutase (PurE) from *Francissella tularensis, Yersinia pestis* and *Bacillus anthracis*
LEADERSHIP
Graduate Student Council (GSC) Department of Chemistry representative (2014-2015)
Skills
Enzyme Activity Assay, FPLC, CD, Fluorescence, cloning, protein purification
Additional Skills
Computer: Pymol, Chimera, Origin-Pro, Microsoft Office Word, Excel, and PowerPoint
Language: Bilingual English/French: Oral and written
Other Responsibilities
Handle ordering, receiving and processing of laboratory supplies.